KTH ROYAL INSTITUTE
OF TECHNOLOGY

Degree Project in Degree Project in Electrical Engineering, specializing in Systems,Control and Spacecraft Engineering

Second cycle, 30 credits

Application of Discrete Time High Order Control Barrier Functions for a prototype multi-spacecraft inspection of the ISS

GREGORIO MARCHESINI

Stockholm, Sweden, 2023

Application of Discrete Time High Order Control Barrier Functions for a prototype multi-spacecraft inspection of the ISS

GREGORIO MARCHESINI

Master's Programme, Aerospace Engineering, 120 credits

Date: January 4, 2023

Supervisor: Pedro Alexandre Delgado Roque

Examiner: Dimos V. Dimarogonas

School of Electrical Engineering and Computer Science

Abstract

In the past few years, the application of Control Barrier Functions (CBF) and High Order Control Barrier Functions (HOCBF) as a suitable framework to ensure *safety* for autonomous systems has attracted increasing interest. In particular, autonomous space systems are frequently subject to safety-critical constraints due to the high costs involved in manufacturing and launching. In the present work, the application of a sample data MPC controller subject to CBF and HOCBF constraints is explored as a suitable solution for spacecraft formation flight operations. Specifically, a prototype inspection mission of the International Space Station through a multi-agent formation of CubeSats is explored. Each CubeSat is assumed to be injected in a passive relative orbit around the ISS and controlled such that the state of each agent is maintained within a prescribed *safe* corridor from its reference relative orbit. Moreover, appropriate conditions on the minimum control authority required to guarantee the constraints satisfaction within the MPC scheme formulation are derived and a numerical procedure to assess the recursive feasibility of the designed controller is presented. Moreover, suitable analytical modifications of the classical CBF and HOCBF constraints definitions are introduced such that the presented sample data MPC control scheme is guaranteed to ensure safety for the state of each agent in between sampling intervals. Lastly, the final control strategy is validated numerically by means of computer simulation.

Keywords

Space Robotics, Control Barrier Functions, Autonomous systems, Multi-agent systems

Sammanfattning

Under de senaste åren har tillämpningen av Kontrollbarriärfunktioner (CBF) och Högre ordningens kontrollbarriärfunktioner (HOCBF) som ett lämpligt ramverk för att säkerställa säkerhet för autonoma system väckt ett ökande intresse. Autonoma rymdsystem är ett område med särskilt fokus på säkerhetsbegränsningar på grund av de höga tillverknings och uppskjutningskostnaderna. I detta arbete undersöks tillämpningen av en MPC-kontroller med CBF och HOCBF bivillkor för applikation inom formationsflygningsoperationer för rymdfarkoster. Detta görs genom att ett prototypinspektionsuppdrag på Internationella Rymdstationen (ISS) genom en multi-agent formation av CubeSats tas fram. Varje CubeSat är ämnad att injiceras i en passiv relativ omloppsbana runt ISS och styras sådant att varje agents tillstånd bevaras inom en föreskriven säker korridor från dess passiva relativa referensomloppsbana. Lämpliga villkor för den minsta styrbarheten som krävs för att garantera att MPC-schemaformuleringens begränsningar är tillfredsställda härleds, och en numerisk procedur för att bedöma den rekursiva genomförbarheten för den designade kontrollern presenteras. Vidare introduceras lämpliga analytiska modifieringar av de klassiska CBF- och HOCBF-begränsningsdefinitionerna så att det presenterade MPC-kontrollschemat med provdata garanterar säkerheten för varje agents tillstånd mellan dess samplingsintervall. Till sist valideras den slutliga kontrollstrategin numeriskt via datorsimuleringar.

Nyckelord

Space Robotics, Control Barrier Functions, Autonomous systems, Multi-agent systems

Acknowledgments

I would like to sincerely thank my supervisor for all the time and afford he invested in supervising my thesis project. I also want to thank my examiner Dimos V. Dimarogonas for accepting my thesis project and for giving me the possibility to pursue my passion for autonomous space systems. Most of all I want to thank all my friends that are in Stockholm and all over Europe. I am extremely grateful for all their support during this long research period and for giving me the possibility to be part of a diverse and culturally reach group of students. In the end, I want to thank my whole family for encouraging me to take all the necessary steps to achieve my dreams.

« *All that is gold does not glitter,*
Not all those who wander are lost;
The old that is strong does not wither,
Deep roots are not reached by the frost.
From the ashes a fire shall be woken,
A light from the shadows shall spring;
Renewed shall be blade that was broken,
The crownless again shall be king »

J.R.R. Tolkien

Stockholm, January 2023
Gregorio Marchesini

Contents

List of Figures

List of Tables

List of acronyms and abbreviations

CBF	Control Barrier Function
CLF	Control Lyapunov Function
DCM	Direction Cosine Matrix
EVA	Extra Vehicular Activity
FHOC	Finite Horizon Optimal Control
HOCBF	High Order Control Barrier Function
ISS	International Space Station
LQR	Linear Quadratic Regulator
MAS	Multi-Agent System
MPC	Model Predictive Control
PRO	Passive Relative Orbit
SD-CBF	Sample Data Control Barrier Function
SD-HOCBF	Sample Data High Order Control Barrier Function

List of Symbols Used

The following symbols will be later used within the body of the thesis.

$\alpha(\cdot) : \mathbb{R} \to \mathbb{R}$ Class K-function, see equation (3.1.3), ... page 26

α_r Out-Of-Plane phase PRO parameter, see equation (2.2.13), . . page 18

α_r Radial phase PRO parameter, see equation (2.2.13), ... page 18

$\bar{\boldsymbol{u}}$ Sequence of control inputs, see equation (2.3.8), ... page 22

$n\bar{u}$ True Longitude, see equation (2.1.9), ... page 6

$\boldsymbol{b}$ implicit keplerian state of the chief, see equation (2.3.3), ... page 20

$\boldsymbol{d}$ Orbital perturbation acceleration vector, see equation (2.1.1), . page 4

$\boldsymbol{e}_{\delta \boldsymbol{r}}$ Relative position errors

$\boldsymbol{e}_{\delta \boldsymbol{x}}$ relative state error, see equation (2.3.6), ... page 21

$\boldsymbol{e}_{\delta \boldsymbol{v}}$ Relative velocity errors

$\boldsymbol{e}_u$ control input error, see equation (2.3.7), ... page 21

$\boldsymbol{r}$ Inertial position, see equation (2.1.1), ... page 4

$\boldsymbol{r}_{ch}$ Position of the chief, see equation (2.2.0), ... page 12

$\boldsymbol{r}_{ch}$ Velocity of the chief in the Hill's frame, see equation (2.2.0), page 12

$\boldsymbol{u}$ Control Input, see equation (2.1.1), ... page 4

$\boldsymbol{V}_{atmo}$ Relative Velocity of the Atmosphere, see equation (2.1.18), . . page 10

$\boldsymbol{v}_{wind}$ Inertial wind velocity, see equation (2.1.18), ... page 10

$\mathcal{C}_S$ Safe set , see equation (3.1.2), ... page 25

$\delta \boldsymbol{a}$ Relative acceleration of the deputy in the Hill's frame, see equation (2.2.6), ... page 16

$\ddot{\boldsymbol{r}}$ Inertial acceleration, see equation (2.1.1), ... page 4

δt Sampling time interval, see equation (2.3.1), ... page 20

$\delta \boldsymbol{r}$ relative position of the deputy w.r.t the chief in the Hill's observer frame, see equation (2.2.4), ... page 14

$\delta \boldsymbol{x}_r$ reference relative state, see equation (2.3.5), ... page 21

$\delta \dot{\boldsymbol{x}}$ relative state

$\delta \tilde{\boldsymbol{x}}$ perturbed relative state, see equation (2.3.3), ... page 20

$\delta \boldsymbol{v}$ relative velocity of the deputy w.r.t the chief in the Hill's observer frame, see equation (2.2.4), ... page 14

$\epsilon_{\delta \boldsymbol{r}}$ Maximum position error inside the safe set, see equation (4.3.1), page 40

$\epsilon_{\delta \boldsymbol{v}}$ Maximum velocity error norm inside the safe set, see equation (4.3.19), page 45

ϵ_f Maximum dynamic acceleration inside the safe set, see equation (4.3.19), ... page 45

$\mathcal{D}$ Domain of the CBF

$\mathcal{L}_f$ Lie derivative along the vector field $\boldsymbol{f}$, see equation (3.1.3), . page 25

$\mathcal{L}_g$ Lie derivative along the vector field $\boldsymbol{g}$, see equation (3.1.3), . . page 25

$\mathcal{T}_k$ Compact time interval, see equation (2.3.1), ... page 20

μ Gravitational parameter, see equation (2.1.1), ... page 4

ν True Anomaly, see equation (2.1.9), ... page 6

Ω longitude of the ascending node , see equation (2.1.9), ... page 6

ω Argument of pericentrum, see equation (2.1.9), ... page 6

$\boldsymbol{\omega}_{\mathcal{H}/\mathcal{I}}$ Angular velocity of the Hill's frame w.r.t an Inertial frame $\mathcal{I}$, see equation (2.1.12), ... page 6

$\partial \mathcal{C}_S$ Border of the safe set , see equation (3.1.2), ... page 25

$\psi : \mathcal{D} \times \mathcal{U} \times \mathcal{I} \to \mathbb{R}$ Control Barrier function constraint, see equation (3.1.4), page 26

$\hat{\boldsymbol{r}}$ Radial Direction in the Hill's frame, see equation (2.1.10), ... page 6

ρ density, see equation (2.1.18), ... page 10

ρ_0 Base density, see equation (2.1.19), ... page 10

ρ_r Radial PRO parameter, see equation (2.2.13), ... page 18

ρ_s Along track PRO parameter, see equation (2.2.13), ... page 18

ρ_w Out-Of-Plane PRO parameter, see equation (2.2.13), ... page 18

$\hat{\boldsymbol{s}}$ Along-track direction in the Hill's frame, see equation (2.1.10), page 6

$\tilde{\boldsymbol{b}}$ perturbed implicit keplerian state of the chief, see equation (2.3.3), page 20

$\tilde{\boldsymbol{e}}_{\delta \boldsymbol{x}}$ perturbed relative state error, see equation (2.3.6), ... page 21

$\mathcal{U}$ MPC control constraint set, see equation (2.3.9), ... page 22

$\hat{\boldsymbol{w}}$ Out-of-Plane direction in the Hill's frame, see equation (2.1.10), page 6

$\mathcal{X}$ MPC state constarint set, see equation (2.3.9), ... page 22

$\mathcal{X}_f$ MPC terminal state set, see equation (2.3.9), ... page 22

$\zeta : \mathcal{D} \times \mathcal{U} \times \mathcal{I} \to \mathbb{R}$ HOCBF constraint, see equation (3.2.5), ... page 28

$C_{\mathcal{A}}^{\mathcal{I}}$ Direction Cosine Matrix from frame $\mathcal{A}$ to frame $\mathcal{B}$, see equation (2.1.11), ... page 6

CD Drag parameter, see equation (2.1.18), ... page 10

Cd Drag coefficient, see equation (2.1.18), ... page 10

d_s Inner safe set threshold distance , see equation (4.3.22), ... page 47

h Angular momentum, see equation (2.1.9), ... page 6

$h(\cdot, \cdot) : \mathcal{X} \times \mathcal{I} \to R$ Control Barrier Function , see equation (3.1.2), page 25

H_s Scale height, see equation (2.1.19), ... page 10

i Inclination, see equation (2.1.9), ... page 6

J_n Zonal Gravity coefficients, see equation (2.1.15), ... page 8

L Lipschitz constant, ... page 29

m mass, see equation (2.1.18), ... page 10

P_n^m Legendre polynomials Order m and degree n, see equation (2.1.15), page 8

$p_{\delta \boldsymbol{r}0}$ Position α function coefficient of order zero

$p_{\delta \boldsymbol{r}1}$ Position α function coefficient of order one

r_{ch} Distance of the chief spacecraft from the Earth Center of Mass, see equation (2.2.0), ... page 12

S Wet surface, see equation (2.1.18), ... page 10

U Gravitational potential, see equation (2.1.2), ... page 5

V_f MPC terminal cost, see equation (2.3.8), ... page 22

V_N MPC Value function, see equation (2.3.8), ... page 22

Chapter 1

Introduction

The application of multi-agent system (Multi-Agent System (MAS)) design to solve complex robotics tasks has received increasing attention in the past few decades [1]. Examples of successful MAS control paradigms for terrestrial and aerial applications are extensive in the literature. Especially the interaction between modern control technique like Reinforcement Learning and distributed autonomous systems design, is raising growing interest due to the broad range of military and civil applications. The advantages of MAS design include redundancy and robustness to single agent failure, reduced complexity in single agent hardware and the possibility to accomplish complex interaction among heterogeneous agents. These same advantages are of critical importance for the next generation of planetary exploration, on-orbit servicing, and on-orbit construction mission concepts, to mention a few. The Starlink and OneWeb mega-constellations are remarkable examples of MAS space-based telecommunication infrastructure, and a few other missions like GRACE and PRISMA proved to be successful MAS space missions with high scientific return. The development of robust MAS control paradigms is particularly appealing for space applications as the distribution of scientific payload over multiple simple and cost effective spacecrafts (alike CubeSats) has the potential to significantly impact the production costs and deployment time [2]. On the other hand, the high computational costs connected to MAS control approaches and the stringent requirements on control and navigation accuracy has considerably hampered the concrete application of MAS mission designs for space applications [2]. In the current work, a prototype MAS mission design is proposed for the inspection of the outer structure of the International Space Station (ISS). Since 1998 the ISS has served as on orbit

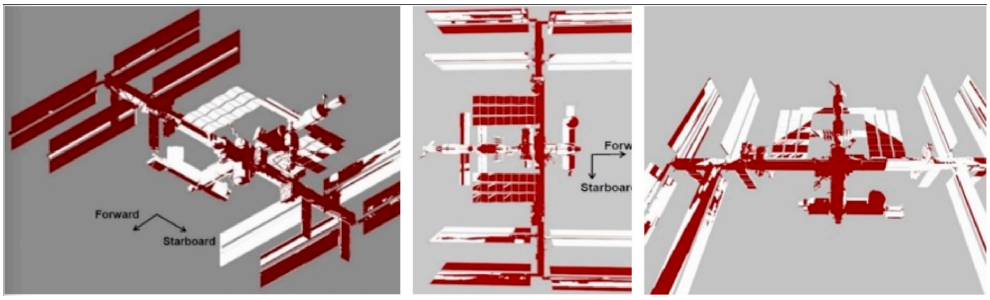

Figure 1.1: Graphical overview of the blind spots for the ISS (from [3]). Dark red areas are areas that cannot be inspected from the interior of the ISS.

science laboratory for micro-gravity experiments. It is known [3] that the outer structure of the space station presents many blind-spots which are not possible to inspect if not by an Extra Vehicular Activity (EVA) or by occasional inspection by cargo missions approaching or leaving the station [3]. Although EVA missions represent an outstanding experience for the astronauts inhabiting the station, they still pose their life in danger while requiring considerable resources in terms of time and energy. This fact motivates the development of an autonomous robotic inspection of the ISS which could significantly reduce the cost of inspecting the critical components of the outer structure of the station while eliminating all the human related risks involved in EVAs. The prototype inspection mission is developed based on the work by [4] : it is assumed that a formation of CubeSats, called the inspectors, is injected into a set of tight Passive Relative Orbit (PRO) around the ISS with the objective of inspecting the outer structure of the station. Each CubeSat is assumed to be controlled through an independent sample data MPC controller which is applied to track the assigned PRO while ensuring control and safety constraints. The application of Control Barrier Function (CBF) has gained particular popularity in the past few years as formal framework to design control invariant sets for dynamical systems where the system state is considered to be *safe* which respect to a given notion of safety introduced during the control design process. Namely, the analytical similarity between the well known Control Lyapunov Function (CLF) applied to synthesise stabilising controllers and the CBF formalism applied to synthesise safe controllers, is the driving reason for its vast theoretical appeal [5]. The application of sample data CBF inside a Finite Horizon Optimal Control scheme (FHOC) alike Model Predictive Control (MPC) has been already explored in [6], but safety in between discrete time steps is not analysed. This problem is addressed in [7] instead, where a corrective term is added to the

continuous time CBF constraint formulation in order ensure safety in between time steps. However, only first relative degree systems are anlysed in [7]. In the current work, the sample data MPC scheme developed by [7] is expanded to address higher relative degree systems. Namely, one High Order Control Barrier Function (HOCBF) and one CBF constraint are included in the MPC control scheme developed by [7] in order to limit the maximum position and velocity tracking errors respectively. The recursive feasibility of the derived MPC control scheme is only proved numerically following an approach similar to the one proposed by [8]. Namely, the set of allowed positions and velocities for each inspector state is densely discretised and each discrete state is test against unfeasibility of the control constraints imposed inside the MPC scheme. The thesis is divided as follows: In Chapter 2 the nonlinear spacecraft relative dynamics is revisited based on the work developed by [9],[10],[11] together with the basic principles of Model Predictive Control and Control Barrier Functions. In Chapter 3 the control strategy developed for the inspection mission is developed and numerically validated in Chapter 4 by means of computer simulation. Eventually in Chapter 5 the results of the specified control scheme are discussed and future research directions are proposed.

Chapter 2

Background

2.1 Fundamentals of Astrodynamics

In this section the fundamental dynamics governing the motion of a point mass as it moves in the gravity field of the Earth is revised. Throughout the section, vectors quantities are represented in bold and scalars are represented in italics. The notation $\|\|$ denotes the standard Euclidean 2-norm while the hat symbol on top a vector quantity $\hat{(\cdot)}$ denotes a direction vector (vectors with unitary norm). When clear from the contest, the norm of a vector is also conveniently denoted by dropping the bold notation used for vectorial quantities so that r is the vector norm of $\boldsymbol{r}$. The symbols $\boldsymbol{a}$, $\boldsymbol{v}$ and $\boldsymbol{r}$ are used to denote acceleration, velocity and position respectively. The notation $\dot{\boldsymbol{r}}$ is used to denote *total* time derivatives while *partial* time derivative of the same vector is denoted by $\frac{\partial \boldsymbol{r}}{\partial t}$. A general inertial frame fixed at the Earth center of mass will be denoted as $\mathcal{I}$.

2.1.1 Single Spacecraft dynamics

The dynamics of a spacecraft as it orbits around the Earth is mathematically described in an inertial frame of reference as

$$\ddot{\boldsymbol{r}} = -\frac{\mu}{r^3}\boldsymbol{r} + \boldsymbol{d} + \boldsymbol{u} \tag{2.1.1}$$

Where μ is the gravitational parameter of the Earth expressed in $\mathrm{m}^3\,\mathrm{s}^{-2}$, $\boldsymbol{d}$ is the sum of the orbital perturbations acting on the spacecraft and $\boldsymbol{u}$ denotes the acceleration due to the propulsion system that is applied to control the

spacecraft. The term $-\frac{\mu}{r^3}\boldsymbol{r}$ is the *point mass* gravity acceleration term. The point mass gravity acceleration can be described by taking the gradient of the conservative gravity field as

$$-\nabla U(\boldsymbol{r}) = -\nabla\left(-\frac{\mu}{r}\right) = -\frac{\mu}{r^3}\boldsymbol{r} \tag{2.1.2}$$

The most relevant perturbing accelerations in Low Earth Orbit (LEO) include atmospheric drag, the gravitational acceleration due to real mass distribution of the Earth. The mass distribution effect is usually modelled as an infinite series of spherical harmonic scalar functions that define a perturbing potential with respect to the single point mass potential defined in (2.1.2) as it is discussed in Section 2.1.2. The dynamics in equation (2.1.1) can be conveniently described in terms of the keplerian elements of the orbit. Namely, the standard notation for the keplerian elements will be applied such that h indicates the angular momentum of the orbit,e inidcates the eccentricity vector, ν indicates the tru anomaly, Ω indicates the RAAN, i indiactes the inclination, ω inidcates the argument of pericentrum and eventually $\bar{\nu}$ indicates the true longitude, which is the sum of the true anomaly and the argument of pericentrum. The *Gauss Variational Equations* (GVE) are broadly applied to describe the dynamics of the keplerian elements when orbital perturbations are introduced in the system [Equation 10.84 in [12]]

$$\dot{h} = r(d_s + u_s) \tag{2.1.3}$$

$$\dot{e} = \frac{h}{\mu} sin(\nu)(d_r + u_r) + \frac{1}{\mu h}\left[\left(h^2 + \mu r\right) cos(\nu) + \mu\, e\, r\right](d_s + u_s) \tag{2.1.4}$$

$$\dot{\nu} = \frac{h}{r^2} + \frac{1}{\boldsymbol{e}\, h}\left[\frac{h^2}{\mu} cos(\nu)(d_r + u_r) - \left(r + \frac{h^2}{\mu}\right) sin(\nu)(d_s + u_s)\right] \tag{2.1.5}$$

$$\dot{\Omega} = \frac{r}{h\, sin(i)} sin(\omega + \nu)(d_w + u_w) \tag{2.1.6}$$

$$\dot{i} = \frac{r}{h} cos(\omega + \nu)(d_w + u_w) \tag{2.1.7}$$

$$\dot{\omega} = -\frac{1}{\boldsymbol{e}h}\left[\frac{h^2}{\mu} cos(\nu)(d_r + u_r) - \left(r + \frac{h^2}{\mu}\right) sin(\nu)(d_s + u_s)\right] - \frac{r\, sin(\omega + \nu)}{h\, tan(i)}(d_w + u_w) \tag{2.1.8}$$

$$\dot{\bar{\nu}} = \frac{h}{r^2} - \frac{r\, sin(\bar{\nu})}{h\, tan(i)}(d_w + u_w) \tag{2.1.9}$$

The orbital perturbation vector $\boldsymbol{d}$ and the propulsive accelerations $\boldsymbol{u}$ appear in equation (2.1.3) as described in the Hill coordinate frame $\mathcal{H}$

$$\boldsymbol{d} = \begin{bmatrix} d_r & d_s & d_w \end{bmatrix} \quad \boldsymbol{u} = \begin{bmatrix} u_r & u_s & u_w \end{bmatrix}$$

The *Hill*'s frame $\mathcal{H}$ is defined from the orbital state of the spacecraft as

$$\begin{aligned} \hat{\boldsymbol{r}} &= \frac{\boldsymbol{r}}{r} \\ \hat{\boldsymbol{w}} &= \frac{\boldsymbol{r} \wedge \dot{\boldsymbol{r}}}{\|\boldsymbol{r} \wedge \dot{\boldsymbol{r}}\|} = \frac{\boldsymbol{h}}{h} \\ \hat{\boldsymbol{s}} &= \hat{\boldsymbol{w}} \wedge \hat{\boldsymbol{r}} \end{aligned} \tag{2.1.10}$$

Intuitively $\hat{\boldsymbol{r}}$ is the direction vector from the Earth to the spacecraft and it is denoted as the *radial* direction. The direction $\hat{\boldsymbol{w}}$ is the direction of the angular momentum, which is always perpendicular to the *instantaneous* orbital plane and it is named *cross-track* direction. The term instantaneous is used because of the time varying geometry of the orbital plane when orbital perturbations are acting on the spacecraft. Eventually the direction $\hat{\boldsymbol{s}}$ closes the orthogonal frame definition and it is denoted as the *along-track* direction. Note that $\hat{\boldsymbol{s}}$ is not generally parallel to the velocity vector apart from the case of purely circular orbits. The Direction Cosine Matrixs (DCMs) that converts the coordinates of a vector from an inertial coordinate frame $\mathcal{I}$ to the frame $\mathcal{H}$ is given by

$$C_{\mathcal{I}}^{\mathcal{H}} = \begin{bmatrix} c_{\bar{\nu}}c_{\Omega} - s_{\bar{\nu}}s_{\Omega}c_i & c_{\bar{\nu}}s_{\Omega} + s_{\bar{\nu}}c_i c_{\Omega} & s_{\bar{\nu}}s_i \\ -s_{\bar{\nu}}c_{\Omega} - c_{\bar{\nu}}s_{\Omega}c_i & -s_{\bar{\nu}}s_{\Omega} + c_{\bar{\nu}}c_i c_{\Omega} & c_{\bar{\nu}}s_i \\ s_i s_{\Omega} & -s_i c_{\Omega} & c_i \end{bmatrix} \tag{2.1.11}$$

Which is the result of a 3-1-3 Euler angles parametrization $(\Omega, i, \bar{\nu})$. The angular velocity of the Hill's frame which respect to the inertial frame $\boldsymbol{\omega}_{\mathcal{H}/\mathcal{I}}$, is expressed in the $\mathcal{H}$ frame coordinates as

$$\begin{aligned} \omega_r &= s_{\bar{\nu}}s_i\dot{\Omega} + \dot{i}c_{\bar{\nu}} \\ \omega_s &= s_i c_{\bar{\nu}}\dot{\Omega} + \dot{i}s_{\bar{\nu}} \\ \omega_w &= \dot{\Omega}c_i + \dot{\bar{\nu}} \end{aligned} \tag{2.1.12}$$

Replacing the definition of $\dot{\Omega}$, $\dot{\omega}$ and $\dot{\bar{\nu}}$ in the definition of $\boldsymbol{\omega}_{\mathcal{H}/\mathcal{I}}$ in equation

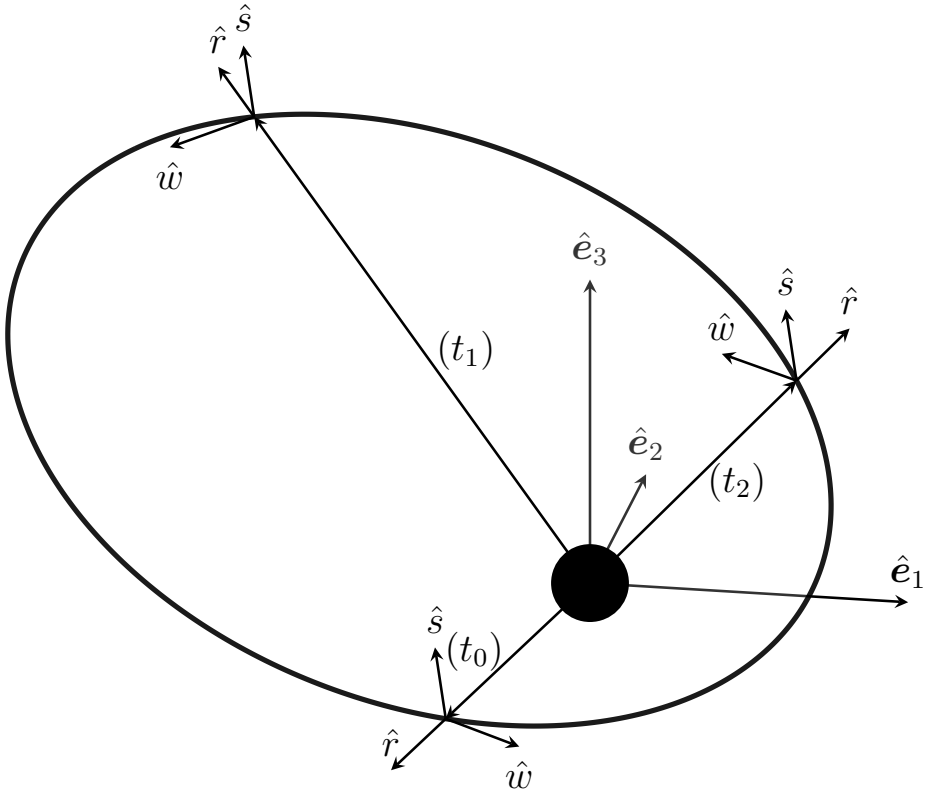

Figure 2.1: Hill's frame $(\hat{\boldsymbol{r}}, \hat{\boldsymbol{s}}, \hat{\boldsymbol{w}})$ at different time steps t along a spacecarft orbit. The inertial frame $\mathcal{I}$ is identified by the base vectors $(\hat{\boldsymbol{e}}_1, \hat{\boldsymbol{e}}_2, \hat{\boldsymbol{e}}_3)$

(2.1.12)

$$\begin{aligned}\omega_r &= \frac{r}{h}(d_w + u_w)\\ \omega_s &= 0\\ \omega_w &= \frac{h}{r^2}\end{aligned} \tag{2.1.13}$$

and the angular acceleration $\dot{\boldsymbol{\omega}}_{\mathcal{H}/\mathcal{I}}$ is then obtained by deriving equation (2.1.13) with respect to time

$$\begin{aligned}\dot{\omega}_r &= \frac{\dot{r}}{h}(d_w + u_w) - \dot{h}\frac{r}{h^2}(d_w + u_w) + \frac{r}{h}(\dot{d}_w + \dot{u}_w)\\ \dot{\omega}_s &= 0\\ \dot{\omega}_w &= \frac{\dot{h}}{r^2} - 2\dot{r}_{ch}\frac{h}{r^3}\end{aligned} \tag{2.1.14}$$

2.1.2 Spherical Harmonics gravity terms perturbation

In the case of the *restricted* two-body problem, the Earth's gravitational field is defined by the potential field of a point mass $U_{pm}(\boldsymbol{r})$ as defined in equation (2.1.2)

$$U_{pm}(\boldsymbol{r}) = -\frac{\mu}{r}$$

Although, the real mass distribution of the Earth is not correctly described by a simple point mass approximation. The most widely used approach to the describe the conservative gravity field of the Earth considering the real mass distribution of the planet is given by a series of spherical harmonic functions [[13],Ch 3.2] as

$$U(\boldsymbol{r}) = \underbrace{-\frac{\mu}{r}}_{U_{pm}} + \underbrace{\frac{\mu}{r}\left[\sum_{n=2}^{N_z}\frac{R^n}{r^n}J_n P_n^0(s_\phi) + \sum_{n=2}^{N_t}\sum_{m=1}^{n}\frac{R^n}{r^n}P_n^m(s_\phi)\left(C_n^m c_{m\psi} + S_n^m s_{m\psi}\right)\right]}_{U_{pert}} \tag{2.1.15}$$

Where the subscripts *pm* and *pert* are applied to identify the point mass potential and the perturbing potential due to the real mass distribution of the Earth. In equation (2.1.15) P_n^m are the Legendre polynomial of degree n and order m, R is the mean radius of the Earth, μ it the gravitational parameter of the Earth, ϕ is longitude ψ geometric latitude. The coefficients J_n, C_n^m and S_n^m are tabulated values obtained from space geodesy missions. The latitude and

longitude are a function of the *Earth Fixed Earth Centered* reference frame, such that evaluating U precisely requires knowledge of the real attitude of the Earth at a given time instant. Although, if only the spherical harmonic terms J_n are considered, only the latitude is required and no information on the planet attitude other than the direction of the rotational axis is required. Among the terms appearing in U_{pert}, the J_n terms are dominant in magnitude. The J_2 term in particular is the largest coefficient among the J_n and it is usually the only one taken into account. The J_3 and J_4 terms (Table 2.1) are three orders of magnitude smaller than J_2. Depending on the application, different

zonal term	value
J_2	0.00108263
J_3	$-J_2 \cdot 2.33936 \times 10^{-3}$
J_4	$-J_2 \cdot 1.49601 \times 10^{-3}$
J_5	$-J_2 \cdot 0.20995 \times 10^{-3}$
J_6	$J_2 \cdot 0.49941 \times 10^{-3}$
J_7	$J_2 \cdot 0.32547 \times 10^{-3}$

Table 2.1: First seven spherical harmonic terms for the planet Earth [14]

levels of accuracy are required in the gravity field description. For example, in Precise Orbit Determination operations (POD), centimeter level accuracy in determining the position of spacecrafts is required and for this reason it is necessary to include as many spherical harmonics as possible in the definition of the potential. However, POD operations involve offline computations for which time is not a stringent requirement. For online applications, where time is a crucial factor, the J_2 term is often the only one taken into account. The gravity potential considering only the zonal harmonics terms is given by

$$U(\boldsymbol{r}) = -\frac{\mu}{r} + \frac{\mu}{r}\sum_{n=2}^{N_z}\frac{R^n J_n P_n^0(sin(\phi))}{r^n} = U_{pm}(\boldsymbol{r}) + U_{zh}(\boldsymbol{r})$$

Note that the latitude is defined from the cartesian position $\boldsymbol{r}$ as

$$sin(\phi) = \frac{\hat{\boldsymbol{e}}_3 \cdot \boldsymbol{r}}{r}$$

Where it is recalled that $\hat{e}$ is a direction vector pointing in the direction of the Earth rotational axis and it is perpendicular to the Earth equatorial plane. From the definition of $U_{zh}(\boldsymbol{r})$, the perturbation due to higher order zonal harmonics

is given by

$$\boldsymbol{d}_{zh} = -\nabla U_{zh}(\boldsymbol{r}) \tag{2.1.16}$$

2.1.3 Atmospheric Drag

The atmospheric drag acceleration is defined as

$$\boldsymbol{d}_{drag} = \frac{1}{2}\frac{\rho\, S\, Cd\|\boldsymbol{V}_{atmo}\|^2}{m}\hat{\boldsymbol{V}}_{atmo} = CD\rho\|\boldsymbol{V}_{atmo}\|^2\hat{\boldsymbol{V}}_{atmo} \tag{2.1.17}$$

In equation (2.1.17), S is the surface perpendicular to the wind direction, ρ is the atmospheric density, m is the mass, Cd is the drag parameter and $\boldsymbol{V}_{atmo}$ is the relative velocity of the atmosphere with respect to the body undergoing the drag acceleration defined as

$$\boldsymbol{V}_{atmo} = \boldsymbol{v}_{wind} - \dot{\boldsymbol{r}} \tag{2.1.18}$$

Where $\boldsymbol{v}_{wind}$ is the inertial velocity of the wind and $\dot{\boldsymbol{r}}$ is the inertial velocity of the body affected by the acceleration. The term CD is the *drag parameter*

$$CD = \frac{1}{2}\frac{SCd}{m}$$

Although the (2.1.17) is a simple analytical formula, the atmospheric density ρ it is a complex function of time, solar activity, altitude and location on the Earth surface. Advanced analytical atmospheric models that take into account for all these variables are available like the *Jacchia* model and the *Harris–Priester* model, but they are difficult to implement on real-time controllers [15]. In the current work a simple analytical exponential atmospheric model is applied which is formally defined as

$$\rho(h) = \rho_0 e^{-\frac{h}{H_s}} \tag{2.1.19}$$

Where ρ_0 is the surface density, h is the altitude of the given spacecraft above the Earth surface and H_s is the *scale height* which is a specific constant for the Earth atmosphere. The model is mostly valid below $100\ km$ altitude but the scale height parameter could be adjusted to fit the density at the altitude range of application.

2.2 Spacecraft Formation Flight

The Spacecraft Formation Flight (SSF) problem is formally defined as follows [11]

The tracking or maintenance of a desired relative separation, orientation or position between or among spacecrafts

While many different approaches to the SSF problem exist [Chapter 1,Section 1.2 in [11]], the Leader/Follower formation approach is the only one analysed which is defined as follows

Given a reference orbit $\mathbb{O}$, called the chief orbit, it is desired to maintain a given number of spacecrafts, named the deputies, in a stable collision-free configuration around $\mathbb{O}$

With the objective of solving the SFF problem applying a Leader/Follower approach, the relative dynamics of a single deputy around the chief orbit is first derived based on the work by [10],[9] and [11]. The same dynamics holds for all the deputies following the prescribed chief orbit. The $\mathcal{H}$ *observer* frame defined by the chief is the reference frame in which the relative dynamics of the deputy is derived. In the continuation of this section, all the inertial accelerations and velocities defined in the $\mathcal{I}$ observer frame are denoted by the dot notation as $\ddot{\boldsymbol{r}}$ and $\dot{\boldsymbol{r}}$. On the other hand, the symbols $\boldsymbol{v}$ and $\boldsymbol{a}$ are applied to denote velocities and accelerations as described in the non-inertial $\mathcal{H}$ observer frame. The *coordinate* frame is assumed to be the $\mathcal{H}$ frame if not else specified. The reader is referred to Appendix A.1 for a brief review of the concept of *observer* and *coordinate* frame*.

2.2.1 Chief dynamics

Given a reference spacecraft called the chief, the Hill's frame $\mathcal{H}$ is defined based on the chief state as presented in equation (2.1.10). The chief state is

*For a comprehensive review of point mass *relative* dynamics and kinematics the reader is referred to Chapter 1 in [16].

then defined in the $\mathcal{H}$ frame as

$$\boldsymbol{r}_{ch} = \begin{bmatrix} r_{ch} \\ 0 \\ 0 \end{bmatrix} \quad \boldsymbol{v}_{ch} = \begin{bmatrix} v_r \\ 0 \\ 0 \end{bmatrix}$$

The inertial acceleration of the chief $\ddot{\boldsymbol{r}}_{ch}$ is given as

$$\ddot{\boldsymbol{r}}_{ch} = \boldsymbol{a}_{ch} + 2\boldsymbol{\omega}_{\mathcal{H}/\mathcal{I}} \wedge \boldsymbol{v} + \dot{\boldsymbol{\omega}}_{\mathcal{H}/\mathcal{I}} \wedge \boldsymbol{r}_{ch} + \boldsymbol{\omega}_{\mathcal{H}/\mathcal{I}} \wedge (\boldsymbol{\omega}_{\mathcal{H}/\mathcal{I}} \boldsymbol{r}_{ch} \wedge \boldsymbol{r}_{ch}) \tag{2.2.1}$$

Replacing the definition of $\boldsymbol{\omega}_{\mathcal{H}/\mathcal{I}}$,$\dot{\boldsymbol{\omega}}_{\mathcal{H}/\mathcal{I}}$ and the chief state, equation (2.2.1) is defined component wise as

$$\ddot{\boldsymbol{r}}_{ch} = (\dot{v}_r - \frac{h^2}{r_{ch}^3})\hat{\boldsymbol{r}} + (\frac{\dot{h}}{r_{ch}})\hat{\boldsymbol{s}} + \omega_r \frac{h}{r_{ch}} \hat{\boldsymbol{w}} \tag{2.2.2}$$

Considering that the chief is unactuated ($\boldsymbol{u}_{ch} = 0$), equation (2.1.1) is specialised on the chief as

$$\ddot{\boldsymbol{r}}_{ch} = -\frac{\mu}{r_{ch}^3} \boldsymbol{r}_{ch} + \boldsymbol{d}_{ch} \tag{2.2.3}$$

It is noted that the direction vector $\hat{\boldsymbol{r}}_{ch}$ is equal to the direction vector $\hat{\boldsymbol{r}}$ of the $\mathcal{H}$ frame since the $\mathcal{H}$ frame is defined from the chief position. The perturbation vector acting on the chief is given by

$$\boldsymbol{d}_{ch} = \boldsymbol{d}_{ch,zh} + \boldsymbol{d}_{ch,drag}$$

The zonal harmonic perturbation $\boldsymbol{d}_{ch,zh}$ is given by

$$\boldsymbol{d}_{ch,zh} = -\nabla \frac{\mu}{r_{ch}} \sum_{n=2}^{N_z} \frac{R^n J_n P_n^0(sin(\phi_{ch}))}{r_{ch}^n}$$

Where $sin(\phi_{ch})$ is related to the orbital elements of the chief as

$$sin(\phi_{ch}) = sin(\bar{\nu}) sin(i)$$

On the other hand the drag perturbation $\boldsymbol{d}_{ch,drag}$ is defined based on the inertial velocity of the atmosphere of the Earth with respect to the deputy velocity. Assuming the atmosphere as rigidly attached to the Earth surface, the inertial

wind speed is given by

$$\boldsymbol{v}_{wind} = \boldsymbol{\omega}_e \wedge \boldsymbol{r}_{ch} = \|\boldsymbol{\omega}_e\| \hat{\boldsymbol{e}}_3 \wedge \boldsymbol{r}_{ch}$$

Where $\|\boldsymbol{\omega}_e\| = 7.292 \times 10^{-3}\ rad/s$ and the inertial velocity of the chief is defined as

$$\dot{\boldsymbol{r}}_{ch} = \boldsymbol{v}_{ch} + \boldsymbol{\omega}_{\mathcal{H}/\mathcal{I}} \wedge \boldsymbol{r}_{ch}$$

The velocity of the wind toward the chief is eventually given by

$$\boldsymbol{V}_{atmo,ch} = \boldsymbol{v}_{wind} - \dot{\boldsymbol{r}}_{ch} = v_r \hat{\boldsymbol{r}} + \left(\frac{h}{r} - \omega_e\ r_{ch}\ cos(i) \right) \hat{\boldsymbol{s}} + (\omega_e\ r_{ch}\ cos(\bar{\nu})\ sin(i))\ \hat{\boldsymbol{w}}$$

and the drag acceleration acting on the chief is then given by

$$\boldsymbol{d}_{ch,drag} = CD_{ch} \rho \|\boldsymbol{V}_{atmo,ch}\|^2 \hat{\boldsymbol{V}}_{atmo,ch}$$

Using the GVE to define the time derivative of i,$\bar{\nu}$ and Ω, the state and dynamics of the chief along its orbit is fully defined by the following set of parameters named here the *implicit* keplerian state (***b***) of the chief

$$\begin{aligned}
\dot{r}_{ch} &= v_r \\
\dot{v}_r &= -\frac{\mu}{r_{ch}} + \frac{h^3}{r_{ch}^3} + d_{r,ch} \\
\dot{h} &= r_{ch} d_{s,ch} \\
\dot{\Omega} &= \frac{r_{ch}}{h\ sin(i)} s(\omega + \nu) d_{w,ch} \\
\dot{i} &= \frac{r}{h} cos(\bar{\nu}) d_{w,ch} \\
\dot{\bar{\nu}} &= \frac{h}{r_{ch}^2} - \frac{r sin(\bar{\nu})}{h\ tan(i)} d_{w,ch}
\end{aligned} \tag{2.2.4}$$

Note that only the orbital elements of the chief are further considered such that the parameters i, $\bar{\nu}$, h and Ω are always considered to be referred to the chief.

2.2.2 Deputy Dynamics

The deputy relative position and velocity with respect to the chief, as described in the $\mathcal{H}$ frame, are defined component wise as

$$\delta \boldsymbol{r} = \begin{bmatrix} \delta r \\ \delta s \\ \delta w \end{bmatrix} \quad \delta \boldsymbol{v} = \begin{bmatrix} \delta v_r \\ \delta v_s \\ \delta v_w \end{bmatrix}$$

While the the absolute position of the deputy is defined by $\boldsymbol{r}_{dep} = \boldsymbol{r}_{ch} + \delta \boldsymbol{r}_{dep}$. The deputy inertial acceleration is defined by equation (2.1.1)

$$\ddot{\boldsymbol{r}}_{dep} = -\frac{\mu}{r_{dep}^3} \boldsymbol{r}_{dep} + \boldsymbol{u}_{dep} + \boldsymbol{d}_{dep} \tag{2.2.5}$$

Where $\boldsymbol{r}_{dep}$ is given component wise as

$$\boldsymbol{r}_{dep} = ((r_{ch} + \delta r)\hat{\boldsymbol{r}} + \delta s \hat{\boldsymbol{s}} + \delta w \hat{\boldsymbol{w}})$$

The zonal harmonic perturbation $\boldsymbol{d}_{dep,zh}$ for the deputy is given by

$$\boldsymbol{d}_{dep,zh} = -\nabla \frac{\mu}{r_{dep}} \sum_{n=2}^{N_z} \frac{R^n J_n P_n^0(sin(\phi_{dep}))}{r_{dep}^n}$$

Where $sin(\phi_{dep})$ is expressed as

$$sin(\phi_{dep}) = \frac{z_{dep}}{r_{dep}} = (r_{ch} + \delta r)\, sin(i) sin\bar{\nu} + \delta s\, sin(i) cos(\bar{\nu}) + \delta w\, cos(i)$$

It is noted that z_{dep} was obtained by multiplying vector $\boldsymbol{r}_{dep}$ by the transpose of the direction cosine matrix $(C_{\mathcal{I}}^{\mathcal{H}})^T = C_{\mathcal{H}}^{\mathcal{I}}$ in (2.1.11) and taking the z component of the resulting vector. Also it is recalled that the orbital elements i and $\bar{\nu}$ are parameters of the chief orbit. The inertial velocity of the deputy is defined identically to the inertial velocity of the chief as

$$\dot{\boldsymbol{r}}_{dep} = \boldsymbol{v}_{dep} + \boldsymbol{\omega}_{\mathcal{H}/\mathcal{I}} \wedge \boldsymbol{r}_{dep}$$

Where $\boldsymbol{v}_{dep}$ is the total velocity of the deputy as seen in the chief frame and it defined as $\boldsymbol{v}_{dep} = \boldsymbol{v}_{ch} + \delta \boldsymbol{v}$. The relative velocity of the wind toward the

deputy is given by

$$\boldsymbol{V}_{dep,atmo} = \boldsymbol{v}_{wind} - \dot{\boldsymbol{r}}_{dep}$$

From the definition of $\boldsymbol{V}_{dep,atmo}$, the drag acceleration acting on the deputy is then derived as

$$\boldsymbol{d}_{dep,drag} = CD_{dep}\rho\|\boldsymbol{V}_{atmo,dep}\|^2\hat{\boldsymbol{V}}_{atmo,dep}$$

Eventually, it is worth highlighting the fact that the deputy inertial dynamics (2.2.5) is a function of the chief implicit keplerian state $\boldsymbol{b}$ and the deputy relative state defined as $\delta\boldsymbol{x}$ such that

$$\delta\boldsymbol{x} = \begin{bmatrix}\delta\boldsymbol{r}\\ \delta\boldsymbol{v}\end{bmatrix}$$

This consideration is further developed in the next section

2.2.3 Nonlinear Relative Dynamics

Now that the dynamics of the chief and deputy are defined, the relative dynamics of the deputy around the chief is developed. Two different approaches are normally applied to derive the relative dynamics of the deputy with respect to the chief in the $\mathcal{H}$ frame. The Lagrangian method, which is based on energy considerations, and the Newtonian method which is based on the direct summation of all the forces involved in the system [Chapter 4 in [11]]. However the resulting dynamics is the same, only the Newton method is presented here as it is considered to involve a lower level of abstraction in comparison to the Lagrangian method. The dynamics of the deputy with respect to the chief orbit as described in the rotating $\mathcal{H}$ *observer* frame is given by

$$\delta\boldsymbol{a} = \delta\ddot{\boldsymbol{r}} - 2\boldsymbol{\omega}_{\mathcal{H}/\mathcal{I}} \wedge \delta\boldsymbol{v} - \dot{\boldsymbol{\omega}}_{\mathcal{H}/\mathcal{I}} \wedge \delta\boldsymbol{r} - \boldsymbol{\omega}_{\mathcal{H}/\mathcal{I}} \wedge (\boldsymbol{\omega}_{\mathcal{H}/\mathcal{I}} \wedge \delta\boldsymbol{r}) \qquad (2.2.6)$$

In equation (2.2.6) the relative inertial acceleration $\delta\ddot{\boldsymbol{r}} := \ddot{\boldsymbol{r}}_{dep} - \ddot{\boldsymbol{r}}_{ch}$ is obtained by subtracting equation (2.2.5) to equation (2.2.1). As discussed previously, the dynamics of the chief is fully defined by the implicit keplerian state $\boldsymbol{b}$ of the chief so that the relative dynamics of the deputy in the $\mathcal{H}$ frame of the chief given by (2.2.6) could be thought as a parametric nonlinear system in the form

$$\delta\boldsymbol{a} = \delta\boldsymbol{a}(\delta\boldsymbol{x}, \boldsymbol{b})$$

Where $\delta\boldsymbol{x}$ is the relative state of the deputy with respect to the chief in the $\mathcal{H}$ frame. After dropping the subscript *dep* from the control $\boldsymbol{u}$ as it is assumed that the deputy is the only capable of actuating, the full form of equation (2.2.6) is given by

$$\begin{aligned}\delta\boldsymbol{a}(\delta\boldsymbol{x},\boldsymbol{b}) = &\underbrace{-\frac{\mu}{r_{dep}^3}\boldsymbol{r}_{dep}+\frac{\mu}{r_{ch}^3}\boldsymbol{r}_{ch}}_{\delta\ddot{\boldsymbol{r}}_g}+\delta\boldsymbol{d}\\ &\underbrace{-2\boldsymbol{\omega}_{\mathcal{H}/\mathcal{I}}\wedge\delta\boldsymbol{v}-\dot{\boldsymbol{\omega}}_{\mathcal{H}/\mathcal{I}}\wedge\delta\boldsymbol{r}-\boldsymbol{\omega}_{\mathcal{H}/\mathcal{I}}\wedge(\boldsymbol{\omega}_{\mathcal{H}/\mathcal{I}}\wedge\delta\boldsymbol{r})}_{\delta\boldsymbol{a}_{fc}}+\boldsymbol{u}\end{aligned} \tag{2.2.7}$$

And the state-space form of the perturbed relative dynamics in equation (2.2.6) becomes

$$\begin{aligned}\delta\dot{\boldsymbol{x}} &= \begin{bmatrix}\delta\boldsymbol{v}\\ \delta\boldsymbol{a}\end{bmatrix} = \boldsymbol{f}(\delta\boldsymbol{x},\boldsymbol{b})+\boldsymbol{g}(\delta\boldsymbol{x},\boldsymbol{b})(\boldsymbol{u}+\delta\boldsymbol{d})\\ \boldsymbol{g}(\delta\boldsymbol{x},\boldsymbol{b}) &= \begin{bmatrix}\boldsymbol{O}_{3x3}\\ \boldsymbol{I}_{3x3}\end{bmatrix}\\ \boldsymbol{f}(\delta\boldsymbol{x},\boldsymbol{b}) &= \begin{bmatrix}\delta\boldsymbol{v}\\ \delta\ddot{\boldsymbol{r}}_g+\delta\boldsymbol{a}_{fc}\end{bmatrix} = \begin{bmatrix}\boldsymbol{f}_r\\ \boldsymbol{f}_v\end{bmatrix}\end{aligned} \tag{2.2.8}$$

Where the relative perturbation vector $\delta\boldsymbol{d}$ is defined as

$$\delta\boldsymbol{d} = \boldsymbol{d}_{dep,drag}-\boldsymbol{d}_{ch,drag}+\boldsymbol{d}_{dep,zh}-\boldsymbol{d}_{ch,zh} = \delta\boldsymbol{d}_{drag}+\delta\boldsymbol{d}_{zh}$$

The perturbation $\delta\boldsymbol{d}_{drag}$ is denoted as *differential* drag perturbation while $\delta\boldsymbol{d}_{ch}$ is the *differential* zonal harmonics term perturbation. It is highlighted that although $\boldsymbol{f}$ is a function of the orbital elements of the chief spacecraft $\boldsymbol{b}$, the relation between $\boldsymbol{b}$ and time is defined by the dynamics in equation (2.2.4) so that $\boldsymbol{f}$ could also be described as a function of time. This point will be recalled in the following sections. The section is concluded noting that in case the perturbation vector is considered to be zero($\delta\boldsymbol{d}=0$) and the chief orbit is considered circular $e=0$, then the implicit keplerian state dynamics becomes

simply

$$\begin{aligned} \dot{r}_{ch} &= v_r \\ \dot{v}_r &= 0 \\ \dot{h} &= 0 \\ \dot{\Omega} &= 0 \\ \dot{i} &= 0 \\ \dot{\bar{\nu}} &= \frac{h}{r^2} \end{aligned} \tag{2.2.9}$$

2.2.4 Linearised relative dynamics

The relative spacecraft dynamics derived in equation (2.2.8) is an highly nonlinear dynamics. Nevertheless, it is possible to linearise equation (2.2.8) around the chief orbit and analyse the linearised system instead of the nonlinear one. Different linearization strategies were developed over the years and an exhaustive list of such linearised solutions to equation (2.2.8) are summarised and compared in [17]. Particularly relevant is the model derived by [18] which included the effect of J_2 and atmospheric drag in a linear time variant model describing the motion of the deputy around the chief by means of the relative keplerian state instead of the relative cartesian state. In current work, only the Clohessy-Wiltshire (CW) linear model will be further analysed. This model is derived based on the assumption that no orbital perturbations are acting on the system, the chief orbit is circular and that the separations between chief and deputy is small compared to the orbital radius of the chief orbit. Under such assumptions, a linearised model for equation (2.2.8) is developed in state-space form as

$$\delta\dot{\boldsymbol{x}}(t) = \begin{bmatrix} \delta\dot{r} \\ \delta\dot{s} \\ \delta\dot{w} \\ \delta\dot{v}_r \\ \delta\dot{v}_s \\ \delta\dot{v}_w \end{bmatrix} = A \begin{bmatrix} \delta r \\ \delta s \\ \delta w \\ \delta v_r \\ \delta v_s \\ \delta v_w \end{bmatrix} + B \begin{bmatrix} u_{r,dep} \\ u_{s,dep} \\ u_{w,dep} \end{bmatrix} \tag{2.2.10}$$

Where A and B are defined as

$$A = \begin{bmatrix} 0 & 0 & 0 & 1 & 0 & 0 \\ 0 & 0 & 0 & 0 & 1 & 0 \\ 0 & 0 & 0 & 0 & 0 & 1 \\ 3\omega_w^2 & 0 & 0 & 2\omega_w & 0 & 0 \\ 0 & 0 & -2\omega_w & 0 & 0 & 0 \\ 0 & -\omega_w^2 & 0 & 0 & 0 & 0 \end{bmatrix} \quad B = \begin{bmatrix} 0 & 0 & 0 \\ 0 & 0 & 0 \\ 0 & 0 & 0 \\ 1 & 0 & 0 \\ 0 & 1 & 0 \\ 0 & 0 & 1 \end{bmatrix} \tag{2.2.11}$$

Systems equation (2.2.10) is a linear time-invariant system for which analytical closed form solutions is available in case of un-actuated dynamics ($\boldsymbol{u}_{dep} = 0$) [[11],Ch 5,pag 85]. In at time t_0 the following condition is met

$$[6\omega_w \delta s(t_0) + 3\delta v_s(t_0)] = 0 \tag{2.2.12}$$

Then the state of the deputy will not drift from the chief (the origin of the Hill's frame). On the other hand, if equation (2.2.12) is satisfied, then the solution to (2.2.10) represent a family of closed periodic orbits, with period equal to the orbital period of the chief ($T = \frac{2\pi}{\omega_z}$). As shown in [11], it is possible to write such closed period orbits in the *amplitude-phase* parametric form

$$\begin{aligned} \delta r(t) &= \rho_r sin\left(\omega_w t + \alpha_r\right) \\ \delta s(t) &= \rho_s + 2\rho_r cos\left(\omega_w t + \alpha_r\right) \\ \delta w(t) &= \rho_w sin\left(\omega_w t + \alpha_w\right) \\ \delta v_r(t) &= \omega_w \rho_r cos\left(\omega_w t + \alpha_r\right) \\ \delta v_s(t) &= -2\omega_w \rho_r sin\left(\omega_w t + \alpha_r\right) \\ \delta v_w(t) &= \omega_w \rho_w cos\left(\omega_w t + \alpha_w\right) \end{aligned} \tag{2.2.13}$$

The parametric form in equation (2.2.13) is particularly suitable for trajectory design purposes. Indeed, equation (2.2.13) highlights the fact that all relative closed orbits of the deputy around the chief could be projected as a 2:1 ellipse on the $\hat{\boldsymbol{r}}\hat{\boldsymbol{s}}$ plane. On the other hand, the cross-track motion can be described as an harmonic oscillator with period equal to the orbital period of the orbit of the chief. Through out the presentation, the notation PRO($\rho_r \times 2\rho_r \times \rho_w - \rho_s$) is applied to define the PRO geometry. The phase and amplitude parameters appearing in equation (2.2.13), are all functions of the initial conditions of the system, so that there is a direct mapping between orbit parameters and initial

conditions

$$\begin{aligned}\rho_r &= \frac{\sqrt{\delta v_r^2(t_0) + \delta r^2(t_0)\omega_w^2}}{\omega_w} \\ \rho_s &= [\delta s(t_0) - 2\delta v_r(t_0)/\omega_w] \\ \rho_w &= \frac{\sqrt{\delta v_w^2(t_0) + \delta w^2(t_0)\omega_w^2}}{\omega_w} \\ \alpha_r &= tan^{-1}\left(\frac{\omega_w\ \delta r(t_0)}{\delta v_r(t_0)}\right) \\ \alpha_w &= tan^{-1}\left(\frac{\omega_w\ \delta w(t_0)}{\delta v_w(t_0)}\right)\end{aligned} \tag{2.2.14}$$

Eventually the discrete model of the continuous linear time-invariant system in (2.2.10) is given by

$$\delta \boldsymbol{x}(k+1) = A_d \delta \boldsymbol{x}(k) + B_d \boldsymbol{u}_{dep}(k) \tag{2.2.15}$$

Where the matrices A_d and B_d are defined as

$$A_d = \begin{bmatrix} 4-3c_{\Delta\omega} & 0 & 0 & \frac{1}{\omega_w}s_{\Delta\omega} & \frac{2}{\omega_w}(1-c_{\Delta\omega}) & 0 \\ 6(s_{\Delta\omega}-(\Delta\omega)) & 1 & 0 & -\frac{2}{\omega_w}(1-c_{\Delta\omega}) & \frac{1}{\omega_w}(4s_{\Delta\omega}-3\Delta\omega) & 0 \\ 0 & 0 & c_{\Delta\omega} & 0 & 0 & \frac{1}{\omega_w}s_{\Delta\omega} \\ 3\omega_w s_{\Delta\omega} & 0 & 0 & c_{\Delta\omega} & 2s_{\Delta\omega} & 0 \\ -6\omega_w(1-c_{\Delta\omega}) & 0 & 0 & -2s_{\Delta\omega} & 4c_{\Delta\omega}-3 & 0 \\ 0 & 0 & -\omega_w s_{\Delta\omega} & 0 & 0 & c_{\Delta\omega} \end{bmatrix}$$

$$B_d = \begin{bmatrix} \frac{1}{\omega_w^2}(1-c_{\Delta\omega}) & \frac{2}{\omega_w^2}((\Delta\omega)-s_{\Delta\omega}) & 0 \\ -\frac{2}{\omega_w^2}((\Delta\omega)-s_{\Delta\omega}) & \frac{4}{\omega_w^2}(1-c_{\Delta\omega})-\frac{3}{2}\Delta t^2 & 0 \\ 0 & 0 & \frac{1}{\omega_w^2}(1-c_{\Delta\omega}) \\ \frac{1}{\omega_w}s_{\Delta\omega} & \frac{2}{\omega_w}(1-c_{\Delta\omega}) & 0 \\ -\frac{2}{\omega_w}(1-c_{\Delta\omega}) & \frac{4}{\omega_w}s_{\Delta\omega}-3\Delta t & 0 \\ 0 & 0 & \frac{1}{\omega_w}s_{\Delta\omega} \end{bmatrix} \tag{2.2.16}$$

The short hand notation $\Delta\omega$ is used to denote the angle $\omega_w \Delta t$.

2.3 Model Predictive Control

Model Predictive Control is an *optimal* control technique based on the *on-line* solution of a finite horizon optimal control Finite Horizon Optimal Control (FHOC) problem. Its superiority to the more classical control strategies like

Linear Quadratic Regulator (LQR) regulator and PID controllers stems from the possibility of defining input and output constraints that are easily inserted in the FOCH problem formulation. Thank to the recent developments in hardware capabilities, it is nowadays possible to solve optimization problems within a fraction of a second, which makes MPC particularly appealing for space systems applications, where fuel and energy consumption are of critical importance. The reader is referred to [19] for a thorough introduction to the history and applications of MPC control while in the following section only the fundamental aspects of sample data MPC control are briefly revised and applied to the deputy dynamics presented in Section 2.2.

2.3.1 Preliminary notation

In the coming presentation, the notation $k\Delta t$ denotes a discrete time instant, where $k \in \mathbb{N}$ defines a finite number of time steps from an initial time t_0 and $\Delta t > 0$ denotes a positive finite sampling interval*. The set $\mathcal{T}_k$ is applied to denote the continuous time interval in between two time steps as

$$\mathcal{T}_k = \{t : t \in [k\Delta t, (k+1)\Delta t]\} \tag{2.3.1}$$

Furthermore the notation $a(i\Delta t|k\Delta t)\ \forall i \in 0 \dots N$ is applied to indicate the value of a at $i-$ steps ahead relative to time step $k\Delta t$. The perturbed and unperturbed dynamics of the deputy relative to the chief are recalled here from (2.2.8),

$$\delta\dot{\boldsymbol{x}} = \boldsymbol{f}(\delta\boldsymbol{x}(t), \boldsymbol{b}(t)) + g(\delta\boldsymbol{x}(t), \boldsymbol{b}(t))\boldsymbol{u}(t) \tag{2.3.2}$$

$$\delta\dot{\tilde{\boldsymbol{x}}} = \boldsymbol{f}(\delta\tilde{\boldsymbol{x}}(t), \tilde{\boldsymbol{b}}(t)) + g(\delta\tilde{\boldsymbol{x}}(t), \tilde{\boldsymbol{b}}(t))(\boldsymbol{u}(t) + \delta\boldsymbol{d}(t)) \tag{2.3.3}$$

Where $\delta\boldsymbol{x} \in \mathcal{X} \subseteq \mathbb{R}^6$ is the nominal relative state of the deputy, $\boldsymbol{b} \in \mathcal{B} \subseteq \mathbb{R}^6$ is the nominal implicit orbital elements vector of the chief, $\delta\boldsymbol{d} \in \mathbb{R}^3$ is the relative orbital perturbations vector and $\boldsymbol{u} \in \mathcal{U} \subseteq \mathbb{R}^3$ is the control input deriving from the propulsion system of the deputy. The variables $\delta\tilde{\boldsymbol{x}}$ and $\tilde{\boldsymbol{b}}$ are used to distinguish between the perturbed and unperturbed system dynamics such that $\delta\tilde{\boldsymbol{x}} \in \tilde{\mathcal{X}} \subseteq \mathbb{R}^6$ is the perturbed relative state of the deputy, and $\tilde{\boldsymbol{b}} \in \tilde{\mathcal{B}} \subseteq \mathbb{R}^6$ is the perturbed implicit keplerian state vector. It is assumed that $\tilde{\mathcal{X}}$, $\mathcal{X}$ and $\mathcal{U}$ are all compact sets containing the origin. Next, the sample time version of the dynamics in equation (2.3.2) and (2.3.3) is obtained through

*$\mathbb{N}$ denotes all natural numbers including zero

a Runge-Kutta integration scheme under *Zero-Order Hold* control such that $\boldsymbol{u}(t) = \boldsymbol{u}(k\Delta t)\ \forall t \in \mathcal{T}_k$

$$\delta\boldsymbol{x}((k+1)\Delta t) = \boldsymbol{F}(\delta\boldsymbol{x}(k\Delta t), \boldsymbol{b}(k\Delta t), \boldsymbol{u}(k\Delta t)) \tag{2.3.4}$$

$$\delta\tilde{\boldsymbol{x}}((k+1)\Delta t) = \boldsymbol{F}(\delta\tilde{\boldsymbol{x}}(k\Delta t), \tilde{\boldsymbol{b}}(k\Delta t), \boldsymbol{u}(k\Delta t) + \delta\boldsymbol{d}(k\Delta t)) \tag{2.3.5}$$

A nominal reference trajectory for the deputy state is additionally defined as $\delta\boldsymbol{x}_r(t) \in \mathcal{X}_r \subseteq \mathcal{X}$ together with its corresponding reference input trajectory $\boldsymbol{u}_r(t) \in \mathcal{U}_r \subseteq \mathcal{U}$ such that

$$\delta\boldsymbol{x}_r((k+1)\Delta t) = \boldsymbol{F}(\delta\boldsymbol{x}_r(k\Delta t), \boldsymbol{b}(k\Delta t), \boldsymbol{u}_r(k\Delta t))$$

It is assumed that $\delta\boldsymbol{x}_r(t)$ is a continuously differentiable function of time. The discrete time state errors with respect to the reference trajectory for the perturbed and unperturbed dynamics are defined as

$$\begin{aligned} \boldsymbol{e}_{\delta\boldsymbol{x}}(k\Delta t) &= \delta\boldsymbol{x}(k\Delta t) - \delta\boldsymbol{x}_r(k\Delta t) \\ \tilde{\boldsymbol{e}}_{\delta\boldsymbol{x}}(k\Delta t) &= \delta\tilde{\boldsymbol{x}}(k\Delta t) - \delta\boldsymbol{x}_r(k\Delta t) \end{aligned} \tag{2.3.6}$$

and the corresponding input error is defined as

$$\boldsymbol{e}_{\boldsymbol{u}}(k\Delta t) = \boldsymbol{u}(k\Delta t) - \boldsymbol{u}_r(k\Delta t) \tag{2.3.7}$$

2.3.2 Sample data MPC control

Consider a state and input reference trajectories $\delta\boldsymbol{x}_r(t)$, $\boldsymbol{u}_r(t)$ as defined in Section 2.3.1. It is desired to steer the perturbed state $\delta\tilde{\boldsymbol{x}}(t)$ toward the reference trajectory $\delta\boldsymbol{x}_r(t)$ by only knowing the nominal discrete dynamics (2.3.4). Given an integer number of *prediction steps* $N \in \mathbb{N}\setminus\{0\}$ and given an initial perturbed state error $\tilde{\boldsymbol{e}}_{\delta\boldsymbol{x}}(k\Delta t)$ at time $k\Delta t$, this objective is formalised by a scalar function $V_N : \mathcal{X} \times \mathcal{U}^N \to \mathbb{R}_{\geq 0}$ referred as the *value function* and formally defined as

$$\begin{aligned} V_N(\boldsymbol{e}_{\delta\boldsymbol{x}}(k\Delta t), \bar{\boldsymbol{u}}(k\Delta t)) := \sum_{i=0}^{N-1} \boldsymbol{e}_{\delta\boldsymbol{x}}^T(i\Delta t|k\Delta t) Q \boldsymbol{e}_{\delta\boldsymbol{x}}(i\Delta t|k\Delta t) + \\ + \boldsymbol{e}_{\boldsymbol{u}}^T(i\Delta t|k\Delta t) R \boldsymbol{e}_{\boldsymbol{u}}(i\Delta t|k\Delta t) + V_f(\boldsymbol{e}_{\delta\boldsymbol{x}}(N\Delta t|k\Delta t)) \end{aligned} \tag{2.3.8}$$

Where the notation $\bar{\boldsymbol{u}}(k\Delta t) \in \mathcal{U}^N$ is used to define an N-steps control sequence as

$$\bar{\boldsymbol{u}}(k\Delta t) = \left[\boldsymbol{u}(0|k\Delta t), \boldsymbol{u}(\Delta t|k\Delta t), ...\boldsymbol{u}((N-1)\Delta t|k\Delta t)\right]$$

The matrices R and Q in equation (2.3.8) are both positive definite matrices and commonly defined as the *control cost* matrix and the *state cost* matrix respectively. The function $V_f : \mathcal{X} \rightarrow \mathbb{R}_{\geq 0}$ is referred as the terminal cost, which penalises the final nominal state error and it is also a positive definite convex function. It is noted that V_N mathematically formalises a cost that decreases as the input and state error tend to zero. The MPC sample data controller then solves the following FHOC problem at every sample time $k\Delta t$ when a new state measurement is available

$$\min_{\bar{\boldsymbol{u}} \in \mathcal{U}^N} \quad V_N(\boldsymbol{e}_{\delta \boldsymbol{x}}(k\Delta t), \bar{\boldsymbol{u}}(k\Delta t)) \tag{2.3.9a}$$

$$\delta \boldsymbol{x}(0|k\Delta t) = \delta \tilde{\boldsymbol{x}}(k\Delta t) \tag{2.3.9b}$$

$$\delta \boldsymbol{x}((i+1)\Delta t|k\Delta t) = \boldsymbol{F}(\delta \boldsymbol{x}(i\Delta t|k\Delta t), \boldsymbol{b}(i\Delta|k\Delta t), \boldsymbol{u}(i\Delta t|k\Delta t)) \quad \forall i \in [0, 1..N-1] \tag{2.3.9c}$$

$$\boldsymbol{u}(i\Delta t|k\Delta t) \in \mathcal{U} \qquad \forall i \in [0, 1, ..N-1] \tag{2.3.9d}$$

$$\delta \boldsymbol{x}(i\Delta t|k\Delta t) \in \mathcal{X} \qquad \forall i \in [0, 1, ..N-1] \tag{2.3.9e}$$

$$\delta \boldsymbol{x}(N\Delta t|k\Delta t) \in \mathcal{X}_f \subseteq \mathcal{X} \qquad \forall i \in [0, 1, ..N-1] \tag{2.3.9f}$$

Where equation (2.3.9b) specifies that the initial predicted state must be equal to the measured state at time step $k\Delta t$ and equation (2.3.9c) specifies that the nominal state must evolve following the discrete nominal dynamics in equation (2.3.4). On the other hand, equation (2.3.9d) and equation (2.3.9e) specify that the control input and state must remain inside the admissible control and state sets respectively while (2.3.9f) constraints the final predicted state to be inside a subset of the nominal state set. The solution to (2.3.9) is a an optimal control sequence $\bar{\boldsymbol{u}}^*(k\Delta t)$ and an optimal predicted nominal state trajectory which minimises the value function V_N at time step $k\Delta t$. It is noted that due to the effect of the perturbations, the predicted nominal state trajectory predicted from the MPC solution will not correspond to the perturbed real state trajectory. For this reason, only the first optimal control input $\boldsymbol{u}^*(0|(k\Delta t))$ is applied to the system in equation (2.3.4) in a *Zero-Order* hold fashion such that $\boldsymbol{u}(t) = \boldsymbol{u}^*(0|(k\Delta t)) \; \forall t \in \mathcal{T}_k$. At the next time step, the optimal control

problem (2.3.9) is solved again and the process is repeated recursively so that a feedback law $K_k(\tilde{\boldsymbol{e}}_{\delta\boldsymbol{x}}(k\Delta t), k\Delta t) := \boldsymbol{u}^*(0|(k\Delta t))$ is obtained. Note that $\tilde{\boldsymbol{e}}_{\delta\boldsymbol{x}}$ was introduced in the feedback law as at time $k\Delta t$ the condition $\tilde{\boldsymbol{e}}_{\delta\boldsymbol{x}} = \boldsymbol{e}_{\delta\boldsymbol{x}}$ is enforced by equation (2.3.9b). Due to the nonlinear dynamics constraint, the FOCH problem (2.3.9) is a non-convex optimisation problem whose solution can only be guaranteed to be *locally* optimal and not *globally* optimal solution.

2.3.3 Stability and Feasibility

A well known problem when dealing with MPC control involves the assessment of the stability of the system under the optimal feedback control law $K_k(\tilde{\boldsymbol{e}}_{\delta\boldsymbol{x}}(k\Delta t), k\Delta t)$ and the feasibility of the FHOC problem (2.3.9) at every time step. Indeed, the fact that $K_k(\tilde{\boldsymbol{e}}_{\delta\boldsymbol{x}}(k\Delta t), k\Delta t)$ is the optimal solution to (2.3.9) does not mean that it is also a stabilising control law for the perturbed system dynamics (see for example the discussion given in [[20],Chapter 1.3.4]). Concerning recursive feasibility, the problem is addressed by defining a terminal set $\mathcal{X}_f$ that is a control invariant set, meaning that for every $\delta\tilde{\boldsymbol{x}} \in \mathcal{X}_f$, it exist a valid control feedback input $K_k(\tilde{\boldsymbol{e}}_{\delta\boldsymbol{x}}(k\Delta t), k\Delta t) \in \mathcal{U}$ such that $\delta\tilde{\boldsymbol{x}}((i+1)\Delta t|k\Delta t) = \boldsymbol{F}(\delta\tilde{\boldsymbol{x}}(i\Delta t|k\Delta t), \tilde{\boldsymbol{b}}(i\Delta|k\Delta t), K_k(\tilde{\boldsymbol{e}}_{\delta\boldsymbol{x}}(k\Delta t), k\Delta t)) \in \mathcal{X}_f$. This conditions guarantees that the MPC controller has at least one feasible solution for every state inside the terminal set that keeps the system inside the terminal set, which then ensures recursive feasibility of the controller [21]. For nonlinear systems, a terminal set is commonly found as follows. First the nonlinear system is linearised around the reference trajectory and a suitable stabilising linear feedback $u(k) = K\tilde{\boldsymbol{e}}(k)$ is found through classic linear control methods (often LQR feedback). Second, a suitable terminal set $\mathcal{X}_f \subseteq \tilde{\mathcal{X}}$ is found considering that $K\tilde{\boldsymbol{e}}_{\delta\boldsymbol{x}}(k) \in \mathcal{U} \quad \forall\delta\tilde{\boldsymbol{x}} \in \mathcal{X}_f$. Concerning stability, this property is normally achieved by ensuring that V_f is a control Lyapunov function within the terminal set. Both these properties are analysed specifically for the deputy dynamics in Chapter 4. The reader is referred to [21] for a deeper analysis of stability and feasibility issues in MCP control.

Chapter 3

Control Barrier Functions for sample data system

In the previous Chapter, the relative dynamics of a deputy around the chief was revised together with the fundamental aspects of MPC control. However, the concept of *safety* was not addressed so far. In most *real* world applications, it is necessary to ensure that the controlled dynamical system remains within a certain *safe* subset of the full state-space. The notion of safety varies from case to case since different constraints apply to different systems. For example, it may be desirable to avoid regions of the state-space where the system is excessively close to an obstacle or where the controller is known to become unstable. In the past few years, the concept of *Control Barrier Function* (CBF) has been developed as suitable framework to analytically define invariant subsets of the state space where the system is allowed to move freely while being safe based on a predefined notion of safety [5]. In the coming subsections, the fundamental theoretical aspects of *Control Barrier Functions* for continuous time and sample data systems are revised. It is noted that for the sake of generality, this section will not be directly specialised to the deputy dynamics, but for a general nonlinear dynamics with the same properties of the deputy dynamics. The results presented here will be then specialised to the deputy dynamics in Section 4.

3.1 Continuous time Control Barrier Functions

A general *control affine* dynamical systems is defined as

$$\dot{\boldsymbol{x}}(t) = \boldsymbol{f}(\boldsymbol{x}(t), t) + \boldsymbol{g}(\boldsymbol{x}(t), t)\boldsymbol{u}(t) \tag{3.1.1}$$

Where $t \in \mathcal{I} \subseteq \mathbb{R}_{\geq 0}$ represents the time, $\boldsymbol{x}(t) \in \mathcal{X} \subseteq \mathbb{R}^n$ defines the state trajectory of the system to be controlled and $\boldsymbol{u}(t) \in \mathcal{U} \subseteq \mathbb{R}^m$ defines the control input. It is assumed that $\mathcal{X}$, $\mathcal{U}$ and $\mathcal{I}$* are all compact and convex sets containing the origin. The functions $\boldsymbol{g} : \mathbb{R}^n \times \mathbb{R}_{\geq 0} \to \mathbb{R}^{n \times m}$ and $\boldsymbol{f} : \mathbb{R}^n \times \mathbb{R}_{\geq 0} \to \mathbb{R}^n$ are at least of class C^1 on $\mathcal{X} \times \mathcal{I}$ (The class of functions C^k consists of all the functions that are k times continuously differentiable). It is then desired that the system remains in a possibly time-varying set $\mathcal{C}(t) \subset \mathcal{X}$, denoted as the safe set, where the system state is considered to be safe. This objective is formalised as follows

Definition 1 (Forward invariance [22])**.** *A set $\mathcal{C}(t)$ is defined as forward invariant for a given control law $\boldsymbol{u}(t)$ if for each $\boldsymbol{x}_0 \in \mathcal{C}(t_0)$ there exists a unique solution $\boldsymbol{x}(t) : [t_0, t_1] \to \mathcal{X}$ to equation (3.1.1) with $\boldsymbol{x}(t_0) = \boldsymbol{x}_0$ such that $\boldsymbol{x}(t) \in \mathcal{C}(t)$ for all $t \in [t_0, t_1]$.*

Consider now a continuously differentiable scalar function $h : \mathcal{D} \times \mathcal{I} \to \mathbb{R}$, with $\mathcal{D} \subseteq \mathcal{X}$ being compact, and consider $\mathcal{C}_S(t)$ and $\partial\mathcal{C}_S(t)$ to be the super level set and the border the of the super level set of h, defied as follows

$$\begin{aligned} \mathcal{C}_S(t) &:= \{\boldsymbol{x} \in \mathcal{D} : h(\boldsymbol{x}, t) \geq 0\} \\ \partial\mathcal{C}_S(t) &:= \{\boldsymbol{x} \in \mathcal{D} : h(\boldsymbol{x}, t) = 0\} \end{aligned} \tag{3.1.2}$$

The following definition of CBF is introduced

Definition 2. *(Control Barrier Function [7]) Given a set $\mathcal{C}_S(t)$ defined as in equation (3.1.2) for a continuously differentiable function $h : \mathcal{D} \times \mathcal{I} \to \mathbb{R}$, then $h(\boldsymbol{x}, t)$ is called Control Barrier Function on the set $\mathcal{D}$ with $\mathcal{C}_S(t) \subset \mathcal{D} \subseteq \mathcal{X}$ $\forall t \geq 0$ if there exist a differentiable extended class $\mathcal{K}$-function $\alpha(\cdot)$ such that*

$$\sup_{\boldsymbol{u} \in \mathcal{U}} \left[\frac{\partial h(\boldsymbol{x}, t)}{\partial t} + \mathcal{L}_f h(\boldsymbol{x}, t) + \mathcal{L}_g h(\boldsymbol{x}, t)\boldsymbol{u} + \alpha(h(\boldsymbol{x}, t)) \right] \geq 0 \tag{3.1.3}$$

Where the symbol $\mathcal{L}$ indicates the Lie derivative†. Differently from [7], it is

*It is clear from the context that $\mathcal{I}$ indicates here a real time interval and not an inertial reference frame

†The Lie derivative of a general scalar function h along a vectorial field f is given by $\mathcal{L}_f h(\boldsymbol{x}, t) := \nabla h(\boldsymbol{x}, t)\boldsymbol{f}(\boldsymbol{x}, t)$

assumed that α is differentiable in the current work. The following Lemma from [22] is then sufficient to guarantee that if condition (3.1.3) is respected, then $\mathcal{C}_S(t)$ from (3.1.2) is forward invariant.

Lemma 1 (Lemma 1 in [22]). *Let $\alpha : \mathbb{R}_{\geq 0} \to \mathbb{R}_{\geq 0}$ be a continuous class $\mathcal{K}$-function and $\boldsymbol{\eta} : [t_0, t_1] \to \mathbb{R}$ be an absolutely continuous function. If $\dot{\boldsymbol{\eta}}(t) \geq -\alpha(\boldsymbol{\eta}(t))$ for every $t \in [t_0, t_1]$, and $\boldsymbol{\eta}(t_0) \geq 0$, then $\boldsymbol{\eta}(t) \geq 0$ for all $t \in [t_0, t_1]$*

Given Definition 2, the set of all *safe* control input to system (3.1.1) is defined as

$$\mathcal{U}_S(\boldsymbol{x}) = \{\boldsymbol{u} \in \mathcal{U} : \frac{\partial h(\boldsymbol{x}, t)}{\partial t} + L_f h(\boldsymbol{x}, t) + L_g h(\boldsymbol{x}, t)\boldsymbol{u}(t) + \alpha(h(\boldsymbol{x}, t)) \geq 0 \, \forall t \geq 0\}$$

If it is possible to guarantee that $\mathcal{U}_S(\boldsymbol{x}) \cap \mathcal{U} \neq \emptyset \, \forall \boldsymbol{x} \in \mathcal{C}_S(t)$, then h is a valid CBF. Additionally, a valid CBF constraint $\psi(\boldsymbol{x}, \boldsymbol{u}, t) : \mathcal{D} \times \mathcal{U} \times \mathcal{I} \to \mathbb{R}$ is defined as

$$\psi(\boldsymbol{x}, \boldsymbol{u}, t) := \frac{\partial h(\boldsymbol{x}, t)}{\partial t} + \mathcal{L}_f h(\boldsymbol{x}, t) + \mathcal{L}_g h(\boldsymbol{x}, t)\boldsymbol{u}(t) + \alpha(h(\boldsymbol{x}, t)) \quad (3.1.4)$$

and safety is ensured by enforcing the condition $\psi(\boldsymbol{x}, \boldsymbol{u}, t) \geq 0$ inside $\mathcal{C}_S(t)$.

3.2 High Order Control Barrier Functions

It often occurs in *real* systems, that the control input does not appear directly in the first time derivative of $h(\boldsymbol{x}, t)$ due to the fact that $\mathcal{L}_g h(\boldsymbol{x}, t)$ is identically zero. As an example from [23], it is considered a simplified one dimensional car model

$$\begin{bmatrix} \dot{x}_1 \\ \dot{x}_2 \end{bmatrix} = \begin{bmatrix} x_2 \\ 0 \end{bmatrix} + \begin{bmatrix} 0 \\ u \end{bmatrix} \quad (3.2.1)$$

Here x_1 could be thought as the position while x_2 could be though as the velocity. Eventually u is the acceleration imposed on the car. Any CBF for which only x_1 appears explicitly in the definition of $h(\boldsymbol{x}, t)$ will not have the control u as argument of $\dot{h}(\boldsymbol{x}, t)$. Although, it could still be desired to define a safe set in terms of *safe* positions of the car. This motivates the definition of an *High Order Barrier Function* (HOCBF) as solution to this problem. First,

the definition of *relative degree* is given

Definition 3 (Definition 5 in [23])**.** *The relative degree of a continuously differentiable function* $h : \mathbb{R}^n \times \mathbb{R}_{\geq 0} \to \mathbb{R}$ *with respect to system equation* (3.1.1) *is the number of times it is needed to differentiate it along the dynamics of equation* (3.1.1) *until control* $\boldsymbol{u}$ *explicitly shows.*

In the case $h(\boldsymbol{x}, t)$ is of *relative-degree r* for system (3.1.1), it is still possible to guarantee safety within the $\mathcal{C}_S(t)$, but at price of reducing the size of $\mathcal{C}_S(t)$. Based on the work developed in [23], an HOCBF is defined starting from the nominal CBF as follows. Given $h(\boldsymbol{x}, t) : \mathcal{D} \times \mathcal{I}$ is a CBF for system equation (3.1.1), a cascade of functions $H_i : \mathcal{D} \times \mathcal{I} \to \mathbb{R}$ is defined

$$\begin{aligned} H_0(\boldsymbol{x}, t) &= h(\boldsymbol{x}, t) \\ H_1(\boldsymbol{x}, t) &= \dot{H}_0(\boldsymbol{x}, t) + \alpha_0(H_0) \\ H_2(\boldsymbol{x}, t) &= \dot{H}_1(\boldsymbol{x}, t) + \alpha_1(H_1) \\ &.... \\ H_{r-1}(\boldsymbol{x}, t) &= \dot{H}_{r-2}(\boldsymbol{x}, t) + \alpha_{r-2}(H_{r-2}) \end{aligned} \tag{3.2.2}$$

Where $\alpha_i(t) : \mathbb{R}_{\geq 0} \to \mathbb{R}_{\geq 0} \, \forall \, i = 0, \dots r-2$ are class $\mathcal{K}$-functions such that α_i is of class C^{r-i}. In addition, a safe set for every H_i is defined as

$$\begin{aligned} \mathcal{C}_{S0}(t) &= \{\boldsymbol{x} \in \mathcal{D} : H_0 \geq 0\} \\ \mathcal{C}_{S1}(t) &= \{\boldsymbol{x} \in \mathcal{D} : H_1 \geq 0\} \\ \mathcal{C}_{S2}(t) &= \{\boldsymbol{x} \in \mathcal{D} : H_2 \geq 0\} \\ &.... \\ \mathcal{C}_{S(r-1)}(t) &= \{\boldsymbol{x} \in \mathcal{D} : H_{r-2} \geq 0\} \end{aligned} \tag{3.2.3}$$

From the definition of the cascade of functions H_i and the cascade of safe sets $\mathcal{C}_{Si}$ the definition of HOCBF is given as follows

Definition 4 (modified from Definition 6 in [23])**.** *Let* $H_i \; \forall i = 0, \dots r-1$ *be defined as in equation* (3.2.2) *and let* $\mathcal{C}_{Si} \; \forall i = 0, \dots r-1$ *be defined as in equation* (3.2.3)*. The function* $h(\boldsymbol{x}, t) : \mathcal{D} \times \mathcal{I} \to \mathbb{R}$ *is a High Order Barrier Functions (HOCBF) for system equation* (3.1.1) *if it is* $r-1$ *times differentiable in* $\boldsymbol{x}$ *and* t*, and there exist* $\alpha_i(t) : \mathbb{R}_{\geq 0} \to \mathbb{R}_{\geq 0} \, \forall \, i = 0, \dots r-2$ *class* $\mathcal{K}$*-functions such that* α_i *is of class* C^{r-1} *and*

$$\frac{\partial H_{r-1}(\boldsymbol{x},t)}{\partial t} + \mathcal{L}_f H_{r-1}(\boldsymbol{x},t) + \mathcal{L}_g H_{r-1}(\boldsymbol{x},t)\boldsymbol{u}(t) + \alpha_{r-1}(H_{r-1}(\boldsymbol{x},t)) = \frac{\partial^r h(\boldsymbol{x},t)}{\partial t^r} + \mathcal{L}_f^r h(\boldsymbol{x},t) + \mathcal{L}_g \mathcal{L}_f^{r-1} h(\boldsymbol{x},t)\boldsymbol{u}(t) + O(h(\boldsymbol{x},t)) + \alpha_{r-1}(H_{r-1}(\boldsymbol{x},t)) \geq 0 \ \forall \boldsymbol{x} \in \bigcap_{i=0..r-1} \mathcal{C}_i(t) \tag{3.2.4}$$

Where $O(h(\boldsymbol{x},t))$ denotes the remaining Lie derivatives along $\boldsymbol{f}$ and partial derivatives with degree less than or equal to r−1.

Furthermore the following essential result is reported from [23].

Theorem 1 (Theorem 4 in [23])**.** *The set $\bigcap_{i=0..r-1} \mathcal{C}_{Si}(t)$ is forward invariant for system (3.1.1) if $h(\boldsymbol{x},t)$ is an HOCBF*

Similarly to the definition of CBF constraint, the HOCBF constraint $\zeta(\boldsymbol{x},\boldsymbol{u},t) : \mathcal{D} \times \mathcal{U} \times \mathcal{I} \to \mathbb{R}$ is defined as

$$\zeta(\boldsymbol{x},\boldsymbol{u},t) := \frac{\partial H_{r-1}(\boldsymbol{x},t)}{\partial t} + \mathcal{L}_f H_{r-1}(\boldsymbol{x},t) + \mathcal{L}_g H_{r-1}(\boldsymbol{x},t)\boldsymbol{u} + \alpha_{r-1}(H_{r-1}(\boldsymbol{x},t)) \tag{3.2.5}$$

And forward invariance of the safe set $\bigcap_{i=0..r-1} \mathcal{C}_{Si}(t)$ is enforced by ensuring that the condition $\zeta(\boldsymbol{x},\boldsymbol{u},t) \geq 0$ is met everywhere inside $\bigcap_{i=0..r-1} \mathcal{C}_{Si}(t)$.

Remark. *In this section, smoothness assumptions were made relative to the α functions appearing in the CBF and HOCBF definition. The original definitions present weaker smoothness assumptions that are instead required in the current work.*

3.3 Sample Data Control Barrier Function

For a sample data system, the state of the system is only available at discrete time steps $k\Delta t$. When a *Zero Order Hold* sample data controller is applied, the control is held constant during the sampling intervals $\mathcal{T}_k := [k\Delta t, (k+1)\Delta t]$ such that only the condition $\psi(\boldsymbol{x}(k\Delta t), \boldsymbol{u}(k\Delta t), k\Delta t) \geq 0$ or $\zeta(\boldsymbol{x}(k\Delta t), \boldsymbol{u}(k\Delta t), k\Delta t) \geq 0$ can be satisfied by the controller. Although, these last conditions only ensures safety at time instant $k\Delta t$ but not inside the interval $\mathcal{T}_k$. This problem is further developed in this sections based on the work by [7]. But first it is relevant to recalled that given a general multivariate

function $f : \mathbb{X} \subseteq \mathbb{R}^n \to \mathbb{Y} \subseteq \mathbb{R}^m$ (not to be confused with $\boldsymbol{f}$ from equation (3.1.1)), then f is Lipschitz continuous on $\mathbb{X}$ if

$$||f(x_2) - f(x_1)|| \leq K||x_2 - x_1|| \quad \forall x_1, x_2 \in \mathbb{X} \tag{3.3.1}$$

where $K \geq 0$ is called the Lipschitz constant for f [[24],Def A.1]. The following lemma generalises the CBF constraint definition to the case of sample data control

Lemma 2. *(modified by [7]) Consider the control affine system (3.1.1) where the functions $\boldsymbol{g} : \mathbb{R}^n \times \mathbb{R}_{\geq 0} \to \mathbb{R}^{n\times m}$ and $\boldsymbol{f} : \mathbb{R}^n \times \mathbb{R}_{\geq 0} \to \mathbb{R}^n$ are both continuously differentiable functions of t and $\boldsymbol{x}$ on the set $\mathcal{I} \times \mathcal{X}$. Let a sampling interval $\mathcal{T}_k := [k\Delta t, (k+1)\Delta t] \subset \mathcal{I}$ for some $\Delta t > 0$ such that (3.1.1) is subject to a constant bounded feedback control input $\boldsymbol{u}(t) = \boldsymbol{u}(\boldsymbol{x}(k\Delta t), k\Delta t) \in \mathcal{U}$ $\forall t \in \mathcal{T}_k$ shorthanded as $\boldsymbol{u}(x(k\Delta t))$. Furthermore consider a valid CBF $h : \mathcal{D} \times \mathcal{I} \to \mathbb{R}$ as in Definition 2 that is at least of class C^2 on $\mathcal{D} \times \mathcal{I}$, its associated safe set $\mathcal{C}_S(t) \subset \mathcal{D}$ and the associated continuous and differentiable CBF constraint $\psi : \mathcal{D} \times \mathcal{U} \times \mathcal{I} \to \mathbb{R}$ as defined in (3.1.4). Given that at time instant $k\Delta t$, $\boldsymbol{x}(k\Delta t) \in \mathcal{C}_S(k\Delta t)$ and that the constant feedback control input $\boldsymbol{u}(\boldsymbol{x}(k\Delta t)) \in \mathcal{U}$ respects the condition*

$$\sup_{\boldsymbol{u}\in\mathcal{U}} \quad \psi(\boldsymbol{x}(k\Delta t), \boldsymbol{u}(k\Delta t), k\Delta t) - L\Delta t \geq 0 \tag{3.3.2}$$

Where L is defined as

$$L = \max_{(\boldsymbol{x},\boldsymbol{u},t)\in\mathcal{D}\times\mathcal{U}\times\mathcal{I}} |\dot{\psi}(\boldsymbol{x}, \boldsymbol{u}, t)|$$

then it holds that

$$\boldsymbol{x}(k\Delta t) \in \mathcal{C}_S(k\Delta t) \Rightarrow \boldsymbol{x}(t) \in \mathcal{C}_S(t) \quad \forall t \in \mathcal{T}_k \tag{3.3.3}$$

Proof. Given a constant feedback input $\boldsymbol{u}(\boldsymbol{x}(k\Delta t))$ on the interval $\mathcal{T}_k$, it is known that $\boldsymbol{u}(\boldsymbol{x}(k\Delta t))$ is bounded on $\mathcal{T}_k$ as $\mathcal{U}$ is compact. Since $\boldsymbol{f}$ and $\boldsymbol{g}$ are differentiable on $\mathcal{X}$ and $\mathcal{I}$ and $\boldsymbol{u}(\boldsymbol{x}(k\Delta t))$ is constant, then the solution $\boldsymbol{x}(t)$ to (3.1.1) is uniquely defined on an interval $[k\Delta t, \tau]$ for some $\tau \leq (k+1)\Delta t$ [[25], Thm. 54]. Furthermore, $\boldsymbol{x}(t)$ is C^2 on $\mathcal{X} \times [k\Delta t, \tau]$ [[25],Prop C.3.11]. The CBF constraint $\psi(\boldsymbol{x}, \boldsymbol{u}, t)$ is defined for a constant feedback input as

$$\psi(\boldsymbol{x}, \boldsymbol{u}(\boldsymbol{x}(k\Delta t)), t) = \frac{\partial h(\boldsymbol{x}, t)}{\partial t} + \mathcal{L}_f h(\boldsymbol{x}, t) + \mathcal{L}_g h(\boldsymbol{x}, t)\boldsymbol{u}(\boldsymbol{x}(k\Delta t)) + \alpha(h(\boldsymbol{x}, t))$$

Since $\boldsymbol{f}$, $\boldsymbol{g}$ and α are C^1 in their respective domains and h is C^2, then $\psi(\boldsymbol{x}, \boldsymbol{u}(\boldsymbol{x}(k\Delta t)), t)$ is also C^1 on $\mathcal{X} \times [k\Delta t, \tau]$ as it is the composition of differentiable functions. Moreover, as $\boldsymbol{x}(t)$ is a continous and differentiable function of t in $[k\Delta t, \tau]$ (as pointed out before) and since $\boldsymbol{x}(k\Delta t) \in C(k\Delta t) \subset \mathcal{D}$, then by continuity of $\boldsymbol{x}(t)$ there must be a time $\tau_0 \in [k\Delta t, \tau]$ for which $\boldsymbol{x}(t) \in \mathcal{D}$. By direct application of the *Mean Value Theorem* [[26],Thm.3.4] it is possible to state that there exist a time $t_c \in [k\Delta t, \tau_0]$ such that

$$\psi(\boldsymbol{x}(t_2), \boldsymbol{u}(\boldsymbol{x}(k\Delta t)), t_2) - \psi(\boldsymbol{x}(t_1), \boldsymbol{u}(\boldsymbol{x}(k\Delta t)), t_1) = \frac{\mathrm{d}}{\mathrm{d}t}\psi(\boldsymbol{x}(t_c), \boldsymbol{u}(\boldsymbol{x}(k\Delta t)), t_c)\ (t_2 - t_1) \forall t_1.t_2 \in [k\Delta t, \tau_0] \tag{3.3.4}$$

Where it is recalled that $\frac{\mathrm{d}\psi}{\mathrm{d}t} \triangleq \dot{\psi}(x(t), u(t), t)$ is the *total* time derivative of ψ. The following chain of inequalities is then derived

$$\begin{aligned} &|\psi(\boldsymbol{x}(t_2), \boldsymbol{u}(\boldsymbol{x}(k\Delta t)), t_2) - \psi(\boldsymbol{x}(t_1), \boldsymbol{u}(\boldsymbol{x}(k\Delta t)), t_1)| \leq \\ &\quad |\frac{\mathrm{d}}{\mathrm{d}t}\psi(\boldsymbol{x}(t_c), \boldsymbol{u}(\boldsymbol{x}(k\Delta t)), t_c)|\ |t_2 - t_1| \leq \\ &\underset{(\boldsymbol{x},\boldsymbol{u},t)\in\mathcal{D}\times\mathcal{U}\times\mathcal{I}}{max} |\frac{\mathrm{d}\psi(\boldsymbol{x}, \boldsymbol{u}, t)}{\mathrm{d}t}|\ |t_2 - t_1| = L\ |\Delta t| \forall t_1, t_2 \in [k\Delta t, \tau_0] \end{aligned} \tag{3.3.5}$$

The first inequality is obtained by direct application of the Cauchy-Schwarz inequality theorem on equation (3.3.4), while the second one is obtained by upper bounding the total time derivative of ψ under constant input $\boldsymbol{u}(\boldsymbol{x}(k\Delta t))$. Note that $\underset{(\boldsymbol{x},\boldsymbol{u},t)\in\mathcal{D}\times\mathcal{U}\times\mathcal{I}}{sup} |\frac{\mathrm{d}}{\mathrm{d}t}\psi(\boldsymbol{x}, \boldsymbol{u}, t)|$ is known to exist as ψ is continuously differentiable on a Cartesian product of compact sets, which is also compact [[27],Tychonoff's Theorem]. Next, it is noted from (3.3.5), that the maximum *negative* variation of $\psi(\boldsymbol{x}, \boldsymbol{u}, t)$ over the interval $[k\Delta t, \tau_0]$ is bounded as

$$\psi(\boldsymbol{x}(t_2), \boldsymbol{u}(\boldsymbol{x}(k\Delta t)), t_2) - \psi(\boldsymbol{x}(t_1), \boldsymbol{u}(\boldsymbol{x}(k\Delta t)), t_1) \geq -L\ |\Delta t|\ \forall t_1, t_2 \in [k\Delta t, \tau_0]$$

Replacing t_1 with $k\Delta t$ and adding inequality (3.3.2) to the right and left hand side yields

$$\psi(\boldsymbol{x}(t_2), \boldsymbol{u}(\boldsymbol{x}(k\Delta t)), t_2) \geq 0\ \forall t_2 \in [k\Delta t, \tau_0] \tag{3.3.6}$$

It is then clear that $\psi(\boldsymbol{x}(t), \boldsymbol{u}(\boldsymbol{x}(k\Delta t)), t) = \dot{h}(\boldsymbol{x}, t) + \alpha(h(\boldsymbol{x}, t)) \geq 0\ \forall t \in [k\Delta t, \tau_0]$ which ensures that $\boldsymbol{x}(t) \in \mathcal{C}_S(t) \forall t \in [k\Delta t, \tau_0]$ by Lemma 1. Now it is proved that $\boldsymbol{x}(t) \in \mathcal{C}_S(t)$ for all $t \in [k\Delta t, \tau]$ by contradiction. Suppose instead that for some $\tau_a \in (\tau_0, \tau]$, $\boldsymbol{x}(\tau_a) \in \mathcal{D} \backslash \mathcal{C}_S(t)$ and $\boldsymbol{x}(t) \in \mathcal{D}$ for all $t \in [k\Delta t, \tau_a]$ (i.e., the solution has left $\mathcal{C}_S(t)$, but not $\mathcal{D}$). Then

$\boldsymbol{x}(t)$ must leave $\mathcal{C}_S(t)$ at some $t < \tau_a$. Furthermore, since the closed-loop dynamics are differentiable on $\mathcal{D}$, $\boldsymbol{x}(t)$ is uniquely defined on $[k\Delta t, \tau_a]$ (this is shown by repeatedly applying [[25], Thm. 54] since $\boldsymbol{x}(t)$ remains in $\mathcal{D}$ over which local differentiability of the closed-loop dynamics holds). To leave $\mathcal{C}_S(t), \dot{h}(\boldsymbol{x}, t) < 0$ must hold on $\partial\mathcal{C}_S(t)$. The maximum negative variation of $\psi(\boldsymbol{x}(t), \boldsymbol{u}(\boldsymbol{x}(k\Delta t)), t)$ is then recomputed over the interval $[k\Delta t, \tau_a]$ and it is obtained again that $\psi(\boldsymbol{x}(t), \boldsymbol{u}(\boldsymbol{x}(k\Delta t)), t) \geq 0 \forall t \in [k\Delta t, \tau_a]$ as L is independent from τ_a as it is from τ_0. Therefore we see that $\dot{h}(\boldsymbol{x}, t) \geq 0$ holds for any $\boldsymbol{x}(t) \in \mathcal{C}(t), t \in [k\Delta t, \tau_a]$. Hence, the contradiction is reached, and so $\boldsymbol{x}(t)$ can never leave $\mathcal{C}(t)$ (and $\mathcal{D}$) on $t \in [k\Delta t, \tau]$. Since it was showed that $\boldsymbol{x}(t)$ remains in a compact subset on the interval $[k\Delta t, \tau]$ (namely $\mathcal{D}$), then $\boldsymbol{x}(t)$ exist and is unique over the whole interval $[k\Delta t, (k+1)\Delta t]$ [[25],Prop. C.3.6]. By the same arguments applied for the previous sub intervals , it is proved again that $\psi(\boldsymbol{x}(t), \boldsymbol{u}(\boldsymbol{x}(k\Delta t)), t) \geq 0 \ \forall t \in [k\Delta t, (k+1)\Delta t]$ which ensures that $\boldsymbol{x}(t) \in \mathcal{C}_S(t) \forall t \in [k\Delta t, (k+1)\Delta t]$ by Lemma 1. □

Following the result from Lemma 2, the definition of sample data CBF (SD-CBF) follows

Definition 5 (SD-CBF modified from [7])**.** *Consider the system* (3.1.1) *and a continuously differentiable function* $h : \mathcal{D} \times \mathcal{I} \to \mathbb{R}$*, the associated safe set* $\mathcal{C}_S(t) \subset \mathcal{D}$ *for all* $t \geq 0$ *as defined in* (3.1.2)*. The function* h *is a Sample Data Control Barrier Function (SD-CBF) if for a given* $\Delta t > 0$ *there exists a differentiable extended class- $\mathcal{K}$ function* α*, where* $\alpha \circ h : \mathcal{D} \times \mathcal{I} \to \mathbb{R}$ *is differentiable on* $\mathcal{D} \times \mathcal{I}$*, such that for any point* $\boldsymbol{x} \in \mathcal{D}$ *and* $k \in \mathbb{N}_0$ *there is a constant feedback input* $\boldsymbol{u}(\boldsymbol{x}(k\Delta t), k\Delta t) \in \mathcal{U}$*, shortened to* $\boldsymbol{u}(k\Delta t)$*, satisfying the condition:*

$$\mathcal{L}_f h(\boldsymbol{x}(k\Delta t), k\Delta t) + \mathcal{L}_g h(\boldsymbol{x}(k\Delta t), k\Delta t) u(k\Delta t) + \alpha(h(\tilde{\boldsymbol{x}}, k\Delta t)) \geq L\Delta t$$

where L *is a valid Lipschitz constant as defined in Lemma 2*

The set of safe control inputs $\mathcal{U}_S$ for a given time step Δt is defined by

$$\mathcal{U}_S(\boldsymbol{x}, \Delta t) = \{\boldsymbol{u} \in \mathcal{U} : \frac{\partial h(\boldsymbol{x}, t)}{\partial t} + \mathcal{L}_f h(\boldsymbol{x}, t) + \mathcal{L}_g h(\boldsymbol{x}, t)\boldsymbol{u} + \alpha(h(\boldsymbol{x}, t)) - L\Delta t \geq 0\}$$

It is worth noting that the constant L is a valid Lipschitz constant for the CBF constraint ψ as it respects condition (3.3.1), and L is a function of the

maximum allowed control $\|\boldsymbol{u}\|_+$, where $\|\boldsymbol{u}\|_+$ is defined as

$$\|\boldsymbol{u}\|_+ = \max_{\boldsymbol{u}\in\mathcal{U}} \|\boldsymbol{u}\|$$

Note that differently from [7], the effect of perturbations on the dynamics (3.1.1) are not yet introduced in the definition of SD-CBF. In Section 3.4, robustness to input perturbations is further analysed. Now that the notion of SD-CBF is formally defined , the following theorem is presented in order to to expand the safety conditions for continuous time HOCBF to sample data systems

Lemma 3. *Consider the control affine system (3.1.1) where the functions $\boldsymbol{g} : \mathbb{R}^n \times \mathbb{R}_{\geq 0} \to \mathbb{R}^{n\times m}$ and $\boldsymbol{f} : \mathbb{R}^n \times \mathbb{R}_{\geq 0} \to \mathbb{R}^n$ are both continuously differentiable functions of time $t \in \mathcal{I} \subset \mathbb{R}_{\geq 0}$ and state $\boldsymbol{x} \in \mathcal{X} \subset \mathcal{R}^n$. Define a sampling interval $\mathcal{T}_k := [k\Delta t, (k+1)\Delta t] \subset \mathcal{I}$ for some $\Delta t > 0$ such that (3.1.1) is subject to a constant bounded feedback control input $\boldsymbol{u}(t) = \boldsymbol{u}(\boldsymbol{x}(k\Delta t), k\Delta t) \in \mathcal{U}\ \forall t \in \mathcal{T}_k$ shorthanded as $\boldsymbol{u}(x(k\Delta t))$. Furthermore consider a valid HOCBF $h : \mathcal{D} \times \mathcal{I} \to \mathbb{R}$ of relative degree r as in Definition 4 that is at least C^{r+1} on $\boldsymbol{x}$ and t, the associated class-$\mathcal{K}$ functions $\alpha_i \forall i = 0, \dots r-2$ such that each α_i is at least C^{r-i}. Also consider the cascade of safe sets $\bigcap_{i=0..r-1} \mathcal{C}_{Si}(t) \subset \mathcal{D}$ where $\mathcal{C}_{Si}(t)$ are defined in (3.2.3), and the continuous and differentiable HOCBF constraint $\zeta(\boldsymbol{x}, \boldsymbol{u}, t) : \mathcal{D}\times\mathcal{U}\times\mathcal{I} \to \mathbb{R}$ as defined in (3.2.5). Given that at time instant $k\Delta t$, $\boldsymbol{x}(k\Delta t) \in \mathcal{C}_S(k\Delta t)$ and that the constant feedback control input $\boldsymbol{u}(\boldsymbol{x}(k\Delta t)) \in \mathcal{U}$ respects the condition*

$$\sup_{\boldsymbol{u}\in\mathcal{U}} \zeta(\boldsymbol{x}(k\Delta t), \boldsymbol{u}(\boldsymbol{x}(k\Delta t)), k\Delta t) - L\Delta t \geq 0 \tag{3.3.7}$$

Where L is defined as

$$L = \max_{(\boldsymbol{x},\boldsymbol{u},t)\in\mathcal{D}\times\mathcal{U}\times\mathcal{I}} |\dot{\zeta}(\boldsymbol{x}, \boldsymbol{u}, t)|$$

then it holds that

$$\boldsymbol{x}(k\Delta t) \in \bigcap_{i=0..r-1} \mathcal{C}_{Si}(k\Delta t) \Rightarrow \boldsymbol{x}(t) \in \bigcap_{i=0..r-1} \mathcal{C}_{Si}(t) \quad \forall t \in \mathcal{T}_k \tag{3.3.8}$$

Proof. The proof is analogous to the the proof of Lemma 2 where the safe set $\mathcal{C}_S(t)$ is replaced by $\bigcap_{i=0..r-1} \mathcal{C}_{Si}(t)$, the CBF constraint $\psi(\boldsymbol{x}, \boldsymbol{u}, t)$ is replaced by the HOCBF constraint $\zeta(\boldsymbol{x}, \boldsymbol{u}, t)$ and $h(\boldsymbol{x}, t)$ is replaced by $H_{r-1}(\boldsymbol{x}, t)$. It is noted that the requirement on the smoothness of the class-$\mathcal{K}$ functions α_i is

required so that $\zeta(\boldsymbol{x}, \boldsymbol{u}, t)$ is a differentiable function on $\mathcal{X} \times \mathcal{U} \times \mathcal{I}$. □

The definition of Sample Data High Order Control Barrier Function (SD-HOCBF) is then introduced similarly to the definition of SD-CBF

Definition 6 (SD-HOCBF)**.** *Consider the system* (3.1.1) *and a continuously differentiable function* $h : \mathcal{D} \times \mathcal{I} \to \mathbb{R}$*, the associated safe set* $\mathcal{C}_S(t) \subset \mathcal{D}$ *for all* $t \geq 0$ *as defined in* (3.1.2) *and consider* r *to be equal to the relative degree of* h *with respect to the dynamics in* (3.1.1)*. The function* h *is a SD-HOCBF for a given* $\Delta t > 0$ *if (1) there exist a set of differentiable extended class* $\mathcal{K}$ *function* $\alpha_i \, \forall i \in 0..r-1$ *as defined in Definition 4 (2) there exists a set of function* $H_i \forall i = 1, ..r-1$ *with the properties defined in Definition 4, (3) for any point* $\boldsymbol{x} \in \mathcal{D}$ *and* $k \in \mathbb{N}_0$ *there is a constant feedback input* $\boldsymbol{u}(\boldsymbol{x}(k\Delta t), k\Delta t) \in \mathcal{U}$*, shortened to* $\boldsymbol{u}(k\Delta t)$*, satisfying the condition:*

$$\frac{\partial H_{r-1}(\tilde{\boldsymbol{x}}, t)}{\partial t} + \mathcal{L}_f H_{r-1}(\tilde{\boldsymbol{x}}, t) + \mathcal{L}_g H_{r-1}(\tilde{\boldsymbol{x}}, t)(\boldsymbol{u} + \boldsymbol{w}) + \alpha_{r-1}(H_{r-1}(\tilde{\boldsymbol{x}}, t)) \geq L\Delta t$$

Where is L is a valid Lipschitz constant as defined in Lemma 3

3.4 Robust SD-CBF and SD-HOCBF

In this section, the notion of SD-CBF and SD-HOCBF is extended to the class of control affine systems subject to input disturbances. Consider the disturbed control affine system

$$\dot{\tilde{\boldsymbol{x}}} = \boldsymbol{f}(\tilde{\boldsymbol{x}}, t) + \boldsymbol{g}(\tilde{\boldsymbol{x}}, t)(\boldsymbol{u}(t) + \boldsymbol{w}(t)) \tag{3.4.1}$$

Where $\tilde{\boldsymbol{x}} \in \tilde{\mathcal{X}} \subseteq \mathbb{R}^n$ while $\boldsymbol{u} \in \mathcal{U}$ and $t \in \mathcal{I} \in \mathbb{R}_{\geq 0}$ are again the control input and time. Note that $\tilde{\mathcal{X}}$ is considered to be a compact and convex as $\mathcal{X}$. The functions $\boldsymbol{f}$ and $\boldsymbol{g}$ are considered to have the same properties as system (3.1.1) on the set $\tilde{\mathcal{X}}$. On the other hand, $\boldsymbol{w}(t) \in \mathcal{W} \subseteq \mathbb{R}^m$ is a bounded unknown input disturbance which is assumed to be *piece-wise differentiable* on a compact and convex set $\mathcal{W}$. The symbol $\|\boldsymbol{w}\|_+$ is applied to denote the maximum norm of the input disturbance. The CBF constraint under perturbed dynamics (3.4.1) is denoted as $\tilde{\psi}(\tilde{\boldsymbol{x}}, \boldsymbol{u}, \boldsymbol{w}, t) : \mathcal{D} \times \mathcal{U} \times \mathcal{W} \times \mathcal{I} \to \mathbb{R}$

$$\tilde{\psi}(\tilde{\boldsymbol{x}}, \boldsymbol{u}, \boldsymbol{w}, t) := \frac{\partial h(\tilde{\boldsymbol{x}}, t)}{\partial t} + \mathcal{L}_f h(\tilde{\boldsymbol{x}}, t) + \mathcal{L}_g h(\tilde{\boldsymbol{x}}, t)(\boldsymbol{u} + \boldsymbol{w}) + \alpha(h(\tilde{\boldsymbol{x}}, t)) \tag{3.4.2}$$

On the other hand, the HOCBF constraint under perturbed dynamics becomes

$$\begin{aligned}\tilde{\zeta}(\tilde{\boldsymbol{x}}, \boldsymbol{u}, \boldsymbol{w}, t) :=& \frac{\partial H_{r-1}(\tilde{\boldsymbol{x}}, t)}{\partial t} + \mathcal{L}_f H_{r-1}(\tilde{\boldsymbol{x}}, t) + \\ & \mathcal{L}_g H_{r-1}(\tilde{\boldsymbol{x}}, t)(\boldsymbol{u} + \boldsymbol{w}) + \alpha_{r-1}(H_{r-1}(\tilde{\boldsymbol{x}}, t))\end{aligned} \tag{3.4.3}$$

Lemma 4. *(modified from [7]) Consider the perturbed control affine system (3.4.1) where the functions $\boldsymbol{g} : \mathbb{R}^n \times \mathbb{R}_{\geq 0} \to \mathbb{R}^{n \times m}$ and $\boldsymbol{f} : \mathbb{R}^n \times \mathbb{R}_{\geq 0} \to \mathbb{R}^n$ are both continuously differentiable functions of t and $\tilde{\boldsymbol{x}}$ on the set $\mathcal{I} \times \tilde{\mathcal{X}}$. Let $\boldsymbol{w}(t) \in \mathcal{W}$ be a bounded unknown piese-wise differentiable disturbance defined on the compact set $\mathcal{W}$ such that $\boldsymbol{w}(t) \leq \|\boldsymbol{w}(t)\|_+ \forall t \in \mathcal{I}$. Let $\mathcal{T}_k := [k\Delta t, (k+1)\Delta t] \subset \mathcal{I}$ be a sampling interval for some $\Delta t > 0$ such that (3.4.1) is subject to a constant bounded feedback control input $\boldsymbol{u}(t) = \boldsymbol{u}(\tilde{\boldsymbol{x}}(k\Delta t), k\Delta t) \in \mathcal{U} \ \forall t \in \mathcal{T}_k$ shorthanded as $u(\tilde{\boldsymbol{x}}(k\Delta t))$. Furthermore consider a valid CBF $h : \mathcal{D} \times \mathcal{I} \to \mathbb{R}$ as in Definition 2 that is at least C^2 on $\mathcal{D} \times \mathcal{I}$ and where α is C^1. Let $\mathcal{C}_S(t) \subset \mathcal{D}$ be the associated safe set as in (3.1.2) and define the associated piece-wise differentiable CBF constraint $\tilde{\psi} : \mathcal{D} \times \mathcal{U} \times \mathcal{W} \times \mathcal{I} \to \mathbb{R}$ as in (3.4.2). Given that at time instant $k\Delta t$, $\tilde{\boldsymbol{x}}(k\Delta t) \in \mathcal{C}_S(k\Delta t)$, $\boldsymbol{x}(k\Delta t) \triangleq \tilde{\boldsymbol{x}}(k\Delta t)$ and that the constant feedback control input $\boldsymbol{u}(\tilde{\boldsymbol{x}}(k\Delta t)) \in \mathcal{U}$ respects the condition*

$$\sup_{\boldsymbol{u} \in \mathcal{U}} \quad \psi(\boldsymbol{x}(k\Delta t), \boldsymbol{u}(k\Delta t), k\Delta t) - L_w \Delta t - c\|\boldsymbol{w}\|_+ \geq 0 \tag{3.4.4}$$

Where ψ is the CBF constraint under nominal dynamics in (3.1.4), evaluated at time $k\Delta t$, and L_w is defined as

$$L_w = \sup_{(\boldsymbol{x}, \boldsymbol{u}, \boldsymbol{w}, t) \in \mathcal{D} \times \mathcal{U} \times \mathcal{W} \times \mathcal{I}} |\dot{\tilde{\psi}}(\tilde{\boldsymbol{x}}, \boldsymbol{u}, \boldsymbol{w}, t)|$$

and the constant c is defined as

$$c = \sup_{(\tilde{\boldsymbol{x}}, t) \in \mathcal{D} \times \mathcal{I}} ||\mathcal{L}_g h(\tilde{\boldsymbol{x}}, t)||$$

Then it holds that

$$\tilde{\boldsymbol{x}}(\Delta t) \in \mathcal{C}_S(k\Delta t) \Rightarrow \tilde{\boldsymbol{x}}(t) \in \mathcal{C}_S(t) \quad \forall t \in \mathcal{T}_k \tag{3.4.5}$$

Proof. The proof follows the same arguments applied to derive Lemma 2. Given a constant feedback input $\boldsymbol{u}(\tilde{\boldsymbol{x}}(k\Delta t))$ on the interval $\mathcal{T}_k$, it is known

that both $\boldsymbol{u}(\tilde{\boldsymbol{x}}(k\Delta t))$ and $\boldsymbol{w}$ are bounded on $\mathcal{T}_k$ as $\mathcal{U}$ and $\mathcal{W}$ are compact. It is also known that $\boldsymbol{f}$ and $\boldsymbol{g}$ in (3.1.1) are both continuously differentiable and $\boldsymbol{w}(t)$ is piece-wise differentiable such that the solution $\tilde{\boldsymbol{x}}(t)$ to (3.4.1) is uniquely defined on an interval $[k\Delta t, \tau]$ for some $\tau \leq (k+1)\Delta t$ [[25], Thm. 54]. The CBF constraint on $[k\Delta t, \tau]$ is then introduced as

$$\tilde{\psi}(\tilde{\boldsymbol{x}}, \boldsymbol{u}(\tilde{\boldsymbol{x}}(k\Delta t)), \boldsymbol{w}, t) = \frac{\partial h(\tilde{\boldsymbol{x}}, t)}{\partial t} + \mathcal{L}_f h(\tilde{\boldsymbol{x}}, t) + \mathcal{L}_g h(\tilde{\boldsymbol{x}}, t)(\boldsymbol{u}(\tilde{\boldsymbol{x}}(k\Delta t)) + \boldsymbol{w}(t)) + \alpha(h(\tilde{\boldsymbol{x}}, t)) \; \forall t \in [k\Delta t, \tau]$$

Now it is noted that $\tilde{\psi}(\tilde{\boldsymbol{x}}(t), \boldsymbol{u}(\tilde{\boldsymbol{x}}(k\Delta t)), \boldsymbol{w}(t), t)$ is a piece-wise differentiable function of time as all the functions appearing in the definition of $\tilde{\psi}$ are continuously differentiable apart from $\boldsymbol{w}(t)$, which is only piece-wise differentiable. Since this function respects the conditions for Prop 4.1.2 in [28], the Lipschitz constant (see equation (3.3.1)) for $\tilde{\psi}(\tilde{\boldsymbol{x}}(t), \boldsymbol{u}(\tilde{\boldsymbol{x}}(k\Delta t)), \boldsymbol{w}(t), t)$ is given by

$$L_w = \sup_{(\boldsymbol{x}, \boldsymbol{u}, \boldsymbol{w}, t) \in \mathcal{D} \times \mathcal{U} \times \mathcal{W} \times \mathcal{I}} |\dot{\tilde{\psi}}(\tilde{\boldsymbol{x}}, \boldsymbol{u}, \boldsymbol{w}, t)|$$

By direct application of the Lipschitz continuity property (3.3.1), it is possible to derive the following inequality

$$|\tilde{\psi}(\tilde{\boldsymbol{x}}(t_2), \boldsymbol{u}(\tilde{\boldsymbol{x}}(k\Delta t)), \boldsymbol{w}(t_2), t_2) - \tilde{\psi}(\tilde{\boldsymbol{x}}(t_1), \boldsymbol{u}(\tilde{\boldsymbol{x}}(k\Delta t)), \boldsymbol{w}(t_1), t_1)| \leq L_w |t_2 - t_1| \quad \forall t_1, t_2 \in [k\Delta t, \tau_0]$$

and the maximum negative variation of $\tilde{\psi}$ over the interval $[k\Delta t, \tau_0]$ becomes

$$\tilde{\psi}(\tilde{\boldsymbol{x}}(t_2), \boldsymbol{u}(\tilde{\boldsymbol{x}}(k\Delta t)), \boldsymbol{w}(t_2), t_2) - \tilde{\psi}(\tilde{\boldsymbol{x}}(t_1), \boldsymbol{u}(\tilde{\boldsymbol{x}}(k\Delta t)), \boldsymbol{w}(t_1), t_1) \geq - L_w |t_2 - t_1| \forall t_1, t_2 \in [k\Delta t, \tau_0] \tag{3.4.6}$$

Next the following relation between $\tilde{\psi}(\tilde{\boldsymbol{x}}(k\Delta t), \boldsymbol{u}(\tilde{\boldsymbol{x}}(k\Delta t)), \boldsymbol{w}(k\Delta t), k\Delta t)$ and $\psi(\boldsymbol{x}(k\Delta t), \boldsymbol{u}(\boldsymbol{x}(k\Delta t)), \boldsymbol{w}(k\Delta t), k\Delta t)$ is introduced recalling that $\tilde{\boldsymbol{x}}(k\Delta t) \triangleq \boldsymbol{x}(k\Delta t)$.

$$\begin{aligned}
&\tilde{\psi}(\tilde{\boldsymbol{x}}(k\Delta t), \boldsymbol{u}(\tilde{\boldsymbol{x}}(k\Delta t)), \boldsymbol{w}(k\Delta t), k\Delta t) = \\
&\psi(\boldsymbol{x}(k\Delta t), \boldsymbol{u}(\boldsymbol{x}(k\Delta t)), k\Delta t) + \mathcal{L}_g h(\boldsymbol{x}(k\Delta t), k\Delta t)\boldsymbol{w}(k\Delta t) \geq \\
&\psi(\boldsymbol{x}(k\Delta t), \boldsymbol{u}(\boldsymbol{x}(k\Delta t)), k\Delta t) - \sup_{(\tilde{\boldsymbol{x}},t)\in\mathcal{D}\times\mathcal{I}} ||\mathcal{L}_g h(\tilde{\boldsymbol{x}}, t)||||\boldsymbol{w}||_+ = \\
&\psi(\boldsymbol{x}(k\Delta t), \boldsymbol{u}(\boldsymbol{x}(k\Delta t)), \boldsymbol{w}(k\Delta t), k\Delta t) - c||\boldsymbol{w}||_+
\end{aligned} \tag{3.4.7}$$

The instant t_1 is replaced with $k\Delta t$, t_2 is replaced with t in (3.4.6) and $\tilde{\psi}(\tilde{\boldsymbol{x}}(k\Delta t), \boldsymbol{u}(\tilde{\boldsymbol{x}}(k\Delta t)), k\Delta t)$ is added on the left and right hand side of (3.4.6) such that the following condition is derived

$$\begin{aligned}
\tilde{\psi}(\tilde{\boldsymbol{x}}(t_2), \boldsymbol{u}(\tilde{\boldsymbol{x}}(k\Delta t)), \boldsymbol{w}(t_2), t_2) &\geq L_w\Delta t + \tilde{\psi}(\tilde{\boldsymbol{x}}(k\Delta t), \boldsymbol{u}(\tilde{\boldsymbol{x}}(k\Delta t)), \boldsymbol{w}(k\Delta t), k\Delta t) \\
&\geq -L_w\Delta t + \psi(\boldsymbol{x}(k\Delta t), \boldsymbol{u}(\boldsymbol{x}(k\Delta t)), \boldsymbol{w}(k\Delta t), k\Delta t) - c||\boldsymbol{w}||_+ \\
&\geq 0 \; \forall t_2 \in [k\Delta t, \tau_0]
\end{aligned}$$

Where the last inequality is obtained by replacing condition (3.4.4) from the lemma statement. As both L_w and c are not specific functions of the time interval considered, the same arguments developed for Lemma 2 are applied to prove that $\tilde{\boldsymbol{x}} \in \mathcal{C}_S(t) \; \forall t \in [k\Delta t, (k+1)\Delta t]$. □

Lemma 4 can be easily extended for SD-HOCBF only in the case the SD-HOCBF has the same relative degree for both $\boldsymbol{u}$ and $\boldsymbol{w}$. This is conditions is formalised as

$$\mathcal{L}_g\mathcal{L}_f^n\boldsymbol{u} = 0 \; \forall n \in [0 \dots r-1] \Rightarrow \mathcal{L}_g\mathcal{L}_f^n\boldsymbol{w} = 0 \; \forall n \in [0 \dots r-1]$$

Where r is the relative degree of the SD-HOCBF. This is due to the fact that if the HOCBF has different relative degree for the control input $\boldsymbol{u}$ and the disturbance $\boldsymbol{w}$, then it is not possible to prove forward invariance of $\bigcap_{i=0..r-1} \mathcal{C}_{Si}(t)$.

Lemma 5. *(modified from [7]) Consider the perturbed control affine system (3.4.1) where the functions $\boldsymbol{g} : \mathbb{R}^n \times \mathbb{R}_{\geq 0} \to \mathbb{R}^{n\times m}$ and $\boldsymbol{f} : \mathbb{R}^n \times \mathbb{R}_{\geq 0} \to \mathbb{R}^n$ are both continuously differentiable functions of t and $\tilde{\boldsymbol{x}}$ on the set $\mathcal{I} \times \tilde{\mathcal{X}}$. Let $\boldsymbol{w}(t) \in \mathcal{W}$ be a bounded unknown piese-wise differentiable disturbance defined on the compact set $\mathcal{W}$ such that $\boldsymbol{w}(t) \leq \|\boldsymbol{w}(t)\|_+ \forall t \in \mathcal{I}$. Let $\mathcal{T}_k := [k\Delta t, (k+1)\Delta t] \subset \mathcal{I}$ be a sampling interval for some $\Delta t > 0$ such that (3.4.1) is subject to a constant bounded feedback control input $\boldsymbol{u}(t) =$*

$\boldsymbol{u}(\tilde{\boldsymbol{x}}(k\Delta t), k\Delta t) \in \mathcal{U} \ \forall t \in \mathcal{T}_k$ shorthanded as $\boldsymbol{u}(\tilde{\boldsymbol{x}}(k\Delta t)$. Furthermore consider a valid HOCBF $h : \mathcal{D} \times \mathcal{I} \to \mathbb{R}$ of relative degree r as in Definition 2 that is at least C^{r+1} on $\mathcal{D} \times \mathcal{I}$ and where α_i is $C^{(r-1)-i}$ $\forall i = 0, \dots r-2$. Let $\underset{i=0..r-1}{\cap} \mathcal{C}_{Si}(t) \subset \mathcal{D}$ be the associated safe set where $\mathcal{C}_{Si}(t)$ are defined as in (3.2.3). Let the associated piece-wise differentiable HOCBF constraint $\tilde{\zeta} : \mathcal{D} \times \mathcal{U} \times \mathcal{W} \times \mathcal{I} \to \mathbb{R}$ as in (3.4.3). Given that at time instant $k\Delta t$, $\tilde{\boldsymbol{x}}(k\Delta t) \in \underset{i=0..r-1}{\cap} \mathcal{C}_{Si}(t)$, $\boldsymbol{x}(k\Delta t) \triangleq \tilde{\boldsymbol{x}}(k\Delta t)$ and that the constant feedback control input $\boldsymbol{u}(\tilde{\boldsymbol{x}}(k\Delta t)) \in \mathcal{U}$ respects the condition

$$\sup_{\boldsymbol{u} \in \mathcal{U}} \quad \zeta(\boldsymbol{x}(k\Delta t), \boldsymbol{u}(k\Delta t), k\Delta t) - L_w \Delta t - c\|\boldsymbol{w}\|_+ \geq 0 \tag{3.4.8}$$

Where ζ is the HOCBF constraint under nominal dynamics in (3.2.5), evaluated at time $k\Delta t$, and L_w is defined as

$$L_w = \sup_{(\boldsymbol{x}, \boldsymbol{u}, \boldsymbol{w}, t) \in \mathcal{D} \times \mathcal{U} \times \mathcal{W} \times \mathcal{I}} |\dot{\tilde{\zeta}}(\tilde{\boldsymbol{x}}, \boldsymbol{u}, \boldsymbol{w}, t)|$$

and the constant c is defined as

$$c = \sup_{(\tilde{\boldsymbol{x}}, t) \in \mathcal{D} \times \mathcal{I}} ||\mathcal{L}_g \mathcal{L}_f^{r-1} h(\tilde{\boldsymbol{x}}, t)||$$

Then it holds that

$$\tilde{\boldsymbol{x}}(k\Delta t) \in \underset{i=0..r-1}{\cap} \mathcal{C}_{Si}(k\Delta t) \Rightarrow \tilde{\boldsymbol{x}}(t) \in \underset{i=0..r-1}{\cap} \mathcal{C}_{Si}(t) \quad \forall t \in \mathcal{T}_k \tag{3.4.9}$$

Proof. The proof is again analogous to the the proof of Lemma 2 where the safe set $\mathcal{C}_S(t)$ is replaced by $\underset{i=0..r-1}{\cap} \mathcal{C}_{Si}(t)$ and the CBF constraint ψ is replaced by the HOCBF constraint ζ. □

Chapter 4

Inspection mission

4.1 Problem Definition

In this Chapter, the theoretical background developed so far will be applied to the spacecraft formation flight problem. It is desired to maintain a formation of CubeSats (denoted as the inspectors from now on) in passive relative orbit (PRO) around the ISS in order to inspect the outer structure of the station while ensuring safety of the formation at all the times. Each agent has the task to track its reference PRO by sparse activation of a sample data MPC controller while maintaining a minimum safe distance from the reference. The driving reason why the agents are set to track PROs stems from the need of minimising the fuel consumption during the mission. In the present work, the PROs design is based on the linearised CW model dynamics (Section 2.2.4). As the ISS orbit is nearly circular (see Table 4.1), the designed PROs are close to be physically stable orbits under zero actuation dynamics. The effects of differential aerodynamic drag and differential zonal harmonic terms cause the inspectors to continuously drift from their reference PROs if periodic correction maneuvers are not undertaken. For this reason an independent MPC controller for each inspector is triggered sparsely during the mission to reset the inspectors on their respective orbits while ensuring safety through the implementation of CBF constraints. A continuous thrust strategy could be applied to perfectly maintain each inspector on its PRO by continuous compensation of the orbital perturbations and linearization errors. Although, it is assumed that each inspector has a limited power distribution capability as well as a payload composed of high resolution cameras applied to undertake the inspection of the outer structure of the ISS. Hence, the effect of continuous

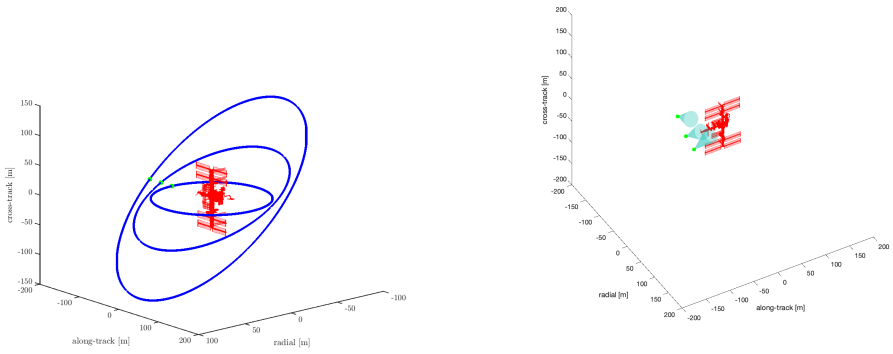

(a) Example of a set of reference PRO geometries for an inspection mission of the International Space Station. The green dot indicates the starting position of each inspector

(b) Graphical representation of the inspection mission with three inspectors. The blue cone indicates the camera cone of view pointing on the ISS structure for the inspection.

actuation could be detrimental for the inspection mission presented as the propulsion system would have a negative effect on the inspectors' payload applied to undertake the inspection. The Chapter is divided as follows: first the nominal and disturbed dynamics of the inspector are recalled from the previous sections. Next, a notion of safety is formalised for the given mission and suitable continuous time and sample data CBF constraints are derived. Eventually the derived CBF constraints are formalised inside the MPC optimal control problem formulation.

mean altitude $[km]$	e	$i\ [deg]$	$a\ [km]$	$T\ [min]$	$\omega_w\ [rad/s]$
417	0.0004751	51.64	6795	92.97	1.126×10^{-3}

Table 4.1: ISS main orbital parameters (these parameters are subject to small daily variations)

4.2 Preliminaries

Each inspector is the equivalent of a deputy as defined in Section 2.2 while the ISS is the equivalent to the chief spacecraft. The nominal unperturbed nonlinear continuous dynamics governing the motions of each inspector is

recalled here for fast reference

$$\begin{aligned} \delta\dot{\boldsymbol{x}} &= \boldsymbol{f}(\delta\boldsymbol{x},t) + \boldsymbol{g}(\delta\boldsymbol{x},t)\boldsymbol{u}(t) \\ \boldsymbol{g}(\delta\boldsymbol{x},t) &= \begin{bmatrix} \boldsymbol{O}_{3x3} \\ \boldsymbol{I}_{3x3} \end{bmatrix} \\ \boldsymbol{f}(\delta\boldsymbol{x},t) &= \begin{bmatrix} \delta\boldsymbol{v} \\ \delta\ddot{\boldsymbol{r}}_g + \delta\boldsymbol{a}_{fc} \end{bmatrix} = \begin{bmatrix} \delta\boldsymbol{v} \\ \boldsymbol{f}_v \end{bmatrix} \end{aligned} \tag{4.2.1}$$

Note that in this case the deputy dynamics is written as a function of time and not as a function of the implicit orbital elements vector $\boldsymbol{b}$. This is possible as the implicit orbital elements dynamics (2.2.4) could be integrated over time independently of the deputy state such that $\boldsymbol{f}$ and $\boldsymbol{g}$ could be rewritten as a function of time without loss of generality. Due to the effect of the differential orbital perturbation vector $\delta\boldsymbol{d}(t)$, the perturbed state dynamics $\delta\dot{\tilde{\boldsymbol{x}}}$ is given as

$$\delta\dot{\tilde{\boldsymbol{x}}} = \boldsymbol{f}(\delta\tilde{\boldsymbol{x}},t) + g(\delta\tilde{\boldsymbol{x}},t)(\boldsymbol{u} + \delta\boldsymbol{d}(t))$$

Given the time varying reference PRO state $\delta\boldsymbol{x}_r(t)$ that it is desired to track over time, the nominal and perturbed state errors are defined as $\boldsymbol{e}_{\delta\boldsymbol{x}} = \delta\boldsymbol{x} - \delta\boldsymbol{x}_r(t)$ and $\tilde{\boldsymbol{e}}_{\delta\boldsymbol{x}} = \delta\tilde{\boldsymbol{x}} - \delta\boldsymbol{x}_r(t)$ respectively.

Through out the section, the notation $\|\boldsymbol{x}\|_+$ will be denote to indicate the maximum norm of a vector $\boldsymbol{x}$ on its domain.

4.3 Safety and HOCBF constraint definition

For the inspection mission of the ISS, the state of each inspector is defined *safe* if the relative position of each inspector has a distance not grater that $\epsilon_{\delta\boldsymbol{r}}$ from the reference relative position defined by the assigned PRO. It is recalled from Section 2.2 that a PRO is a bounded periodic relative orbit around the ISS. Based on this notion of safety a suitable candidate CBF constraint is given by

$$h_{\delta\boldsymbol{r}}(\delta\boldsymbol{x},t) = \epsilon_{\delta\boldsymbol{r}}^2 - \|\delta\boldsymbol{r} - \delta\boldsymbol{r}_r(t)\|^2 \tag{4.3.1}$$

Where $\delta\boldsymbol{r}$ denotes the relative position of the inspector with respect to the ISS and $\delta\boldsymbol{r}_r(t)$ denotes the reference position along the PRO which is only a function of time (see Section 2.2.4). The constant $\epsilon_{\delta\boldsymbol{r}}$ defines the radius of a ball around the reference $\delta\boldsymbol{r}_r$ where the inspector is considered safe. The domain set $\mathcal{X}$ for the inspector relative state can be simply considered as a

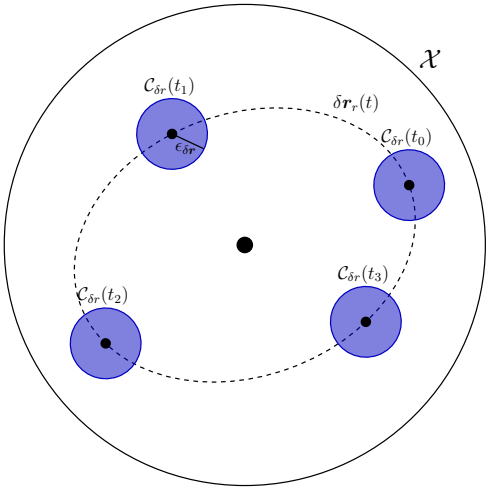

Figure 4.2: Schematic representation of the safe set $\mathcal{C}_{\delta \boldsymbol{r}}(t)$ for four different reference times. The dashed line represents a 2D PRO which is the reference trajectory to track over time ($\delta \boldsymbol{r}_r(t)$). The radius of each safe set is indicated by the parameter $\epsilon_{\delta \boldsymbol{r}}$

convex set such that

$$\mathcal{X} = \{\delta \boldsymbol{x} \in \mathbb{R}^6 : \|\delta \boldsymbol{x}_r\| \leq k \|\delta \boldsymbol{x}_r\|_+\}$$

Where k is a non-negative constant and $\|\delta \boldsymbol{x}_r\|_+$ is the maximum state reference norm along the PRO (which is known to exist as the PRO is a bounded periodic reference). The constant k is chosen based on the value of $\epsilon_{\delta \boldsymbol{r}}$, so that the safe set for $h(\delta \boldsymbol{x}, t)$ is always a strict subset of $\mathcal{X}$. The domain of definition of $h(\delta \boldsymbol{x}, t)$, $\mathcal{D}$, is considered to be $\mathcal{X}$ without loss of generality. Taking the total time derivative of $h(\delta \boldsymbol{x}, t)$ leads to

$$\dot{h}_{\delta \boldsymbol{r}}(\delta \boldsymbol{x}, t) = -2(\delta \boldsymbol{r}(\delta \boldsymbol{x}, t) - \delta \boldsymbol{r}_r(t))^T (\delta \boldsymbol{v}(\delta \boldsymbol{x}, t) - \delta \boldsymbol{v}_r(t)) \tag{4.3.2}$$

where

$$\begin{aligned} \frac{\partial h_{\delta \boldsymbol{r}}(\delta \boldsymbol{x}, t)}{\partial t} &= -2(\delta \boldsymbol{r}(\delta \boldsymbol{x}, t) - \delta \boldsymbol{r}_r(t))^T \delta \boldsymbol{v}_r(t) \\ \mathcal{L}_{\boldsymbol{f}} h_{\delta \boldsymbol{r}}(\delta \boldsymbol{x}, t) &= -2(\delta \boldsymbol{r}(\delta \boldsymbol{x}, t) - \delta \boldsymbol{r}_r(t))^T \delta \boldsymbol{v}(\delta \boldsymbol{x}, t) \\ \mathcal{L}_{\boldsymbol{g}} h_{\delta \boldsymbol{r}}(\delta \boldsymbol{x}, t) &= 0 \end{aligned} \tag{4.3.3}$$

The control $\boldsymbol{u}(t)$ is not directly present in equation (4.3.2) as $\mathcal{L}_{\boldsymbol{g}} h_{\delta \boldsymbol{r}}(\delta \boldsymbol{x}, t)$ is zero. As a consequence, $h_{\delta \boldsymbol{r}}(\delta \boldsymbol{x}, t)$ is an HOCBF for system (4.2.1). The

second total time derivative for $h_{\delta \boldsymbol{r}}(\delta \boldsymbol{x}, t)$ under nominal dynamics is then derived as follows

$$\begin{aligned}\ddot{h}_{\delta \boldsymbol{r}}(\delta \boldsymbol{x}, t) = &-2(\delta \boldsymbol{v}(\delta \boldsymbol{x}, t) - \delta \boldsymbol{v}_r(t))^T(\delta \boldsymbol{v}(\delta \boldsymbol{x}, t) - \delta \boldsymbol{v}_r(t)) - \\ &2(\delta \boldsymbol{r}(\delta \boldsymbol{x}, t) - \delta \boldsymbol{r}_r(t))^T(\boldsymbol{f}_v(\delta \boldsymbol{x}, t) + \boldsymbol{u}(t) - \delta \boldsymbol{a}_r(t))\end{aligned} \tag{4.3.4}$$

Where the relative acceleration $\delta \boldsymbol{a}(\delta \boldsymbol{x}, t)$ is replaced with its definition from equation (4.2.1). The decomposition of equation (4.3.4) into its Lie and partial time derivatives is considered unnecessary complex to be presented. Although, it is pointed out that the Lie derivative of $\dot{h}_{\delta \boldsymbol{r}}$ along $\boldsymbol{g}(\delta \boldsymbol{x}, t)$ is given by

$$\mathcal{L}_{\boldsymbol{g}} \mathcal{L}_{\boldsymbol{f}} h_{\delta \boldsymbol{r}} = -2 \boldsymbol{e}_{\delta \boldsymbol{r}}^T \tag{4.3.5}$$

For convenience the reference acceleration $\delta \boldsymbol{a}_r$ is set to zero while the position and velocity tracking errors $\boldsymbol{e}_{\delta \boldsymbol{v}}(\delta \boldsymbol{x}, t)$, $\boldsymbol{e}_{\delta \boldsymbol{r}}(\delta \boldsymbol{x}, t)$ are introduced as

$$\begin{aligned}\boldsymbol{e}_{\delta \boldsymbol{v}}(\delta \boldsymbol{x}, t) &= \delta \boldsymbol{v}(\delta \boldsymbol{x}, t) - \delta \boldsymbol{v}_r(t) \\ \boldsymbol{e}_{\delta \boldsymbol{r}}(\delta \boldsymbol{x}, t) &= \delta \boldsymbol{r}(\delta \boldsymbol{x}, t) - \delta \boldsymbol{r}_r(t)\end{aligned}$$

The HOCBF and its time derivatives are then summarised as

$$\begin{aligned}h_{\delta \boldsymbol{r}}(\delta \boldsymbol{x}, t) &= \epsilon_{\delta \boldsymbol{r}}^2 - \|\boldsymbol{e}_{\delta \boldsymbol{r}}(\delta \boldsymbol{x}, t)\|^2 \\ \dot{h}_{\delta \boldsymbol{r}}(\delta \boldsymbol{x}, t) &= -2 \boldsymbol{e}_{\delta \boldsymbol{r}}(\delta \boldsymbol{x}, t)^T \boldsymbol{e}_{\delta \boldsymbol{v}}(\delta \boldsymbol{x}, t) \\ \ddot{h}_{\delta \boldsymbol{r}}(\delta \boldsymbol{x}, t) &= -2 \boldsymbol{e}_{\delta \boldsymbol{v}}(\delta \boldsymbol{x}, t)^T \boldsymbol{e}_{\delta \boldsymbol{v}}(\delta \boldsymbol{x}, t) \\ &\quad - 2 \boldsymbol{e}_{\delta \boldsymbol{r}}(\delta \boldsymbol{x}, t)^T(\boldsymbol{f}_v(\delta \boldsymbol{x}, t) + \boldsymbol{u}(t))\end{aligned} \tag{4.3.6}$$

Since the control $\boldsymbol{u}(t)$ directly appears at the second derivative of $h_{\delta \boldsymbol{r}}(\delta \boldsymbol{x}, t)$, the defined HOCBF is of relative degree 2 for the system (4.2.1). Developing a cascade of barrier functions as in equation (3.2.2) and assuming that all the class $\mathcal{K}$-functions $\alpha(\cdot)$ are polynomial functions in the form $\alpha_n(x) = p_n x^{a_n}$ with $a_n \geq 0$ being a general exponent (note this class of functions respect the smoothness conditions introduced in Section 3), the following cascade of CBFs is derived

$$\begin{aligned}H_0(\delta \boldsymbol{x}, t) &= h_{\delta \boldsymbol{r}}(\delta \boldsymbol{x}, t) \\ H_1(\delta \boldsymbol{x}, t) &= \dot{h}_{\delta \boldsymbol{r}}(\delta \boldsymbol{x}, t) + p_0(h_{\delta \boldsymbol{r}}(\delta \boldsymbol{x}, t))^{a_0}\end{aligned} \tag{4.3.7}$$

and the general HOCBF constraint is derived as follows

$$\zeta(\delta \boldsymbol{x}, \boldsymbol{u}, t) = \ddot{h}_{\delta \boldsymbol{r}} + a_0\, p_0\, \dot{h}_{\delta \boldsymbol{r}} h_{\delta \boldsymbol{r}}^{a_0 - 1} + p_1\, (p_0\, h_{\delta \boldsymbol{r}}^{a_0} + \dot{h}_{\delta \boldsymbol{r}})^{a_1} \tag{4.3.8}$$

where the dependence from the state and time was dropped for convenience. In order to limit the complexity of the derivations we will only consider linear alpha functions in the form $\alpha_n(x) = p_n x$ such that the following definition H_i are derived

$$\begin{aligned} H_0(\delta\boldsymbol{x}, t) &= h_{\delta\boldsymbol{r}}(\delta\boldsymbol{x}, t) \\ H_1(\delta\boldsymbol{x}, t) &= \dot{h}_{\delta\boldsymbol{r}}(\delta\boldsymbol{x}, t) + p_{\delta\boldsymbol{r}0} h_{\delta\boldsymbol{r}}(\delta\boldsymbol{x}, t) \end{aligned} \tag{4.3.9}$$

The consequences of this simplification will be analysed in the conclusion of the work with reference to the remarks highlighted in [23] regarding the application of high order polynomials alpha functions instead of simple linear functions as it is the case for the current work. The safe sets for H_0 and H_1 are defined as :

$$\begin{aligned} \mathcal{C}_0(t) &= \{\delta\boldsymbol{x} \in \mathcal{X} : H_0(\delta\boldsymbol{x}, t) \geq 0\} \\ \mathcal{C}_1(t) &= \{\delta\boldsymbol{x} \in \mathcal{X} : H_1(\delta\boldsymbol{x}, t) \geq 0\} \end{aligned} \tag{4.3.10}$$

And the global safe set is given as

$$\mathcal{C}_{\delta\boldsymbol{r}}(t) := \mathcal{C}_1(t) \cap \mathcal{C}_0(t)$$

The condition for the system to be in $\mathcal{C}_0(t)$ is simply to be inside the ball defined by equation (4.3.1). On the other hand, the condition for the system to be in $\mathcal{C}_1(t)$ is less evident. Namely, the function $\dot{h}_{\delta\boldsymbol{r}} + p_{\delta\boldsymbol{r}0} h_{\delta\boldsymbol{r}}$ is positive in the following two situations : (1) the velocity error $\boldsymbol{e}_{\delta\boldsymbol{v}}$ has a negative projection along the position error $\boldsymbol{e}_{\delta\boldsymbol{r}}$, which intuitively corresponds to the inspector moving toward the reference (2) the projection of $\boldsymbol{e}_{\delta\boldsymbol{v}}$ along $\boldsymbol{e}_{\delta\boldsymbol{r}}$ is positive but the value of $\boldsymbol{e}_{\delta\boldsymbol{v}}^T \boldsymbol{e}_{\delta\boldsymbol{r}}$ is smaller than $p_{\delta\boldsymbol{r}0} h(\delta\boldsymbol{x}, t)$.

Now that a HOCBF is defined together with the safe set $\mathcal{C}_{\delta\boldsymbol{r}}(t)$, the HOCBF constraint is defined as

$$\zeta_{\delta\boldsymbol{r}}(\delta\boldsymbol{x}, \boldsymbol{u}, t) = \dot{H}_1(\delta\boldsymbol{x}, t) + p_{\delta\boldsymbol{r}1} H_1(\delta\boldsymbol{x}, t) \tag{4.3.11}$$

Replacing the relations in equation (4.3.9) and (4.3.6) in equation (4.3.11) the HOCBF constraint becomes

$$\begin{aligned} \zeta_{\delta\boldsymbol{r}}(\delta\boldsymbol{x}, \boldsymbol{u}, t) = &- 2\|\boldsymbol{e}_{\delta\boldsymbol{v}}\|^2 - 2\boldsymbol{e}_{\delta\boldsymbol{r}}^T(\boldsymbol{f}_v(\delta\boldsymbol{x}, t) + \boldsymbol{u}(t)) \\ &- 2(p_{\delta\boldsymbol{r}0} + p_{\delta\boldsymbol{r}1})(\boldsymbol{e}_{\delta\boldsymbol{r}}^T \boldsymbol{e}_{\delta\boldsymbol{v}}) + p_{\delta\boldsymbol{r}0} p_{\delta\boldsymbol{r}1}(\epsilon_{\delta\boldsymbol{r}}^2 - \|\boldsymbol{e}_{\delta\boldsymbol{r}}\|^2) \end{aligned} \tag{4.3.12}$$

It is desired to study the feasibility of the condition $\zeta_{\delta\boldsymbol{r}}(\delta\boldsymbol{x}, \boldsymbol{u}, t) \geq 0$ for any given state condition within the set $\mathcal{C}_{\delta\boldsymbol{r}}(t)$ as this condition must be ensured in order to maintain the system inside the safe set (see Lemma 1). The control

set $\mathcal{U}$ is first defined

Definition 7. *The available control set $\mathcal{U}$ for the dynamics system in (4.2.1) is a compact set defined as*

$$\mathcal{U} = \{\boldsymbol{u} \in \mathbb{R}^3 : \|\boldsymbol{u}\| \leq \|\boldsymbol{u}\|_+\}$$

where $\|\boldsymbol{u}\|_+$ denoted the maximum available control norm.

The following proposition is then given

Proposition 1. *Given the HOCBF constraint defined in equation (4.3.12), the associated safe set $\mathcal{C}_{\delta \boldsymbol{r}}(t)$ and the feasible control input set $\mathcal{U}$ as in Definition 7, it holds that*

$$\max_{\boldsymbol{u} \in \mathcal{U}} \quad \zeta_{\delta \boldsymbol{r}}(\delta \boldsymbol{x}, \boldsymbol{u}, t) = \|\boldsymbol{u}\|_+ - \beta_{\delta \boldsymbol{r}}(\delta \boldsymbol{x}, t) \quad \forall \delta \boldsymbol{x} \in \mathcal{C}_{\delta \boldsymbol{r}}(t) \tag{4.3.13}$$

where

$$\begin{aligned} \beta_{\delta \boldsymbol{r}}(\delta \boldsymbol{x}, t) = \frac{1}{\|\boldsymbol{e}_{\delta \boldsymbol{r}}\|} \big(\|\boldsymbol{e}_{\delta \boldsymbol{v}}\|^2 + \boldsymbol{e}_{\delta \boldsymbol{r}}^T \boldsymbol{f}_v + (p_{\delta \boldsymbol{r}0} + p_{\delta \boldsymbol{r}1})(\boldsymbol{e}_{\delta \boldsymbol{r}}^T \boldsymbol{e}_{\delta \boldsymbol{v}}) \\ - \frac{p_{\delta \boldsymbol{r}0} p_{\delta \boldsymbol{r}1}}{2} (\epsilon_{\delta \boldsymbol{r}}^2 - \|\boldsymbol{e}_{\delta \boldsymbol{r}}\|^2) \end{aligned} \tag{4.3.14}$$

Proof. The value of the inner product $\boldsymbol{e}_{\delta \boldsymbol{r}}^T \boldsymbol{u}$ is bounded by applying the inner product inequality

$$-\|\boldsymbol{e}_{\delta \boldsymbol{r}}\| \|\boldsymbol{u}\| \leq \boldsymbol{e}_{\delta \boldsymbol{r}}^T \boldsymbol{u} \leq \|\boldsymbol{e}_{\delta \boldsymbol{r}}\| \|\boldsymbol{u}\| \tag{4.3.15}$$

Considering that inside the set $\mathcal{U}$ the relation $\|\boldsymbol{u}\| \leq \|\boldsymbol{u}\|_+$ holds, then the inner product $\boldsymbol{e}_{\delta \boldsymbol{r}}^T \boldsymbol{u}$ is further bounded as

$$-\|\boldsymbol{e}_{\delta \boldsymbol{r}}\| \|\boldsymbol{u}\|_+ \leq \boldsymbol{e}_{\delta \boldsymbol{r}}^T \boldsymbol{u} \leq \|\boldsymbol{e}_{\delta \boldsymbol{r}}\| \|\boldsymbol{u}\|_+ \tag{4.3.16}$$

Hence the HOCBF constraint $\zeta_{\delta \boldsymbol{r}}$ is always maximised with respect to the control input $\boldsymbol{u}$ for any possible state in $\mathcal{C}_{\delta \boldsymbol{r}}(t)$ as

$$\begin{aligned} \max_{\boldsymbol{u} \in \mathcal{U}} \zeta_{\delta \boldsymbol{r}}(\delta \boldsymbol{x}, \boldsymbol{u}, t) = -2\|\boldsymbol{e}_{\delta \boldsymbol{v}}\|^2 - 2\boldsymbol{e}_{\delta \boldsymbol{r}}^T \boldsymbol{f}_v + 2\|\boldsymbol{e}_{\delta \boldsymbol{r}}\| \|\boldsymbol{u}\|_+ \\ - 2(p_{\delta \boldsymbol{r}0} + p_{\delta \boldsymbol{r}1})(\boldsymbol{e}_{\delta \boldsymbol{r}}^T \boldsymbol{e}_{\delta \boldsymbol{v}}) + p_{\delta \boldsymbol{r}0} p_{\delta \boldsymbol{r}1} (\epsilon_{\delta \boldsymbol{r}}^2 - \|\boldsymbol{e}_{\delta \boldsymbol{r}}\|^2) \geq 0 \end{aligned} \tag{4.3.17}$$

Isolating $\|\boldsymbol{u}\|_+$ in (4.3.17) yields then the result of the proposition □

From the result of Proposition 1, a minimum maximum control magnitude $\|\boldsymbol{u}\|_+$ such that the condition $\zeta_{\delta \boldsymbol{r}}(\delta \boldsymbol{x}, \boldsymbol{u}, t) \geq 0$ is always satisfied for any possible state condition is found by maximising the function $\beta_{\delta \boldsymbol{r}}(\delta \boldsymbol{x}, t)$ for the state and time. Considering the system state to be inside safe set $\mathcal{C}_{\delta \boldsymbol{r}}(t)$, an upper bound on $\beta_{\delta \boldsymbol{r}}(\delta \boldsymbol{x}, t)$ is developed as

$$
\begin{aligned}
&\beta_{\delta \boldsymbol{r}}(\delta \boldsymbol{x}, t) \leq \\
&\frac{1}{\|\boldsymbol{e}_{\delta \boldsymbol{r}}\|}\left(\|\boldsymbol{e}_{\delta \boldsymbol{v}}\|^2+\|\boldsymbol{e}_{\delta \boldsymbol{r}}\| \epsilon_f+\left(p_{\delta \boldsymbol{r} 0}+p_{\delta \boldsymbol{r} 1}\right)\left(\boldsymbol{e}_{\delta \boldsymbol{r}}^T \boldsymbol{e}_{\delta \boldsymbol{v}}\right)_+-\frac{p_{\delta \boldsymbol{r} 0} p_{\delta \boldsymbol{r} 1}}{2}\left(\epsilon_{\delta \boldsymbol{r}}^2-\|\boldsymbol{e}_{\delta \boldsymbol{r}}\|^2\right)\right)= \\
&\frac{1}{\|\boldsymbol{e}_{\delta \boldsymbol{r}}\|}\left(\epsilon_{\delta \boldsymbol{v}}^2+\|\boldsymbol{e}_{\delta \boldsymbol{r}}\| \epsilon_f+\left(p_{\delta \boldsymbol{r} 0}+p_{\delta \boldsymbol{r} 1}\right) \frac{p_{\delta \boldsymbol{r} 0}}{2}\left(\epsilon_{\delta \boldsymbol{r}}^2-\|\boldsymbol{e}_{\delta \boldsymbol{r}}\|^2\right)-\frac{p_{\delta \boldsymbol{r} 0} p_{\delta \boldsymbol{r} 1}}{2}\left(\epsilon_{\delta \boldsymbol{r}}^2-\|\boldsymbol{e}_{\delta \boldsymbol{r}}\|^2\right)\right)= \\
&\frac{1}{\|\boldsymbol{e}_{\delta \boldsymbol{r}}\|}\left(\epsilon_{\delta \boldsymbol{v}}^2+\|\boldsymbol{e}_{\delta \boldsymbol{r}}\|\left(\epsilon_f\right)+\left(\left(p_{\delta \boldsymbol{r} 0}+p_{\delta \boldsymbol{r} 1}\right) \frac{p_{\delta \boldsymbol{r} 0}}{2}-\frac{p_{\delta \boldsymbol{r} 0} p_{\delta \boldsymbol{r} 1}}{2}\right)\left(\epsilon_{\delta \boldsymbol{r}}^2-\|\boldsymbol{e}_{\delta \boldsymbol{r}}\|^2\right)\right)= \\
&\frac{\epsilon_{\delta \boldsymbol{v}}^2}{\|\boldsymbol{e}_{\delta \boldsymbol{r}}\|}+\epsilon_f+\frac{p_{\delta \boldsymbol{r} 0}^2}{2} \frac{\left(\epsilon_{\delta \boldsymbol{r}}^2-\|\boldsymbol{e}_{\delta \boldsymbol{r}}\|^2\right)}{\|\boldsymbol{e}_{\delta \boldsymbol{r}}\|}=\bar{\beta}_{\delta \boldsymbol{r}}
\end{aligned}
\tag{4.3.18}
$$

Where the variables ϵ_f and $\epsilon_{\delta \boldsymbol{v}}$ are defined as follows

$$
\begin{aligned}
\underset{(\delta \boldsymbol{x}, t) \in \mathcal{X} \times \mathbb{R}_{\geq 0}}{max} \quad & \|\boldsymbol{e}_{\delta \boldsymbol{v}}\|=\|\boldsymbol{e}_{\delta \boldsymbol{v}}\|_+=\epsilon_{\delta \boldsymbol{v}} \\
\underset{(\delta \boldsymbol{x}, t) \in \mathcal{X} \times \mathbb{R}_{\geq 0}}{max} \quad & \|\boldsymbol{f}_v\|=\|\boldsymbol{f}_v\|_+=\epsilon_f
\end{aligned}
\tag{4.3.19}
$$

While ϵ_f can be obtained analytically (Appendix A.3), the upper bound $\epsilon_{\delta \boldsymbol{v}}$ must be enforced from the satisfaction of a second barrier constraint on the velocity error (which is developed in the next section). If it is not possible to bound $\|\boldsymbol{e}_{\delta \boldsymbol{v}}\|$, then it is not possible to give any guarantee about the satisfaction of the HOCBF constraint. Note that this conclusion is not dependant from the particular choice of the linear α functions inside the HOCBF definition due to the fact the the second time derivative of $h_{\delta \boldsymbol{r}}$ will eventually appear as evident form equation (4.3.8). At last, the maximum of the inner product $\boldsymbol{e}_{\delta \boldsymbol{r}}^T \boldsymbol{e}_{\delta \boldsymbol{v}}$ was bounded within the safe set $\mathcal{C}_1 \supset \mathcal{C}_{\delta \boldsymbol{r}}$ as

$$
\begin{aligned}
H_1 \geq 0 & \Rightarrow -2 \boldsymbol{e}_{\delta \boldsymbol{r}}^T \boldsymbol{e}_{\delta \boldsymbol{v}}+\alpha_0(h(\boldsymbol{x}, t)) \geq 0 \\
& \Rightarrow\left(\boldsymbol{e}_{\delta \boldsymbol{r}}^T \boldsymbol{e}_{\delta \boldsymbol{v}}\right) \leq \frac{\alpha_0(h(\boldsymbol{x}, t))}{2}=\frac{p_{\delta \boldsymbol{r} 0}}{2}\left(\epsilon_{\delta \boldsymbol{r}}^2-\|\boldsymbol{e}_{\delta \boldsymbol{r}}\|^2\right)
\end{aligned}
\tag{4.3.20}
$$

From the definition of $\bar{\beta}_{\delta \boldsymbol{r}}$ the maximum control norm tends to infinity as the position error norm tends to zero. This problem derives from the fact that $\mathcal{L}_g \mathcal{L}_f h(\boldsymbol{x}, t)$ is singular at the origin. If the available control is limited (as it is the case in every real application), the satisfaction of the HOCBF constraint

can only be strictly ensured in a restricted safe set $\tilde{\mathcal{C}}_{\delta \boldsymbol{r}}(t) \subset \mathcal{C}_{\delta \boldsymbol{r}}(t)$ defined as

$$\tilde{\mathcal{C}}_{\delta \boldsymbol{r}}(t) = \{\delta \boldsymbol{x} \in \mathcal{C}_{\delta \boldsymbol{r}}(t) : d_s \leq \|\boldsymbol{e}_{\delta \boldsymbol{r}}\| \leq \epsilon_{\delta \boldsymbol{r}}\}$$

On the other hand, inside the set $\mathcal{C}_{\delta \boldsymbol{r}}(t) \backslash \tilde{\mathcal{C}}_{\delta \boldsymbol{r}}(t)$ the satisfaction of the HOCBF constraint can only be assumed under an appropriate feedback law. The higher is the control authority and the smaller will be the minimum value of d_s such that $\zeta_{\delta \boldsymbol{r}}(\delta \boldsymbol{x}, \boldsymbol{u}, t) \geq 0$ is ensured for every state condition in $\tilde{\mathcal{C}}_{\delta \boldsymbol{r}}(t)$. A second relevant issue needs to be solved before moving further. Namely, the maximum speed error norm $\epsilon_{\delta \boldsymbol{v}}$ has to be bounded inside $\mathcal{C}_{\delta \boldsymbol{r}}(t)$ in order to provide any guarantee on the HOCBF constraint satisfaction. In the present work it is considered that the maximum relative speed error bound $\epsilon_{\delta \boldsymbol{v}}$ is enforced to be equal to

$$\epsilon_{\delta \boldsymbol{v}} \leq \frac{p_{\delta \boldsymbol{r}0}}{2} \frac{(\epsilon_{\delta \boldsymbol{r}}^2 - d_s^2)}{d_s} \tag{4.3.21}$$

which is the maximum outward radial speed component allowed inside $\mathcal{C}_1(t)$

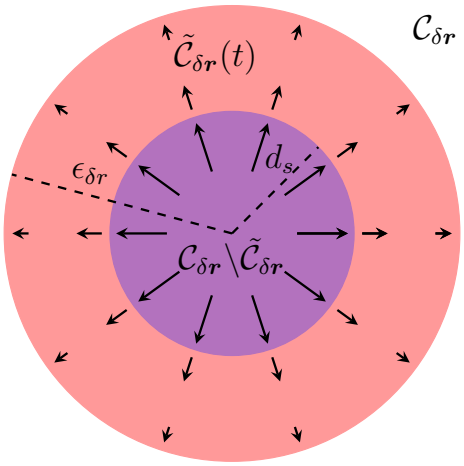

Figure 4.3: Schematic representation of the sets $\tilde{\mathcal{C}}_{\delta \boldsymbol{r}}$,$\mathcal{C}_{\delta \boldsymbol{r}}$ and $\mathcal{C}_{\delta \boldsymbol{r}} \backslash \tilde{\mathcal{C}}_{\delta \boldsymbol{r}}$. The black arrows indicate the maximum radial component of the speed error $\boldsymbol{e}_{\delta \boldsymbol{v}}$ as allowed inside $\mathcal{C}_{\delta \boldsymbol{r}}$. The dashed lines are applied to indicate the inner distance d_s and the outer safe set limit $\epsilon_{\delta \boldsymbol{r}}$

when $\|\boldsymbol{e}_{\delta \boldsymbol{r}}\| = d_s$. This value lower bounds the maximum outward radial speed inside $\mathcal{C}_{\delta \boldsymbol{r}}(t) \backslash \tilde{\mathcal{C}}_{\delta \boldsymbol{r}}(t)$, and upper bounds the maximum allowed radial speed in $\tilde{\mathcal{C}}_{\delta \boldsymbol{r}}(t)$ as evident from equation (4.3.20). Replacing d_s and Definition (4.3.21) for the maximum relative speed upper bound $\epsilon_{\delta \boldsymbol{v}}$ in equation (4.3.18), leads to a closed form analytical solution for the maximum control required to

satisfy the HOCBF constraint inside $\tilde{\mathcal{C}}_{\delta \boldsymbol{r}}(t)$

$$\|\boldsymbol{u}\|_+ \geq \frac{p_{\delta \boldsymbol{r}0}^2}{4} \frac{(\epsilon_{\delta \boldsymbol{r}}^2 - d_s^2)^2}{d_s^3} + \epsilon_f + \frac{p_{\delta \boldsymbol{r}0}^2}{2} \frac{(\epsilon_{\delta \boldsymbol{r}}^2 - d_s^2)}{d_s} \tag{4.3.22}$$

It is instead not possible to prove analytically that such control authority is sufficient to satisfy the HOCBF constarint inside $\mathcal{C}_{\delta \boldsymbol{r}}(t) \backslash \tilde{\mathcal{C}}_{\delta \boldsymbol{r}}(t)$ as subject to the defined upper limit in the speed error magnitude defined in (4.3.21)

4.4 Velocity CBF

In the previous subsection it was assumed that a maximum value for the norm of the relative velocity error exist as $\epsilon_{\delta \boldsymbol{v}}$. In order to impose such upper bound on the maximum relative velocity error norm, a second barrier function is introduced as

$$h_{\delta \boldsymbol{v}}(\delta \boldsymbol{x}, t) = \epsilon_{\delta \boldsymbol{v}}^2 - \|\delta \boldsymbol{v} - \delta \boldsymbol{v}_r(t)\|^2 \tag{4.4.1}$$

Replacing $\delta \boldsymbol{v} - \delta \boldsymbol{v}_r(t)$ with $\boldsymbol{e}_{\delta \boldsymbol{v}}$ and taking the time derivative of $h_{\delta \boldsymbol{v}}(\delta \boldsymbol{x}, t)$ with respect to time leads to

$$\dot{h}_{\delta \boldsymbol{v}}(\delta \boldsymbol{x}, t) = -2 \boldsymbol{e}_{\delta \boldsymbol{v}}^T (\boldsymbol{f}_v + \boldsymbol{u}) \tag{4.4.2}$$

Since the control $\boldsymbol{u}$ appears in the first time derivative of $h_{\delta \boldsymbol{v}}(\delta \boldsymbol{x}, t)$, then $h_{\delta \boldsymbol{v}}(\delta \boldsymbol{x}, t)$ is of relative degree one for the system (4.2.1) with $\mathcal{L}_{\boldsymbol{g}} h_{\delta \boldsymbol{v}}(\delta \boldsymbol{x}, t)$ defined as

$$\mathcal{L}_{\boldsymbol{g}} h_{\delta \boldsymbol{v}}(\delta \boldsymbol{x}, t) = -2 \boldsymbol{e}_{\delta \boldsymbol{v}}^T$$

And a valid CBF constraint is directly imposed as

$$\begin{aligned} \psi_{\delta \boldsymbol{v}}(\delta \boldsymbol{x}, \boldsymbol{u}, t) &:= \dot{h}_v(\delta \boldsymbol{x}, t) + p_{\delta \boldsymbol{v}0}(h_{\delta \boldsymbol{v}}(\delta \boldsymbol{x}, t)) \\ &= -2 \boldsymbol{e}_{\delta \boldsymbol{v}}^T (\boldsymbol{f}_v(\delta \boldsymbol{x}, t) + \boldsymbol{u}(t)) + p_{\delta \boldsymbol{v}0}(\epsilon_{\delta \boldsymbol{v}}^2 - \|\boldsymbol{e}_{\delta \boldsymbol{v}}(\delta \boldsymbol{x}, t)\|^2) \geq 0 \end{aligned} \tag{4.4.3}$$

The safe set for the velocity CBF is simply defined by

$$\mathcal{C}_{\delta \boldsymbol{v}}(t) = \{\delta \boldsymbol{x} \in \mathcal{X} : h_{\delta \boldsymbol{v}}(\delta \boldsymbol{x}, t) \geq 0\} \tag{4.4.4}$$

Similarly to Proposition 1, the following proposition is given to analytically derive a lower bound and the minimum control authority required to satisfy the velocity CBF constraint

Proposition 2. *Given the CBF constraint defined in equation (4.4.3), the*

associated safe set $\mathcal{C}_{\delta \boldsymbol{v}}(t)$ *from* (4.4.4) *and the feasible control input set* $\mathcal{U}$ *as in Definition 7, it holds that*

$$\max_{\boldsymbol{u} \in \mathcal{U}} \quad \psi_{\delta \boldsymbol{v}}(\delta \boldsymbol{x}, \boldsymbol{u}, t) = \|\boldsymbol{u}\|_+ - \beta_{\delta \boldsymbol{v}}(\delta \boldsymbol{x}, t) \tag{4.4.5}$$

where

$$\beta_{\delta \boldsymbol{v}}(\delta \boldsymbol{x}, t) = \frac{\boldsymbol{e}_{\delta \boldsymbol{v}}^T \boldsymbol{f}_v}{\|\boldsymbol{e}_{\delta \boldsymbol{v}}\|} - p_{\delta \boldsymbol{r} 0} \frac{(\epsilon_{\delta \boldsymbol{v}}^2 - \|\boldsymbol{e}_{\delta \boldsymbol{v}}\|^2)}{2\|\boldsymbol{e}_{\delta \boldsymbol{v}}\|} \tag{4.4.6}$$

Proof. The value of the inner product $\boldsymbol{e}_{\delta \boldsymbol{v}}^T \boldsymbol{u}$ is bounded as

$$-\|\boldsymbol{e}_{\delta \boldsymbol{v}}\| \|\boldsymbol{u}\| \leq \boldsymbol{e}_{\delta \boldsymbol{v}}^T \boldsymbol{u} \leq \|\boldsymbol{e}_{\delta \boldsymbol{v}}\| \|\boldsymbol{u}\| \tag{4.4.7}$$

Considering that inside $\mathcal{U}$ the relation $\|\boldsymbol{u}\| \leq \|\boldsymbol{u}\|_+$ holds, then the inner product $\boldsymbol{e}_{\delta \boldsymbol{v}}^T \boldsymbol{u}$ is further bounded as

$$-\|\boldsymbol{e}_{\delta \boldsymbol{v}}\| \|\boldsymbol{u}\|_+ \leq \boldsymbol{e}_{\delta \boldsymbol{v}}^T \boldsymbol{u} \leq \|\boldsymbol{e}_{\delta \boldsymbol{v}}\| \|\boldsymbol{u}\|_+ \tag{4.4.8}$$

Replacing this last inequality in the definition of $\psi_{\delta \boldsymbol{v}}(\delta \boldsymbol{x}, \boldsymbol{u}, t)$ gives the result of the proposition □

Applying Proposition 2 it is possible to derive a lower bound on the maximum control authority $\|\boldsymbol{u}\|_+$ as function of the state such that the CBF condition $\psi_{\delta \boldsymbol{v}}(\delta \boldsymbol{x}, \boldsymbol{u}, t) \geq 0$ is respected as

$$\|\boldsymbol{u}\|_+ \geq \beta_{\delta \boldsymbol{v}}(\delta \boldsymbol{x}, t) = -p_{\delta \boldsymbol{v} 0} \frac{(\epsilon_{\delta \boldsymbol{v}}^2 - \|\boldsymbol{e}_{\delta \boldsymbol{v}}\|^2)}{2\|\boldsymbol{e}_{\delta \boldsymbol{v}}\|} + \frac{1}{\|\boldsymbol{e}_{\delta \boldsymbol{v}}\|} \boldsymbol{e}_{\delta \boldsymbol{v}}^T \boldsymbol{f}_v \tag{4.4.9}$$

In order to find a minimum maximum control magnitude $\|\boldsymbol{u}\|_+$ such that the condition $\psi_{\delta \boldsymbol{v}}(\delta \boldsymbol{x}, \boldsymbol{u}, t) \geq 0$ is always satisfied, the lower bound $\beta_{\delta \boldsymbol{v}}(\delta \boldsymbol{x}, t)$ is maximised for the state and time, considering that the system is inside the safe set $\mathcal{C}_{\delta \boldsymbol{v}}(t)$. Applying the Cauchy-Schwarz inequality on the term $\boldsymbol{e}_{\delta \boldsymbol{v}}^T \boldsymbol{f}$, the function $\beta_{\delta \boldsymbol{v}}(\delta \boldsymbol{x}, t)$ is upper bounded as

$$\beta(\delta \boldsymbol{x}, t) \leq -p_{\delta \boldsymbol{r} 0} \frac{(\epsilon_{\delta \boldsymbol{v}}^2 - \|\boldsymbol{e}_{\delta \boldsymbol{v}}\|^2)}{2\|\boldsymbol{e}_{\delta \boldsymbol{v}}\|} + \epsilon_f \tag{4.4.10}$$

And eventually the maximum minimum control input required to satisfy the CBF constraint is obtained by noting that the RHS in equation (4.4.10) is

maximised within the safe set $\mathcal{C}_{\delta \boldsymbol{v}}$ by the condition $\|\boldsymbol{e}_{\delta \boldsymbol{v}}\| = \epsilon_{\delta \boldsymbol{v}}$ such that

$$\|\boldsymbol{u}\|_+ \geq \epsilon_f \tag{4.4.11}$$

This subsection is concluded noting that for the first order barrier function $h_{\delta \boldsymbol{v}}$ the minimum maximum control authority is only given by the maximum dynamic acceleration which is a much simpler result than the one obtained for the HOCBF.

4.5 From continuous to sample data

As developed in Section 3.3, a suitable margin should be defined for the position and velocity barrier constraints so that safety is not only ensured at the time steps $k\Delta t$, but also in between the time intervals $\mathcal{T}_k = [k\Delta t, (k+1)\Delta t]$. Namely, the constants L_w and c appearing in Lemma 4 and 5 are to be defined for the position HOCBF constraint and the velocity CBF constraints under perturbed dynamics. For clarity, $L_{\delta \boldsymbol{r}}$ and $c_{\delta \boldsymbol{r}}$ will be applied to define the constants L_w and c from Lemma 4 and 5 for the position HOCBF constraint, while $L_{\delta \boldsymbol{v}}$ and $c_{\delta \boldsymbol{v}}$ are applied for the velocity CBF constraint.

4.5.1 Robust position SD-HOCBF

The HOCBF constraint under perturbed dynamics $\tilde{\zeta}_{\delta \boldsymbol{r}}(\delta \tilde{\boldsymbol{x}}, t)$ is defined as

$$\begin{aligned}\tilde{\zeta}_{\delta \boldsymbol{r}}(\delta \tilde{\boldsymbol{x}}, \boldsymbol{u}, \delta \boldsymbol{d}, t) := &- 2\|\tilde{\boldsymbol{e}}_{\delta \boldsymbol{v}}\|^2 - 2\tilde{\boldsymbol{e}}_{\delta \boldsymbol{r}}^T(\boldsymbol{f}_v + \delta \boldsymbol{d}) + 2\|\tilde{\boldsymbol{e}}_{\delta \boldsymbol{r}}\|\|\boldsymbol{u}\|_+ \\ &- 2(p_{\delta \boldsymbol{r}0} + p_{\delta \boldsymbol{r}1})(\tilde{\boldsymbol{e}}_{\delta \boldsymbol{r}}^T \tilde{\boldsymbol{e}}_{\delta \boldsymbol{v}}) + p_{\delta \boldsymbol{r}0} p_{\delta \boldsymbol{r}1}(\epsilon_{\delta \boldsymbol{r}}^2 - \|\tilde{\boldsymbol{e}}_{\delta \boldsymbol{r}}\|^2)\end{aligned}$$

and its time derivative is given as

$$\begin{aligned}\dot{\tilde{\zeta}}_{\delta \boldsymbol{r}}(\delta \tilde{\boldsymbol{x}}, \boldsymbol{u}, \delta \boldsymbol{d}, t) = -6\tilde{\boldsymbol{e}}_{\delta \boldsymbol{v}}^T(\boldsymbol{f}_v + \boldsymbol{u} + \delta \boldsymbol{d}) - 2\tilde{\boldsymbol{e}}_{\delta \boldsymbol{r}}^T(\frac{\mathrm{d}\boldsymbol{f}_v}{\mathrm{d}t} + \frac{\mathrm{d}\delta \boldsymbol{d}}{\mathrm{d}t}) \\ -2(p_{\delta \boldsymbol{r}0} + p_{\delta \boldsymbol{r}1})(\tilde{\boldsymbol{e}}_{\delta \boldsymbol{v}}^T \tilde{\boldsymbol{e}}_{\delta \boldsymbol{v}} + \tilde{\boldsymbol{e}}_{\delta \boldsymbol{r}}^T(\boldsymbol{f}_v + \boldsymbol{u} + \delta \boldsymbol{d})) - p_{\delta \boldsymbol{r}0} p_{\delta \boldsymbol{r}1}(2\tilde{\boldsymbol{e}}_{\delta \boldsymbol{v}}^T \tilde{\boldsymbol{e}}_{\delta \boldsymbol{r}})\end{aligned} \tag{4.5.1}$$

Where $\delta \boldsymbol{d} \in \mathcal{W}$ is the orbital perturbations vector. It is noted that $\frac{\mathrm{d}\boldsymbol{u}}{\mathrm{d}t} = 0 \ \forall t \in \mathcal{T}_k$ applying the *Zero-Order Hold* control scheme. The constraint $\tilde{\zeta}_{\delta \boldsymbol{r}}$ is a piece-wise differentiable function of time (as all the functions appearing in its definition are at least piece-wise differentiable). A valid Lipschitz constant

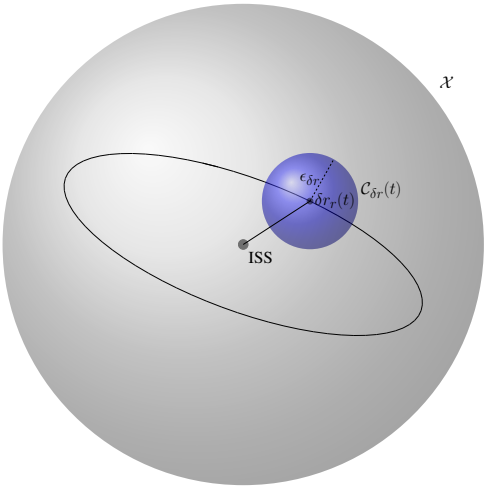

Figure 4.4: 3D representation of the safe $\mathcal{C}_{\delta \boldsymbol{r}}$ set compared to the set $\mathcal{X}$.

$L_{\delta \boldsymbol{r}}$ for $\dot{\tilde{\zeta}}_{\delta \boldsymbol{r}}$ is then given by Lemma 5 as

$$L_{\delta \boldsymbol{r}} = \sup_{(\delta \boldsymbol{x}, \boldsymbol{u}, \delta \boldsymbol{d}, t) \in \mathcal{X} \times \mathcal{U} \times \mathcal{W} \times \mathbb{R}_{\geq 0}} |\dot{\tilde{\zeta}}_{\delta \boldsymbol{r}}(\delta \boldsymbol{x}, \boldsymbol{u}, \delta \boldsymbol{d}, t)|$$

A critical issue arise as upper bounding $L_{\delta \boldsymbol{r}}$ over $\mathcal{X}$ is excessively conservative for the current mission scenario as $\mathcal{C}_{\delta \boldsymbol{r}}(t)$ is only a small subset of $\mathcal{X}$. Indeed, the safe set is a moving sphere of a few meters in diameter, while the set $\mathcal{X}$ is commonly a sphere with a diameter that is roughly one order of magnitude higher in diameter (See Figure 4.4 for example). This problem is solved by finding a set that minimally upper bounds the safe set $\mathcal{C}_{\delta \boldsymbol{r}}$. Given that each inspector has a finite maximum acceleration, and that the state is started from within $\mathcal{C}_{\delta \boldsymbol{r}}$, it is possible to find a set $\mathcal{S}_{\delta \boldsymbol{r}}(\|\boldsymbol{u}\|, \Delta t, t)$ that contains all the possible states of the system at time step $k(\Delta t + 1)$. This set will be defined shortly. First, it is noted that inside the safe set, a valid Lipschitz constant $L_{\delta \boldsymbol{r}}$ for $\dot{\tilde{\zeta}}_{\delta \boldsymbol{r}}(\delta \boldsymbol{x}, \boldsymbol{u}, \delta \boldsymbol{d}, t)$ can be obtained by direct application of the Cauchy-Schwarz inequality over all the dot products present in the analytical form of $\dot{\tilde{\zeta}}_{\delta \boldsymbol{r}}$ and assuming all vectors have their maximum norm

$$L_{\delta \boldsymbol{r}}(\|\boldsymbol{u}\|_+, \Delta t) = 6\epsilon_{\delta \boldsymbol{v}}(\epsilon_f + \epsilon_d + \|\boldsymbol{u}\|_+) + 2\epsilon_{\delta \boldsymbol{r}} \left(\|\frac{\mathrm{d}f_v}{\mathrm{d}t}\|_+ + \|\frac{\mathrm{d}\delta \boldsymbol{d}}{\mathrm{d}t}\|_+ \right) + 2(p_{\delta \boldsymbol{r}0} + p_{\delta \boldsymbol{r}1})(\epsilon_{\delta \boldsymbol{v}}^2 + \epsilon_{\delta \boldsymbol{r}}(\epsilon_f + \epsilon_d + \|\boldsymbol{u}\|_+)) + 2p_{\delta \boldsymbol{r}0} p_{\delta \boldsymbol{r}1}(\epsilon_{\delta \boldsymbol{v}} \epsilon_{\delta \boldsymbol{r}}) \tag{4.5.2}$$

Where term $\|\frac{\mathrm{d}\boldsymbol{f}_v}{\mathrm{d}t}\|_+$ is the maximum norm of the total time derivative of $\boldsymbol{f}_v$ and it is a complex function of the maximum control input $\|\boldsymbol{u}\|_+$ and the desired

PRO geometry, while ϵ_d is the defined as

$$\epsilon_d = \underset{\delta \boldsymbol{d} \in \mathcal{W}}{max} \|\delta \boldsymbol{d}\| = \|\delta \boldsymbol{d}\|_+$$

In Appendix A.4 a full analytical first order approximation for $\|\frac{\mathrm{d}\boldsymbol{f}_v}{\mathrm{d}t}\|_+$ is developed for circular orbits only (which is the case for the ISS orbit). Given the approximately constant angular velocity ω_w for the ISS orbit, the definition of $\|\frac{\mathrm{d}f_v}{\mathrm{d}t}\|_+$ from Appendix A.4 is

$$\begin{aligned}\|\frac{\mathrm{d}\boldsymbol{f}_v}{\mathrm{d}t}\|_+ =& \|\delta \ddot{\boldsymbol{r}}_g\|_+ + 3\omega_w \epsilon_f + 3\omega_w^2 \|\delta \boldsymbol{v}\|_+ + \omega_w^3 \|\delta \boldsymbol{r}\|_+ + \|\delta \dot{\boldsymbol{d}}\|_+ + 3\omega_w \|\boldsymbol{u}\|_+ \\ =& qq + 3\omega_w(\epsilon_f + \|\boldsymbol{u}\|_+ + \epsilon_d)\end{aligned} \tag{4.5.3}$$

Where the term qq is defined as

$$qq = \|\ddot{\boldsymbol{r}}_g\|_+ + 3\omega_w^2 \|\delta \boldsymbol{v}\|_+ + \|\delta \dot{\boldsymbol{d}}\|_+ + \omega_w^3 \|\delta \boldsymbol{r}\|_+ \tag{4.5.4}$$

The upper bounds $\|\delta \boldsymbol{v}\|_+$ and $\|\delta \boldsymbol{r}\|_+$ are the maximum absolute relative distance and the maximum relative velocity of the inspector relative to the ISS. Both these parameters could be approximated as

$$\begin{aligned}\|\delta \boldsymbol{v}\|_+ &\approx \|\delta \boldsymbol{v}_r\|_+ \\ \|\delta \boldsymbol{r}\|_+ &\approx \|\delta \boldsymbol{r}_r\|_+\end{aligned}$$

where $\|\delta \boldsymbol{v}_r\|_+$ and $\|\delta \boldsymbol{r}_r\|_+$ are computed from the analytical definition of the reference PRO (Section 2.2.4). This approximation is valid for relatively small velocity and position errors compared to the reference trajectory. From the nominal maximum velocity error $\epsilon_{\delta \boldsymbol{v}}$ and maximum nominal position error $\epsilon_{\delta \boldsymbol{v}}$, it is possible to define a set $\mathcal{S}_{\delta \boldsymbol{r}}(\|\boldsymbol{u}\|, \Delta t, t) \supset \mathcal{C}_{\delta \boldsymbol{r}}(t)$ such that

$$\mathcal{S}_{\delta \boldsymbol{r}}(\|\boldsymbol{u}\|, \Delta t, t) = \{\delta \boldsymbol{x} \in \mathcal{X} : \|\tilde{\boldsymbol{e}}_{\delta \boldsymbol{r}}\| \leq \tilde{\epsilon}_{\delta \boldsymbol{r}}(\Delta t, \|\boldsymbol{u}\|_+) \wedge \|\tilde{\boldsymbol{e}}_{\delta \boldsymbol{v}}\| \leq \tilde{\epsilon}_{\delta \boldsymbol{v}}(\Delta t, \|\boldsymbol{u}\|_+)\}$$

Where

$$\begin{aligned}\tilde{\epsilon}_{\delta \boldsymbol{r}}(\Delta t, \|\boldsymbol{u}\|_+) &= \epsilon_{\delta \boldsymbol{r}} + (\epsilon_f + \epsilon_d + \|\boldsymbol{u}\|_+)\frac{\Delta t^2}{2} + \epsilon_{\delta \boldsymbol{v}} \Delta t \\ \tilde{\epsilon}_{\delta \boldsymbol{v}}(\Delta t, \|\boldsymbol{u}\|_+) &= \epsilon_{\delta \boldsymbol{v}} + (\epsilon_f + \epsilon_d + \|\boldsymbol{u}\|_+)\Delta t\end{aligned} \tag{4.5.5}$$

Informally, $\mathcal{S}_{\delta \boldsymbol{r}}(\|\boldsymbol{u}\|, \Delta t, t)$ represents the set that minimally upper bounds $\mathcal{C}_{\delta \boldsymbol{r}}(t)$ under worse case scenario acceleration. Indeed, given that at time $k\Delta t$ the system is started at the condition $\boldsymbol{e}_{\delta \boldsymbol{r}} = \epsilon_{\delta \boldsymbol{r}}$ and $\boldsymbol{e}_{\delta \boldsymbol{v}} = \epsilon_{\delta \boldsymbol{v}}$, the maximum

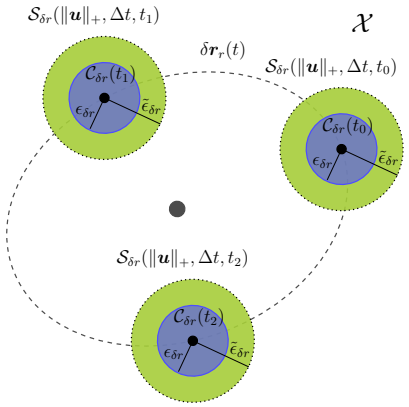

Figure 4.5: Graphical representation of the set $\mathcal{S}_{\delta \boldsymbol{r}}(\|\boldsymbol{u}\|, \Delta t, t)$ for three different time steps. In green is the set $\mathcal{S}_{\delta \boldsymbol{r}}(\|\boldsymbol{u}\|, \Delta t, t)$ and in light blue is the safe set $\mathcal{C}_{\delta \boldsymbol{r}}(t)$. The size of the set $\mathcal{S}_{\delta \boldsymbol{r}}(\|\boldsymbol{u}\|, \Delta t, t)$ depends upon the defined maximum input control and maximum time step. Increasing $\|\boldsymbol{u}\|_+$ or Δt has the effect of increasing the size of $\mathcal{S}_{\delta \boldsymbol{r}}(\|\boldsymbol{u}\|, \Delta t, t)$ compared to $\mathcal{C}_{\delta \boldsymbol{r}}(t)$

velocity and position error variations for a given maximum constant control input norm $\|\boldsymbol{u}\|_+$ and a given time interval Δt are upper bounded on the interval $\mathcal{T}_k = [k\Delta t, (k+1\Delta t)]$ as

$$\begin{aligned} \|\tilde{\boldsymbol{e}}_{\delta \boldsymbol{v}}(t) - \tilde{\boldsymbol{e}}_{\delta \boldsymbol{v}}(k\Delta t)\| &\leq (\epsilon_f + \epsilon_d + \|\boldsymbol{u}\|_+)\Delta t \quad \forall t \in \mathcal{T}_k \\ \|\tilde{\boldsymbol{e}}_{dr}(t) - \tilde{\boldsymbol{e}}_{dr}(k\Delta t)\| &\leq (\epsilon_f + \epsilon_d + \|\boldsymbol{u}\|_+)\frac{\Delta t^2}{2} + \epsilon_{\delta \boldsymbol{v}}\Delta t \quad \forall t \in \mathcal{T}_k \end{aligned} \tag{4.5.6}$$

Hence, inside the set $\mathcal{S}_{\delta \boldsymbol{r}}(\Delta t, \|\boldsymbol{u}\|_+, t)$ a valid Lipschitz constant $L_{\delta \boldsymbol{r}}$ is given by

$$\begin{aligned} L_{\delta \boldsymbol{r}}(\|\boldsymbol{u}\|_+, \Delta t) \leq & 6\tilde{\epsilon}_{\delta \boldsymbol{v}}(\epsilon_f + \epsilon_d + \|\boldsymbol{u}\|_+) + 2\tilde{\epsilon}_{\delta \boldsymbol{r}}\left(\|\frac{\mathrm{d}f_v}{\mathrm{d}t}\|_+\right) + \\ & 2(p_{\delta \boldsymbol{r}0} + p_{\delta \boldsymbol{r}1})(\tilde{\epsilon}^2_{\delta \boldsymbol{v}} + \tilde{\epsilon}_{\delta \boldsymbol{r}}(\epsilon_f + \epsilon_d + \|\boldsymbol{u}\|_+)) + \\ & 2p_{\delta \boldsymbol{r}0}p_{\delta \boldsymbol{r}1}(\tilde{\epsilon}_{\delta \boldsymbol{v}}\tilde{\epsilon}_{\delta \boldsymbol{r}}) \end{aligned} \tag{4.5.7}$$

It is noted that $L_{\delta \boldsymbol{r}}(\|\boldsymbol{u}\|_+, \Delta t)$ is only a valid Lipschitz constant on the set $S_{\delta \boldsymbol{r}}(\|\boldsymbol{u}\|_+, \Delta t, t)$ and not a globally valid Lipschitz constant over the full domain $\mathcal{X}$. Finding a globally valid Lipschitz constant is considered impractical as it would require extremely high control authorities to satisfy the CBF and HOCBF constraints. Regarding the constant $c_{\delta \boldsymbol{r}}$ from Lemma

5 (identified as c in the Lemma statement), the same issue arises as upper bounding $c_{\delta \boldsymbol{r}}$ over the full set $\mathcal{X}$ would be overly conservative. For this reason, a maximum value for $c_{\delta \boldsymbol{r}}$ is only found for the set $\mathcal{S}_{\delta \boldsymbol{r}}(\Delta t, \|\boldsymbol{u}\|_+, t)$ as

$$c_{\delta \boldsymbol{r}} = 2\tilde{\epsilon}_{\delta \boldsymbol{r}}$$

The continuous time HOCBF constraint $\zeta_{\delta \boldsymbol{r}}$ is then modified according to Lemma 5, in order to obtain a valid robust SD-HOCBF constraint as

$$\zeta_{\delta \boldsymbol{r}}(\boldsymbol{x}(k\Delta t), \boldsymbol{u}(k\Delta t), k\Delta t) - c_{\delta \boldsymbol{r}}\epsilon_d - L_{\delta \boldsymbol{r}}(\|\boldsymbol{u}\|_+, \Delta t)\Delta t \geq 0$$

The pair of maximum control afford and time steps, $(\|\boldsymbol{u}\|_+, \Delta t)$, for which it is possible to respect the SD-HOCBF constraint $\zeta_{\delta \boldsymbol{r}} - c_{\delta \boldsymbol{r}}\epsilon_d - L_{\delta \boldsymbol{r}}\Delta t \geq 0$ is then found on the semi-half space $\phi_{\delta \boldsymbol{r}}(\|\boldsymbol{u}\|_+, \Delta t)$ defined by the condition $\phi_{\delta \boldsymbol{r}}(\|\boldsymbol{u}\|_+, \Delta t) \geq 0$ where $\phi_{\delta \boldsymbol{r}}$ is defined as

$$\phi_{\delta \boldsymbol{r}}(\|\boldsymbol{u}\|_+, \Delta t) = \|\boldsymbol{u}\|_+ - \bar{\beta}_{\delta \boldsymbol{r}} - c_{\delta \boldsymbol{r}}\epsilon_d - L_{\delta \boldsymbol{r}}(\|\boldsymbol{u}\|_+, \Delta t)\Delta t \tag{4.5.8}$$

4.5.2 Robust velocity SD-CBF

Similarly to the previous subsection, the perturbed CBF constraint $\tilde{\psi}_{\delta \boldsymbol{v}}(\delta\tilde{\boldsymbol{x}}, \boldsymbol{u}, \delta\boldsymbol{d}, t)$ is defined as

$$\tilde{\psi}_{\delta \boldsymbol{v}}(\delta\tilde{\boldsymbol{x}}, \boldsymbol{u}, \delta\boldsymbol{d}, t) := -2\tilde{\boldsymbol{e}}_{\delta \boldsymbol{v}}^T(\boldsymbol{f}_v + \boldsymbol{u} + \delta\boldsymbol{d}) + p_{\delta \boldsymbol{v}0}(\epsilon_{\delta \boldsymbol{v}}^2 - \|\tilde{\boldsymbol{e}}_{\delta \boldsymbol{v}}\|^2) \tag{4.5.9}$$

and its first time derivative is given by

$$\begin{aligned}\dot{\tilde{\psi}}_{\delta \boldsymbol{v}}(\delta\tilde{\boldsymbol{x}}, \boldsymbol{u}, \delta\boldsymbol{d}, t) = -2\tilde{\boldsymbol{e}}_{\delta \boldsymbol{v}}^T\left(\frac{\mathrm{d}\boldsymbol{f}_v}{\mathrm{d}t} + \frac{\mathrm{d}\delta\boldsymbol{d}}{\mathrm{d}t}\right) - 2\|\boldsymbol{f}_v + \boldsymbol{u} + \delta\boldsymbol{d}\|^2 + \\ p_{\delta \boldsymbol{v}0}(-2\tilde{\boldsymbol{e}}_v^T(\boldsymbol{f}_v + \boldsymbol{u} + \delta\boldsymbol{d}))\end{aligned} \tag{4.5.10}$$

By the same arguments developed for the SD-HOCBF, a set $\mathcal{S}_{\delta \boldsymbol{v}}(\|\boldsymbol{u}\|_+, \Delta t, t) \supset \mathcal{C}_{\delta \boldsymbol{v}}(t)$ is defined such that

$$\mathcal{S}_{\delta \boldsymbol{v}}(\|\boldsymbol{u}\|_+, \Delta t, t) := \{\delta\boldsymbol{x} \in \mathcal{X} : \|\tilde{\boldsymbol{e}}_{\delta \boldsymbol{v}}\| \leq \tilde{\epsilon}_{\delta \boldsymbol{v}}\}$$

Where the definition of $\tilde{\epsilon}_{\delta \boldsymbol{v}}$ is given in equation (4.5.5). Hence inside $\mathcal{S}_{\delta \boldsymbol{v}}$ a valid Lipschitz constant for $\tilde{\psi}(\delta\tilde{\boldsymbol{x}}, \boldsymbol{u}, t)$ in equation (4.5.10) is obtained again by applying the Cauchy–Schwarz inequality and by setting all the vectors to

their maximum norm inside $\mathcal{S}_{\delta \boldsymbol{v}}$

$$L_{\delta \boldsymbol{v}}(\|\boldsymbol{u}\|_+, \Delta t) = 2\tilde{\epsilon}_{\delta \boldsymbol{v}} \left(\|\frac{\mathrm{d}\boldsymbol{f}_v}{\mathrm{d}t}\|_+ + \|\frac{\mathrm{d}\delta \boldsymbol{d}}{\mathrm{d}t}\|_+ \right) + 2(\epsilon_f + \|\boldsymbol{u}\|_+ + \epsilon_d)^2 + p_{\delta \boldsymbol{v}0}(2\tilde{\epsilon}_{\delta \boldsymbol{v}}(\epsilon_f + \|\boldsymbol{u}\|_+ + \epsilon_d)) \tag{4.5.11}$$

and a suitable constant $c_{\delta \boldsymbol{v}}$ is given from Lemma 4 as

$$c_{\delta \boldsymbol{v}} = 2\tilde{\epsilon}_{\delta \boldsymbol{v}}$$

The continuous time CBF constraint $\psi_{\delta \boldsymbol{v}}$ is then modified in order to obtain a valid robust SD-CBF constraint as

$$\psi_{\delta \boldsymbol{v}}(\boldsymbol{x}(k\Delta t), \boldsymbol{u}(k\Delta t), k\Delta t) - L_{\delta \boldsymbol{v}}(\|\boldsymbol{u}\|_+, \Delta t)\Delta t - c_{\delta \boldsymbol{v}}\epsilon_d \geq 0$$

As already developed in the case of the SD-HOCBF, the space of minimum maximum control authorities and time steps for which it is possible to respect the SD-CBF constraint is found on the semi-half space $\phi_{\delta \boldsymbol{v}}(\|\boldsymbol{u}\|_+, \Delta t) \geq 0$ where $\phi_{\delta \boldsymbol{v}}(\|\boldsymbol{u}\|_+, \Delta t)$ is defined by

$$\phi_{\delta \boldsymbol{v}}(\|\boldsymbol{u}\|_+, \Delta t) = \|\boldsymbol{u}\|_+ - \bar{\beta}_{\delta \boldsymbol{v}} - c_{\delta \boldsymbol{v}}\epsilon_d - L_{\delta \boldsymbol{v}}(\|\boldsymbol{u}\|_+, \Delta t)\Delta t \tag{4.5.12}$$

4.5.3 Zero-actuation Lipschitz constants

In addition to the constants $L_{\delta \boldsymbol{r}}$ and $L_{\delta \boldsymbol{v}}$ developed in the previous section, it is relevant to define two new constants $L^z_{\delta \boldsymbol{r}}$ and $L^z_{\delta \boldsymbol{v}}$ as

$$\begin{aligned} L^z_{\delta \boldsymbol{r}} &= L_{\delta \boldsymbol{r}}(\boldsymbol{0}, \Delta t) \\ L^z_{\delta \boldsymbol{v}} &= L_{\delta \boldsymbol{v}}(\boldsymbol{0}, \Delta t) \end{aligned} \tag{4.5.13}$$

Where $L^z_{\delta \boldsymbol{v}}$ and $L^z_{\delta \boldsymbol{r}}$ are defined as

$$\begin{aligned} L^z_{\delta \boldsymbol{r}} &= 6\tilde{\epsilon}_{\delta \boldsymbol{v}}\epsilon_f + 2\tilde{\epsilon}_{\delta \boldsymbol{r}} \left(\|\frac{\mathrm{d}\boldsymbol{f}_v}{\mathrm{d}t}\|_+ + \|\frac{\mathrm{d}\delta \boldsymbol{d}}{\mathrm{d}t}\|_+ \right) + \\ &\quad 2(p_{\delta \boldsymbol{r}0} + p_{\delta \boldsymbol{r}1})(\tilde{\epsilon}^2_{\delta \boldsymbol{v}} + \tilde{\epsilon}_{\delta \boldsymbol{r}}(\epsilon_f + \epsilon_d)) + 2p_{\delta \boldsymbol{r}0}p_{\delta \boldsymbol{r}1}(\tilde{\epsilon}_{\delta \boldsymbol{v}}\tilde{\epsilon}_{\delta \boldsymbol{r}}) \\ L^z_{\delta \boldsymbol{v}} &= 2\tilde{\epsilon}_{\delta \boldsymbol{v}} \left(\|\frac{\mathrm{d}\boldsymbol{f}_v}{\mathrm{d}t}\|_+ + \|\frac{\mathrm{d}\delta \boldsymbol{d}}{\mathrm{d}t}\|_+ \right) + \\ &\quad 2(\epsilon_f + \epsilon_d)^2 + 2p_{\delta \boldsymbol{v}0}(\tilde{\epsilon}_{\delta \boldsymbol{v}}(\epsilon_f + \epsilon_d)) \end{aligned} \tag{4.5.14}$$

Note that the values of $\tilde{\epsilon}_{\delta \boldsymbol{v}}$ and $\tilde{\epsilon}_{\delta \boldsymbol{r}}$ in this case are given as in equation (4.5.5) considering $\|\boldsymbol{u}\|_+ = 0$. Moreover, the following short hand notation is applied to denote the nominal HOCBF and CBF constraints under zero actuation.

$$\zeta^z_{\delta \boldsymbol{r}}(\delta \boldsymbol{x}, t) = \zeta_{\delta \boldsymbol{r}}(\delta \boldsymbol{x}, \boldsymbol{0}, t)$$
$$\psi^z_{\delta \boldsymbol{v}}(\delta \boldsymbol{x}, t) = \psi_{\delta \boldsymbol{v}}(\delta \boldsymbol{x}, \boldsymbol{0}, t)$$

In the next section it will be clear how these definitions will become useful for triggering activation of the MPC controller.

4.6 MPC Control Scheme

In the previous subsections, an analytical form for the position SD-HOCBF constraints and the velocity SD-CBF were appropriately defined. In the present subsection, the analytical MPC control scheme is developed based on the definition of these constraints. Three major issues are highlighted

1. While the SD-CBF constraint and the SD-HOCBF constraint could be independently satisfied, it is possible that there are certain state conditions inside $\mathcal{C}_{\delta \boldsymbol{r}} \cap \mathcal{C}_{\delta \boldsymbol{v}}$ for which there is no feasible control solution that satisfies both constraints.

2. It is necessary to define a triggering conditions such that the MPC controller is activated sparsely and such that the activation always occurs while the systems is still inside the safe set

3. The determination of the parameters $p_{\delta \boldsymbol{r}0}$,$p_{\delta \boldsymbol{r}1}$, $p_{\delta \boldsymbol{v}0}$ and d_s represent a hard design problem as there is no analytical procedure that yields a direct solution for these parameters.

Concerning the first issue, a solution similar to [8] is applied. Namely, the safe set $\mathcal{C}_{\delta \boldsymbol{r}} \cap \mathcal{C}_{\delta \boldsymbol{v}}$ is uniformly discretised and the following convex optimization

problem is solved

$$\min_{\boldsymbol{t},\boldsymbol{u}} -\boldsymbol{t}^T\boldsymbol{t} \tag{4.6.1a}$$

$$I\boldsymbol{t} \geq \boldsymbol{0} \tag{4.6.1b}$$

$$\|\boldsymbol{u}\|^2 \leq \|\boldsymbol{u}\|_+^2 \tag{4.6.1c}$$

$$\begin{aligned} -2\|\boldsymbol{e}_{\delta\boldsymbol{v}}\|^2 - 2\|\boldsymbol{e}_{\delta\boldsymbol{r}}\|\epsilon_f + 2\boldsymbol{e}_{\delta\boldsymbol{r}}^T\boldsymbol{u} - 2(p_{\delta\boldsymbol{r}0} + p_{\delta\boldsymbol{r}1})(\boldsymbol{e}_{\delta\boldsymbol{r}}^T\boldsymbol{e}_{\delta\boldsymbol{v}}) + \\ p_{\delta\boldsymbol{r}0}p_{\delta\boldsymbol{r}1}(\epsilon_{\delta\boldsymbol{r}}^2 - \|\boldsymbol{e}_{\delta\boldsymbol{r}}\|^2) - (L_{\delta\boldsymbol{r}}\Delta t - c_{\delta\boldsymbol{r}}\epsilon_d) - t_1 \geq 0 \end{aligned} \tag{4.6.1d}$$

$$-2\|\boldsymbol{e}_{\delta\boldsymbol{v}}\|\epsilon_f - 2\boldsymbol{e}_{\delta\boldsymbol{v}}^T\boldsymbol{u}(t) + p_{\delta\boldsymbol{v}0}(\epsilon_{\delta\boldsymbol{v}}^2 - \|\boldsymbol{e}_{\delta\boldsymbol{v}}\|^2) - L_{\delta\boldsymbol{v}}\Delta t + c_{\delta\boldsymbol{v}}\epsilon_d - t_2 \geq 0 \tag{4.6.1e}$$

(4.6.1f)

Where $\boldsymbol{t} = [t_1, t_2]$ is simply a dummy vector constrained to have only positive values from constraint (4.6.1b)(the symbol I is applied to denote the identity matrix). Constraint (4.6.1d) and (4.6.1e) are worst case scenario modification of the SD-HOCBF and SD-CBF constraints respectively for which it is assumed that the dynamic acceleration of the system is always directioned to maximally decrease the value of the SD-CBF and SF-HOCBF constraints. If a feasible solution to problem (4.6.1) is found over a sufficiently dense discretization of the set $\mathcal{C}_{\delta\boldsymbol{r}} \cap \mathcal{C}_{\delta\boldsymbol{v}}$, it is then considered possible to satisfy both the SD-HOCBF and SD-CBF constraints over the continuous set of safe states. Regarding the trigger condition, it is recalled again that each inspector is not continuously actuated. The controller should only be actuated when the state of the inspector is sufficiently close to the border of the safe set $\mathcal{C}_{\delta\boldsymbol{r}} \cap \mathcal{C}_{\delta\boldsymbol{v}}$ while the inspector is left free to follow it reference PRO until the state reaches the border of the safe set again. The following two conditions are defined in order to trigger the activation of the MPC controller when the inspectors are not actuated.

$$\zeta_{\delta\boldsymbol{r}}(\delta\boldsymbol{x}, \boldsymbol{0}, k\Delta t) \leq L_{\delta\boldsymbol{r}}^z\Delta t + c_{\delta\boldsymbol{r}}\epsilon_d \tag{4.6.2a}$$

$$\psi_{\delta\boldsymbol{v}}(\delta\boldsymbol{x}, \boldsymbol{0}, k\Delta t) \leq L_{\delta\boldsymbol{v}}^z\Delta t + c_{\delta\boldsymbol{v}}\epsilon_d \tag{4.6.2b}$$

When either of these last two conditions becomes true, the MPC controller is activated to reset the system to along it reference trajectory. Indeed equations (4.6.2a) and (4.6.2b) are first hit when the state of the system is still inside the safe set as the maximum variation of the constraint $\zeta_{\delta\boldsymbol{r}}$ and $\psi_{\delta\boldsymbol{v}}$ over an interval Δt is given by $L_{\delta\boldsymbol{r}}^z\Delta t + c_{\delta\boldsymbol{r}}\epsilon_d$ and $L_{\delta\boldsymbol{v}}^z\Delta t + c_{\delta\boldsymbol{v}}\epsilon_d$ when the inspector is not actuated. The final issue related to the consistent definition of parameters $p_{\delta\boldsymbol{r}0}$,$p_{\delta\boldsymbol{r}1}$, $p_{\delta\boldsymbol{v}0}$ and d_s that are able to satisfy all the feasibility

conditions specified so far is faced by simple trial and error in the current thesis. The problem is commonly approached empirically by parameter optimization algorithms which are not considered in the current work. An example of parameters optimization is given in [23]. With reference to all the aforementioned considerations, the final general FHOC problem to be solved by the MPC for each inspector is defined as follows

$$\min_{\bar{\boldsymbol{u}} \in \mathcal{U}^N} \quad V_N(\boldsymbol{e}_{\delta \boldsymbol{x}}(k\Delta t), \bar{\boldsymbol{u}}(k\Delta t)) \tag{4.6.3a}$$

$$\delta \boldsymbol{x}(0, k\Delta t) = \delta \tilde{\boldsymbol{x}}(k\Delta t) \tag{4.6.3b}$$

$$\delta \boldsymbol{x}((i+1)\Delta t | k\Delta t) = \boldsymbol{F}(\delta \boldsymbol{x}(i\Delta t), \boldsymbol{b}(i\Delta t), \boldsymbol{u}(i\Delta t)) \, \forall i \in [0, 1..N-1] \tag{4.6.3c}$$

$$\|\boldsymbol{u}(i\Delta t | k\Delta t)\|^2 \leq \|\boldsymbol{u}\|_+^2 \qquad \forall i \in [0, 1, ..N-1] \tag{4.6.3d}$$

$$\zeta_{\delta \boldsymbol{r}}(\delta \boldsymbol{x}(0|k\Delta t), \boldsymbol{u}(k\Delta t), k\Delta t) \geq L_{\delta \boldsymbol{r}} \Delta t + c_{\delta \boldsymbol{r}} \epsilon_d \, \forall i \in [0, 1, ..N-1] \tag{4.6.3e}$$

$$\psi_{\delta \boldsymbol{v}}(\delta \boldsymbol{x}(0|k\Delta t), \boldsymbol{u}(k\Delta t), k\Delta t) \geq L_{\delta \boldsymbol{v}} \Delta t + c_{\delta \boldsymbol{v}} \epsilon_d \qquad \forall i \in [0, 1, ..N-1] \tag{4.6.3f}$$

Where the constraint (4.6.3b) is the initial condition constraint for which the initial nominal state $\delta \boldsymbol{x}$ is equal to the measured perturbed state $\delta \tilde{\boldsymbol{x}}$, the constraint (4.6.3c) is the dynamic constraint where $\boldsymbol{F}$ is the nominal inspector discrete dynamics from (2.3.4), constraint (4.6.3d) is the convex constraint on the maximum control authority. Constraint (4.6.3e) and (4.6.3f) are the SD-HOCBF constraint on the position and the SD-CBF constraint on the velocity respectively. The value function to be optimised is defined as

$$\begin{aligned} V_N(\boldsymbol{e}_{\delta \boldsymbol{x}}(k\Delta t), \bar{\boldsymbol{u}}(k\Delta t)) := \sum_{i=0}^{N-1} \boldsymbol{e}_{\delta \boldsymbol{x}}^T(i\Delta t | k\Delta t) Q \boldsymbol{e}_{\delta \boldsymbol{x}}(i\Delta t | k\Delta t) + \\ \boldsymbol{e}_{\boldsymbol{u}}^T(i\Delta t | k\Delta t) R \boldsymbol{e}_{\boldsymbol{u}}(i\Delta t | k\Delta t) + V_f(\boldsymbol{e}_{\delta \boldsymbol{x}}(N\Delta t | k\Delta t)) \end{aligned} \tag{4.6.4}$$

Where the terminal cost $V_f(\boldsymbol{e}_{\delta \boldsymbol{x}}(N\Delta t|k\Delta t))$ is defined as

$$\boldsymbol{e}_{\delta \boldsymbol{x}}(N\Delta t|k\Delta t))^T P^* \boldsymbol{e}_{\delta \boldsymbol{x}}(N\Delta t|k\Delta t)))$$

with terminal cost matrix $P^* := \mu P$ and $\mu \geq 1$ such that P solves the *Discrete Algebraic Riccati Equation* (DARE)

$$P = A_d^T P A_d - (A_d^T P_d B)(R + B_d^T P B_d)^{-1}(B_d^T P A_d) + Q. \tag{4.6.5}$$

The matrices A_d and B_d appearing in the DARE directly derive from the sample data CW model in equation (2.2.16). On the other hand, R and Q are parameters of the problem that can be chosen to give the best control performance.

4.6.0.1 Recursive feasibility and stability

As mentioned in the previous section, the simultaneous feasibility of the SD-CBF and SD-HOCBF constraints inside the safe set is determined through a gird search method over a dense discretization of the safe set $\mathcal{C}_{\delta \boldsymbol{r}} \cap \mathcal{C}_{\delta \boldsymbol{v}}$. The resulting state space that would need to be sampled is a six dimensional state space (since $\delta \boldsymbol{x} \in \mathbb{R}^6$). Due to the spherical symmetry of the sets $\mathcal{C}_{\delta \boldsymbol{r}}$ and $\mathcal{C}_{\delta \boldsymbol{v}}$ it is possible to reduce the problem to three dimensions only. Namely, the position error norm $\|\boldsymbol{e}_{\delta \boldsymbol{r}}\|$, the velocity error norm $\|\boldsymbol{e}_{\delta \boldsymbol{v}}\|$ and the angle θ between these two vectors (See Figure 4.6). The cartesian product $[0, \epsilon_{\delta \boldsymbol{r}}] \times [0, \pi] \times [0, \epsilon_{\delta \boldsymbol{v}}]$ is hence discretised and applied to search for unfeasible solutions to (4.6.1). It is recalled that for angles θ that are smaller than $\pi/2$ (See Figure 4.6), the radial component of the speed error should be clipped to satisfy equation (4.3.20), which is required to maintain the state of the inspector inside the safe set. Once this feasibility analysis is numerically developed, the definition of a terminal set becomes unnecessary. Concerning the stability, the problem is solved following the approach defined by [7]. Namely, it assumed that the cost function in (4.6.4) is a Lyapunov functions for every state $\delta \boldsymbol{x}$ within the safe set $\mathcal{C}_{\delta \boldsymbol{r}} \cap \mathcal{C}_{\delta \boldsymbol{v}}$. From this assumption, the stability of the specified MPC scheme can be proved similarly to [7]. Note that differently form [7], the feasibility of the MPC scheme is only proved numerically and not analytically due to the multiple CBF constraints involved, such the the stability and feasibility results are weaker than the ones developed in [7].

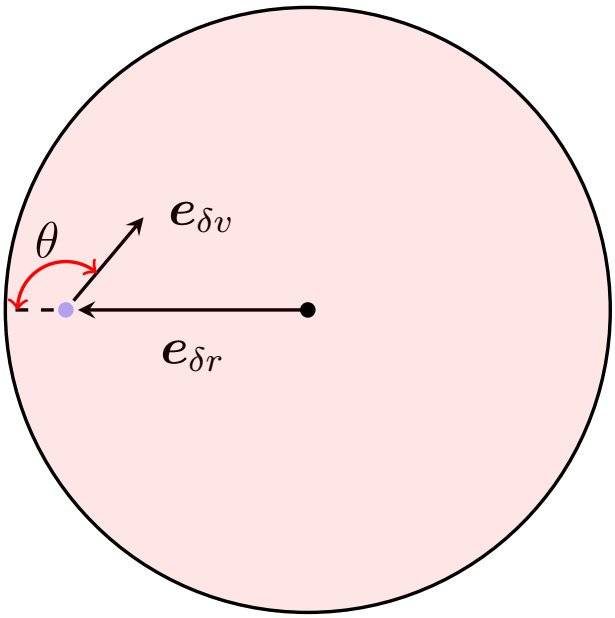

Figure 4.6: Graphical representation of the three main vectors involved in the grid search for unfeasible simultaneous satisfaction of the SD-HOCBF and the SD-CBF constraints. The position error vector $\boldsymbol{e}_{\delta \boldsymbol{r}}$ is maintained in fixed direction and its magnitude its varied from its minimum to maximum value. On the other hand, the velocity vector $\boldsymbol{e}_{\delta \boldsymbol{v}}$ is modified both in direction and magnitude during the grid search algorithm.

Chapter 5

Simulations and Results

In this subsection the control scheme developed in the previous Chapters is tested by means of computer simulation for a single inspector and a multi-agent inspection mission. The simulation is fully developed in *Python* and the optimization library *CasADi* is applied to solve the nonlinear optimal control problem (4.6.3) by means of the Interior Point Method algorithm. The simulations were preformed on a 2,3 GHz Dual-Core Intel Core i5 CPU with 8GB of RAM. The simulation environment in which the inspector and the ISS are propagated takes into account for zonal harmonic terms up to order 6 and exponential atmospheric drag. The *open source* astrodynamics toolbox *TuDat*[*] was applied to asses the accuracy of the implemented model.

5.1 Single inspector simulation

In this subsection the performance of the MPC controller designed in the previous section is evaluated in simulation for a single inspector, while the multi-agent case is analysed in the next subsection. For both the multi-agent and single agent mission scenarios, the inspector is assumed to be a 6U-CubeSat with a total mass of $10\ kg$ and an omnidirectional propulsion system capable of delivering a maximum of $200\ mN$ of thrust corresponding to a maximum acceleration of $0.02\ m/s^2$

[*]TuDat main wiki page : https://docs.tudat.space/en/stable/

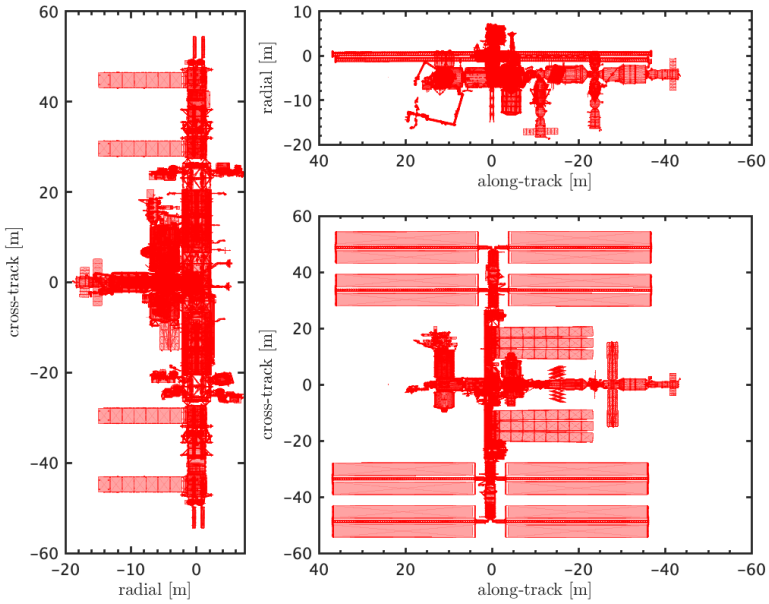

Figure 5.1: Plant of the ISS as seen in the $\mathcal{H}$ frame

	$m\ [kg]$	C_d	$S\ [m^2]$	CD	$f_{th}\ [N]$
ISS	4.194×10^5	2.2	1.300×10^2	3.409×10^{-4}	-
Inspector	1.000×10^1	2.2	6.000×10^{-2}	6.600×10^{-3}	2.00×10^{-1}

Table 5.1: Specific simulation parameters for the inspector parameters CubeSat and the ISS. The parameters presented for the ISS are obtained from [29]. The inspector parameters are obtained from [4]

These same specifications are applied in [4] for a similar mission and are considered to give a realistic operative scenario for the inspection mission. The ISS has a mass of $419400\ kg$ and no actuation capabilities. The reference ISS orbit parameters are given is Table 4.1 while the physical specifics of the inspector and the ISS are summarised in Table 5.1. It is futher assumed that the inspector is already engaged into a PRO$(70 \times 140 \times 0 - 0)$ around the ISS. As pointed out in [4], CubeSats are commonly deployed directly from the ISS thanks to the *Nanorack* system *, but the injection phase into the PRO is not considered in the present work. The maximum safety distance $\epsilon_{\delta r}$ is selected

*https://nanoracks.com/products/iss-launch/

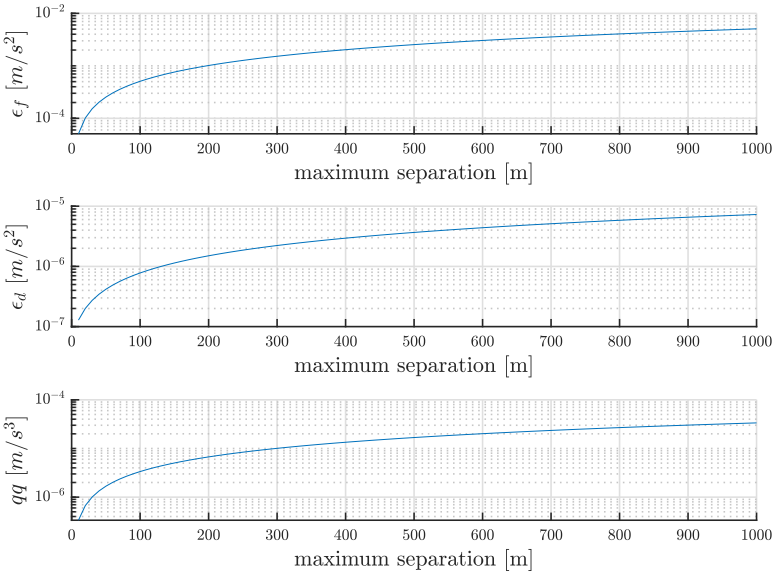

Figure 5.2: Computed value for ϵ_f,ϵ_d and qq as a function of the separation between the inspector and the ISS. Analytical formulation for ϵ_f,ϵ_d and qq is given in Appendix A.3. The atmospheric density is considered to be 3 g/km^3 at the altitude of the ISS assuming mean solar activity while the darg parameters for the inspector and the ISS are reported in Table 5.1

to be $10\ m$ with a maximum ISS-inspector separation of approximately 170 m for the selected PRO geometry. The parameter d_s is selected to be equal to $3\ m$ such that the maximum allowed speed error ϵ_v is computed based on the defined safe distance d_s as

$$\epsilon_v = \frac{p_{\delta \boldsymbol{r}0}}{2}\frac{\epsilon_r^2 - d_s^2}{d_s} = 15.2 \quad cm/s \tag{5.1.1}$$

Figure 5.2 shows the value of the maximum dynamic acceleration ϵ_f, maximum perturbation acceleration ϵ_d and the parameters qq (from (4.5.3)) as a function of the separation between the inspector and the ISS. These values are computed analytically in first order approximation in Appendix A.3. The maximum control authority of the inspector is one order of magnitude higher than ϵ_f for the given PRO geometry, while the worst case contribution from the orbital perturbations (ϵ_d) is three orders of magnitude lower. The further is the inspector position with respect to the ISS and the higher are the differential orbital perturbations and differential dynamical accelerations as shown in Figure 5.2. The parameters set $p_{\delta \boldsymbol{r}0}$,$p_{\delta \boldsymbol{r}1}$ and $p_{\delta \boldsymbol{v}0}$ are obtained by a trial and error approach such that a feasible region $(\|\boldsymbol{u}\|_+, \Delta t)$ for which the condition $\phi_{\delta \boldsymbol{r}}(\|\boldsymbol{u}\|_+, \Delta t) \geq 0$ (4.5.8) and $\phi_{\delta \boldsymbol{v}}(\|\boldsymbol{u}\|_+, \Delta t) \geq 0$ (4.5.12) exist (Figure 5.3b) and such that the problem (4.6.1) always has a feasible solution over a dense discretization of the set $[0, \epsilon_{\delta \boldsymbol{r}}] \times [0, \pi] \times [0, \epsilon_{\delta \boldsymbol{v}}]$ (Figure 5.3a). In Figure 5.3a the states for which problem (4.6.1) is feasible are represented in black and unfeasible states are represented in red. It is noted from Figure 5.3a that both the SD-CBF and SD-HOCBF constraint can be simultaneously satisfied over the full discrete configuration space as no unfeasible solution was found for (4.6.1). For this particular case, the position error norm $\|\boldsymbol{e}_{\delta \boldsymbol{r}}\|$ is discretised in steps of $6\ cm$, the velocity magnitude step is discretised in steps of $0.1\ cm/s$ and the angle range is discretised in steps of $1\ deg$. The curvature shown in the lower right part of the grid is due to the clipping of the speed norm as the radial velocity error component allowed inside the safe set $\mathcal{C}_{\delta \boldsymbol{v}}$ is limited for angle θ between 0 and 90 degrees For this simulation, the parameters $p_{\delta \boldsymbol{r}0}$ and $p_{\delta \boldsymbol{r}1}$ are selected to be equal to 0.01 and 0.1 for the position SD-HOBF and $p_{\delta \boldsymbol{v}0}$ is selected to be equal to 0.1 for the velocity SD-CBF. The resulting feasible $(\|\boldsymbol{u}\|_+, \Delta t)$ region is shown in the right panel of Figure 5.3b while the constants $L_{\delta \boldsymbol{r}}$,$L_{\delta \boldsymbol{v}}$,$L^z_{\delta \boldsymbol{v}}$,$L^z_{\delta \boldsymbol{r}}$ are summarised in Table 5.2. The size of the feasible $(\|\boldsymbol{u}\|_+, \Delta t)$ space in Figure 5.3b is sensible to the parameters $p_{\delta \boldsymbol{v}0}$,$p_{\delta \boldsymbol{r}1}$ and $p_{\delta \boldsymbol{r}0}$ such that a very narrow corridor exist for the selection of these parameters. The main reason for this high sensibility is due to the low control authority allowed by the propulsion system of the

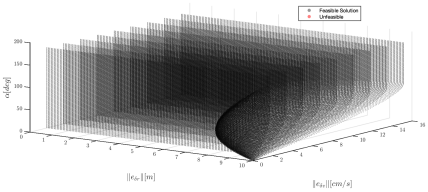

(a) 3D representation of the discrete grid over the set $[0, \epsilon_{\delta \boldsymbol{r}}] \times [0, \pi] \times [0, \epsilon_{\delta \boldsymbol{v}}]$.

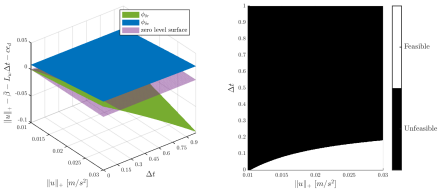

(b) (left) 3D representation of the functions $\phi_{\delta \boldsymbol{r}}$ and $\psi_{\delta \boldsymbol{v}}$ from (4.5.8) and (4.5.12)(right) 2D projection of the region $\phi_{\delta \boldsymbol{r}} \geq 0 \wedge \phi_{\delta \boldsymbol{v}} \geq 0$ on the $\|\boldsymbol{u}\|_+ - \Delta t$ plane

Figure 5.3

inspector. From Figure 5.3b, the sampling time Δt is set at $150\ ms$ which is the maximum allowed for a maximum control authority of $0.02\ m/s^2$. In order to asses the performance of the MPC controller designed, a set of 50 simulations with random initial conditions inside the safe set are undertaken. For all the simulations the initial velocity error norm $\|\epsilon_{\delta \boldsymbol{v}}\|$ is considered to be equal to the maximum allowed speed error $\epsilon_{\delta \boldsymbol{v}}$. Additionally the condition

$$\boldsymbol{e}_{\delta \boldsymbol{r}}^T(\delta \boldsymbol{x}(t_0), t_0)\boldsymbol{e}_{\delta \boldsymbol{v}}(\delta \boldsymbol{x}(t_0), t_0) = \frac{p_{\delta r 0}}{2} \frac{(\epsilon_r^2 - \boldsymbol{e}_{\delta \boldsymbol{r}}(\delta \boldsymbol{x}(t_0), t_0)^2)}{\boldsymbol{e}_{\delta \boldsymbol{r}}(\delta \boldsymbol{x}(t_0), t_0)}$$

is enforced at time t_0 of the simulation such that the inspector state is at the border of $\mathcal{C}_{\delta \boldsymbol{v}}$ at time t_0. The time evolution of the SD-HOBF and SD-CBF constraints together with the related CBF and HOCBF is shown in Figure 5.4. All the barriers and barrier constraint remain positive during the whole system operation. The simulation terminates when the position and speed errors decrease to $1\ mm$ and $1\ mm/s$ respectively. It is highlighted how the SD-CBF constraint $\psi_{\delta \boldsymbol{v}}$ remains extremely close to its lower limit for all the simulations due to the fact that the controller tries to reach the reference as fast as possible while the barrier keeps the speed error norm constrained to its maximum value $\epsilon_{\delta \boldsymbol{v}}$. This behaviour could be tuned for different choices of the state cost and control cost matrices Q ad R.

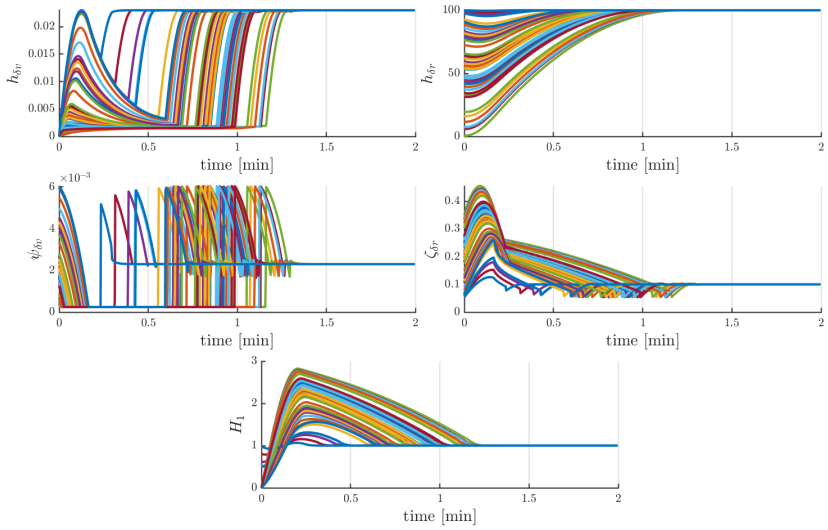

Figure 5.4: Time evolution of the SD-CBF constraint ($\psi_{\delta \boldsymbol{v}}(t)$), SD-HOBF constraint ($\zeta_{\delta \boldsymbol{r}}(t)$), velocity SD-CBF ($h_{\delta \boldsymbol{v}}(t)$), position SD-HOBF ($h_{\delta \boldsymbol{r}}(t)$) and relative degree 1 position barrier ($H_1(t)$). The different line plots correspond to fifty different simulations with different initial conditions inside the safe set $\mathcal{C}_{\delta \boldsymbol{r}} \cap \mathcal{C}_{\delta \boldsymbol{v}}$

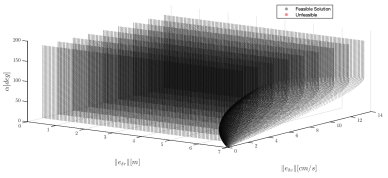

(a) 3D representation of the discrete grid over the set $[0, \epsilon_{\delta \boldsymbol{r}}] \times [0, \pi] \times [0, \epsilon_{\delta \boldsymbol{v}}]$.

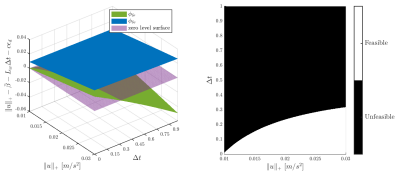

(b) (left)3D representation of the functions $\phi_{\delta \boldsymbol{r}}$ and $\psi_{\delta \boldsymbol{v}}$ from (4.5.8) and (4.5.12)(right) 2D projection of the region $\phi_{\delta \boldsymbol{r}} \geq 0 \wedge \phi_{\delta \boldsymbol{v}} \geq 0$ on the $(\|\boldsymbol{u}\|_+, \Delta t)$ plane

Figure 5.5

Parameters	Value	Unit	Parameters	Value	Unit
$\epsilon_{\delta \boldsymbol{r}}$	10.00	m	$L_{\delta \boldsymbol{r}}$	$7.58e^{-2}$	-
$\epsilon_{\delta \boldsymbol{v}}$	$1.33e^{-1}$	m/s	$L_{\delta \boldsymbol{v}}$	$1.16e^{-3}$	-
d_s	3.00	m	$L^z_{\delta \boldsymbol{r}}$	$1.15e^{-2}$	-
$p_{\delta r0}$	$1.00e^{-2}$	$1/s$	$L^z_{\delta \boldsymbol{v}}$	$3.64e^{-5}$	-
$p_{\delta r1}$	$1.00e^{-1}$	$1/s$	$c_{\delta \boldsymbol{r}}$	$20.05e^{-2}$	m
$p_{\delta v0}$	$5.00e^{-2}$	$1/s$	$c_{\delta \boldsymbol{v}}$	$3.10e^{-1}$	m/s

Table 5.2: List of barriers parameters for the single agent mission

5.2 Multi-agent inspection

Similar to the single agent mission, a multi-agent mission is simulated over a period of two orbits for three inspectors inserted into three different PROs. A close up 3D view of the three different PROs is shown in Figure 4.1a, while a graphical representation of the three inspectors orbiting around the the ISS during the inspection is given in Figure 4.1b. The parameters defining each inspector's relative orbit are summarised in Table 5.3. The maximum corridor width for each inspector is reduced to 7 m for this simulation while the parameter d_s is left unchanged at 3 m. All the agents are assumed to have the same parameters $p_{\delta v0}$,$p_{\delta r0}$ and $p_{\delta r1}$ as summarised in Table 5.4. The constants $L_{\delta \boldsymbol{r}}$,$L_{\delta \boldsymbol{v}}$,,$L^z_{\delta \boldsymbol{r}}$,$L^z_{\delta \boldsymbol{v}}$,$c_{\delta \boldsymbol{v}}$ and $c_{\delta \boldsymbol{r}}$ are computed for the inspector in the outer most PRO and they are applied to all the three inspectors. This is a conservative solution as the inner most inspectors present lower values for ϵ_f,ϵ_d,$\|\delta \boldsymbol{r}_r\|_+$ and $\|\delta \boldsymbol{v}_r\|_+$. The maximum speed error $\epsilon_{\delta \boldsymbol{v}}$ is set at 13.3 cm/s (applying (5.1.1) as for the single agent simulation) while the value ϵ_f and ϵ_d

$\rho_x\ [m]$	$\rho_{y0}\ [m]$	$\rho_z\ [m]$	$\alpha_x\ [deg]$	$\alpha_z\ [deg]$	$\|\delta\boldsymbol{r}\|_+\ [m]$	$\|\delta\boldsymbol{v}\|_+\ [m/s]$
50.00	0.00	0.00	90.00	0.00	100	0.10
64.00	0.00	60.00	90.00	0.50	143.00	0.18
78.00	0.00	140.00	90.00	0.00	223.00	0.29

Table 5.3: List of parameters defining a unique PRO for each of the three inspectors

Parameters	Value	Unit	Parameters	Value	Unit
$\epsilon_{\delta\boldsymbol{r}}$	7.00	m	$L_{\delta\boldsymbol{v}}$	$1.20e^{-3}$	-
$\epsilon_{\delta\boldsymbol{v}}$	$1.33e^{-1}$	m/s	$L^z_{\delta\boldsymbol{r}}$	$6.30e^{-3}$	-
d_s	3.00	m	$L_{\delta\boldsymbol{r}}$	$4.35e^{-2}$	-
$p_{\delta\boldsymbol{r}0}$	$2.00e^{-2}$	$1/s$	$L^z_{\delta\boldsymbol{v}}$	$1.89e^{-5}$	-
$p_{\delta\boldsymbol{r}1}$	$5.00e^{-2}$	$1/s$	$c_{\delta\boldsymbol{r}}$	14.04	m
$p_{\delta\boldsymbol{v}0}$	$5.00e^{-2}$	$1/s$	$c_{\delta\boldsymbol{v}}$	0.27	m/s

Table 5.4: List of barriers parameters for the multiagent mission

for each inspector are computed analytically identically to the single inspector case (Figure 5.2).The selected sampling time is $100\ ms$, but the maximum allowed sampling time is as high as $200\ ms$ as shown from the set of feasible points $(\|\boldsymbol{u}\|_+, \Delta t)$ in Figure 5.5b). On the other hand, Figure 5.5a shows the solution to problem 4.6.1 for the outermost agent (the graphic is identical for all the three agents as the same parameters are applied to all of them) which shows that a feasible control exist over the full discretised safe set. The time evolution of the SD-CBF and SD-HOBF together with their respective constraint is shown in Figure 5.6a. The simulation is run over two full orbits. The SD-CBF and SD-HOBF are respected during the whole mission duration while the MPC controller is maintained inactive during approximately 96% of the whole mission duration corresponding to 180 min of inspection under zero actuation. The remaining 4% of the mission duration the MPC controller is actuated. Eventually, Figure 5.6b shows the relative distance between the three agents which always remains above zero for the whole duration of the mission even when the agents are at the closest point along their reference.

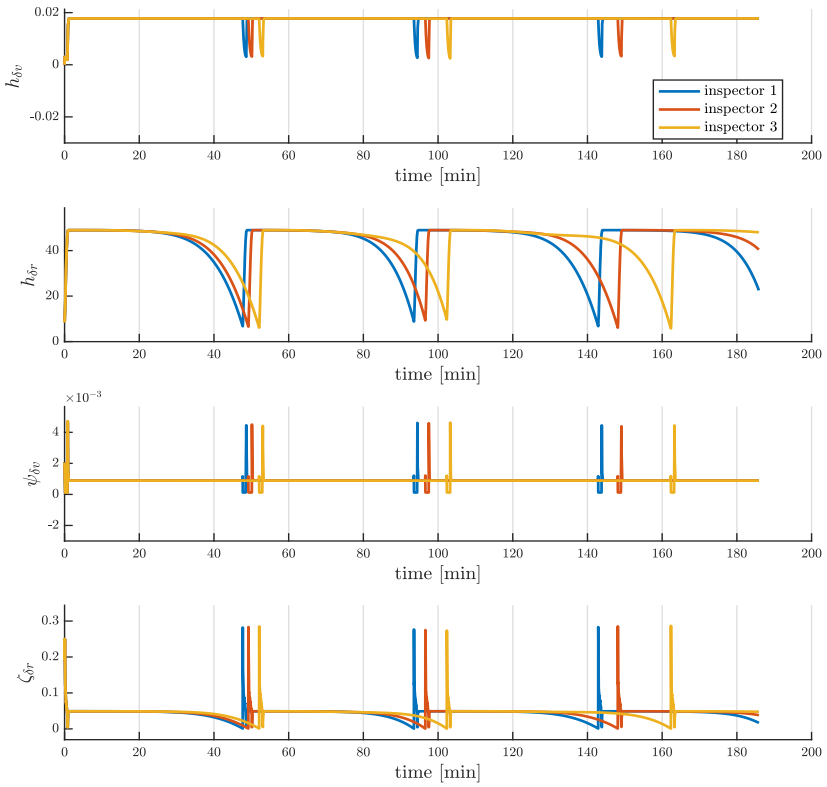

(a) Time evolution of relative position error, relative velocity error, HOBF $h_{\delta \boldsymbol{r}}$, CBF $h_{\delta \boldsymbol{v}}$ and H_1 for the three inspectors involved in the inspection mission

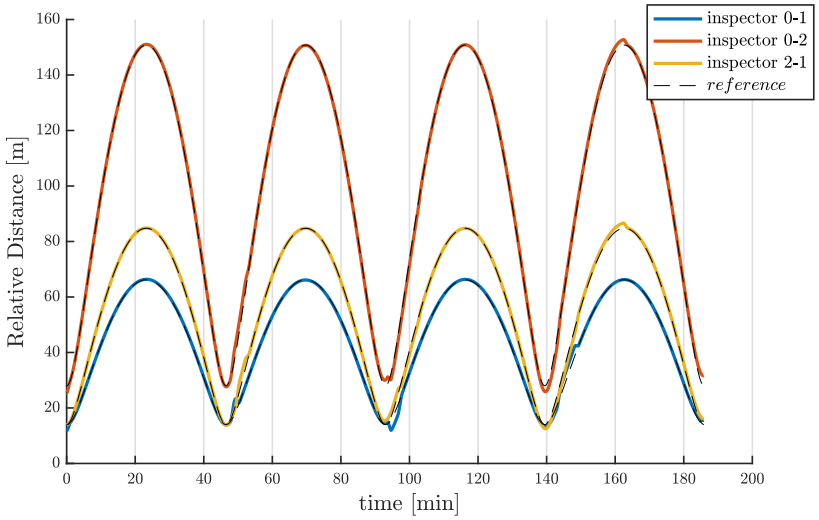

(b) Relative distance between the inspectors over two orbital periods. A dashed line represents the relative distance between the agents under zero tracking error.

Figure 5.6

Chapter 6

Conclusions

The numerical simulations presented show that the derived control approach meets the safety requirements established for the inspection mission both for the case of multi-agent and single agent inspection. In addition, the definition of SD-CBF from [7] was successfully extended to SD-HOCBF for the particular choice of linear α functions. Although, many practical issues are highlighted

- The derivation of suitable margins applied for ensuring safety in between sapling intervals has been particularly challenging even for simple linear α functions. It is considered that for more complicated α functions, upper bounding the Lipschitz constant for the HOCBF constraint could yield excessively small sampling times. This is a fact that remains to be explored for future work.
- The attempt to derive a suitable minimum maximum control authority $\|\boldsymbol{u}\|_+$ for the considered HOCBF constraint resulted in two main fundamental conclusions: (1) under worse case scenario conditions infinite control is required to satisfy the HOCBF constraint and this happens exactly at the origin of the safe set where $\mathcal{L}_g\mathcal{L}_f h_{\delta \boldsymbol{r}} = 0$. This conclusion does not depend on the applied linear α functions, but it is generalizable to more complex functions as $\mathcal{L}_g\mathcal{L}_f h_{\delta \boldsymbol{r}}$ eventually goes to zero at the origin of the safe set for every choice of the functions α. This same problem does not arise in [23] for example where the objective is to a void a given spherical $unsafe$ set wrapped around an obstacle to be avoided (the opposite case of the current work). In this case, the position error will never reach zero norm inside the safe set.

(2) It is not possible to make any consideration on the satisfaction of the HOCBF constraint defined in the present work if the system speed is not bounded. In the presentation, a solution to the problem has been explored by the introduction of a barrier constraint on the velocity error. This solution comes with the cost of dealing with possibly colliding barrier constraints. Other choices are left to be explored as future work

- A formal and solid paradigm to determine the coefficients $p_{\delta \boldsymbol{v}0}$,$p_{\delta \boldsymbol{r}0}$,$p_{\delta \boldsymbol{r}1}$ remains an open question from the current work

However the controller has shown to be successful for the given simulation, it is acknowledge that practical implementation could present many difficulties related to the precision of the navigation system applied on board the inspectors. The GNSS system remains the only navigation systems capable of a satisfying the precision and accuracy required for the mission, although the capabilities of GNSS receivers are not yet technologically ready for the requirements of the presented mission. Further research should be conducted in order to address the robustness of the presented control strategy under sensor noise and measurement error.

6.1 Future work

Throughout the current thesis project, some relevant aspects of the inspection mission concept presented need to be addressed as future work. Namely, the thesis work mainly focused on the development of a safe controller for the inspectors, while aspects related to the visual inspection through the camera payload mounted on each inspector was left unaddressed. As a future work, it is interesting to design a proper Machine Vision architecture that could take advantage of the PRO geometry of each inspector to obtain an high resolution screening of the outer structure of the ISS. In addition to that, an attitude controller that takes care of the camera pointing should also be designed. It is envisaged that some of the most interesting challenges to solve will be (1)designing a controller with high pointing accuracy,(2) handling of differential lightning conditions between the cameras due to the ISS orbit around the Earth (3)the design of a computer vision architecture that can handle information from different cameras to achieve an high resolution map of the outer structure of the ISS so that critical failures can be identified or prevented.

Appendix A

Appendices

A.1 Relative kinematics

In this section, the equations of motion of a point mass p as described in a rotating frame are derived. First, an inertial frame $\mathcal{J}$ and a rotating frame $\mathcal{K}$ are defined as in Fig A.1 It is known from rational mechanics that the time derivative of a vector quantity observed from the inertial frame $\mathcal{J}$, relates to the time derivative in the rotating frame $\mathcal{K}$ as [Equation 1.20 in [16]]

$$\frac{\partial(\cdot)}{\partial t}|_{\mathcal{J}} = \frac{\partial(\cdot)}{\partial t}|_{\mathcal{K}} + \boldsymbol{\omega}_{\mathcal{K}/\mathcal{J}} \wedge (\cdot) \tag{A.1.1}$$

In equation (A.1.1), the angular velocity of frame $\mathcal{K}$ with respect to frame $\mathcal{J}$ is denoted as $\boldsymbol{\omega}_{\mathcal{K}/\mathcal{J}}$. The vertical bar symbol $|$ is used to define the *observer* frame. The *observer* is the frame of reference with respect to which the time derivatives of vectors are developed. This definition of the *observer* frame is fundamentally different from the definition of the *coordinate* frame, which is the reference frame in which vectors are described component wise. A vector could be both described in the same observer and coordinate frame, or it is possible that these last two are different. When writing equation (A.1.1) it is always assumed that the coordinate frame is consistent for the RHS and LHS. The following remarkable property derives from equation (A.1.1)

$$\frac{\partial \boldsymbol{\omega}_{\mathcal{K}/\mathcal{J}}}{\partial t}|_{\mathcal{J}} = \frac{\partial \boldsymbol{\omega}_{\mathcal{K}/\mathcal{J}}}{\partial t}|_{\mathcal{K}} + \boldsymbol{\omega}_{\mathcal{K}/\mathcal{J}} \wedge \boldsymbol{\omega}_{\mathcal{K}/\mathcal{J}} = \frac{\partial \boldsymbol{\omega}_{\mathcal{K}/\mathcal{J}}}{\partial t}|_{\mathcal{J}} \tag{A.1.2}$$

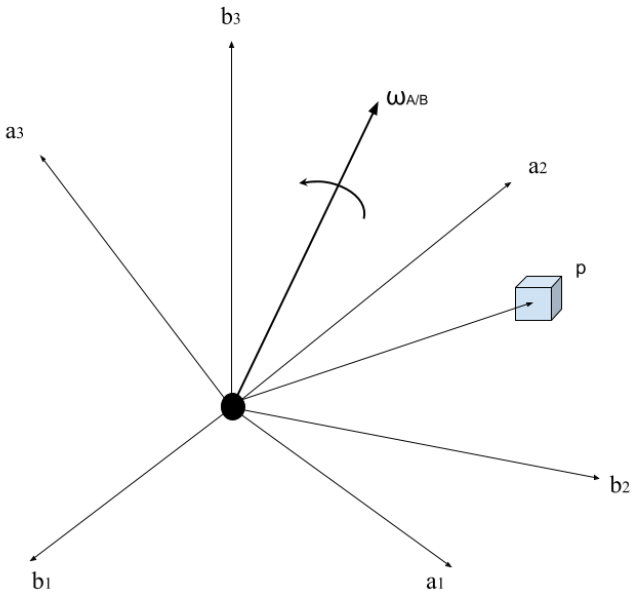

Figure A.1: Inertial frame B and rotating frame $\mathcal{K}$. The point mass body p is represented as a cube in the Figure

Hence the time derivative of the relative angular velocity is the same in $\mathcal{J}$ and $\mathcal{K}$.

Building on equation (A.1.1), it possible to relate the time derivative of the vector $\boldsymbol{p}$ in the *observer* frame $\mathcal{J}$ to the one obtained in the *observer* frame $\mathcal{K}$.

$$\frac{\partial \boldsymbol{p}}{\partial t}|_{\mathcal{J}} = \frac{\partial \boldsymbol{p}}{\partial t}|_{\mathcal{K}} + \boldsymbol{\omega}_{\mathcal{K}/\mathcal{J}} \wedge \boldsymbol{p} \tag{A.1.3}$$

The relative acceleration is obtained by differentiating again

$$\frac{\partial^2 \boldsymbol{p}}{\partial^2 t}|_{\mathcal{K}} = \frac{\partial}{\partial t}|_{\mathcal{K}}(\frac{\partial \boldsymbol{p}}{\partial t}|_{\mathcal{J}}) + \frac{\partial}{\partial t}|_{\mathcal{K}}(\boldsymbol{\omega}_{\mathcal{K}/\mathcal{J}} \wedge \boldsymbol{p}) \tag{A.1.4}$$

Every quantity on the right must be expanded again following the rule expressed in equation (A.1.1)

$$\frac{\partial^2 \boldsymbol{p}}{\partial^2 t}|_{\mathcal{K}} = \frac{\partial^2 \boldsymbol{p}}{\partial^2 t}|_{\mathcal{J}} + \boldsymbol{\omega}_{\mathcal{K}/\mathcal{J}} \wedge \frac{\partial \boldsymbol{p}}{\partial t}|_{\mathcal{J}} + \dot{\boldsymbol{\omega}}_{\mathcal{K}/\mathcal{J}} \wedge \boldsymbol{p} + \boldsymbol{\omega}_{\mathcal{K}/\mathcal{J}} \wedge (\frac{\partial \boldsymbol{p}}{\partial t}|_{\mathcal{J}} + \boldsymbol{\omega}_{\mathcal{K}/\mathcal{J}} \wedge \boldsymbol{p}) \tag{A.1.5}$$

Where property equation (A.1.2) is used to take the time derivative of $\boldsymbol{\omega}_{\mathcal{K}/\mathcal{J}}$. Re-arranging equation (A.1.5) leads to

$$\frac{\partial^2 \boldsymbol{p}}{\partial^2 t}|_{\mathcal{K}} = \frac{\partial^2 \boldsymbol{p}}{\partial^2 t}|_{\mathcal{J}} + 2\boldsymbol{\omega}_{\mathcal{K}/\mathcal{J}} \wedge \frac{\partial \boldsymbol{p}}{\partial t}|_{\mathcal{J}} + \dot{\boldsymbol{\omega}}_{A/B} \wedge \boldsymbol{p} + \boldsymbol{\omega}_{\mathcal{K}/\mathcal{J}} \wedge (\boldsymbol{\omega}_{\mathcal{K}/\mathcal{J}} \wedge \boldsymbol{p}) \tag{A.1.6}$$

A.2 Direction cosine matrix

Vectors could be represented in multiple coordinate frames of reference and the most convenient choice should always be made in order to describe a given systems. Nevertheless, it is essential to be able to change from one coordinate frame to another when required. This is important especially in astrodynamics applications where many different frames of reference are applied. Given a frame of reference $\mathcal{A}$ $(\hat{\boldsymbol{a}}_1, \hat{\boldsymbol{a}}_2, \hat{\boldsymbol{a}}_3)$ and a frame of reference $\mathcal{B}$ $(\hat{\boldsymbol{b}}_1, \hat{\boldsymbol{b}}_2, \hat{\boldsymbol{b}}_3)$, it is possible to compute a mapping $C_{\mathcal{A}}^{\mathcal{B}} : \mathbb{R}^3 \to \mathbb{R}^3$ that transforms any vector described in $\mathcal{A}$ coordinates to frame $\mathcal{B}$ coordinates by computing the following matrix

$$C_{\mathcal{A}_{ij}}^{\mathcal{B}} = \hat{\boldsymbol{b}}_i \cdot \hat{\boldsymbol{a}}_j = cos(\alpha_{ij}) \tag{A.2.1}$$

The matrix $C_{\mathcal{A}}^{\mathcal{B}}$ takes the name of *Direction Cosine Matrix* due to the fact that each entry represents the cosine of the angle between the base vector $\hat{\boldsymbol{a}}_j$ of the $\mathcal{A}$ frame and the base vector $\hat{\boldsymbol{b}}_i$ from the $\mathcal{B}$ frame. Thanks to $C_{\mathcal{A}}^{\mathcal{B}}$ it is possible to change coordinates from frame $\mathcal{A}$ to frame $\mathcal{B}$. Due to the nice ortho-normality property, the inverse coorindate transformation is given by $(C_{\mathcal{A}}^{\mathcal{B}})^{-1} = (C_{\mathcal{A}}^{\mathcal{B}})^T$.

A.3 Derivation of the maximum relative spacecraft dynamics acceleration

In this section, a suitable upper bound on the relative acceleration between the deputy and the chief is derived. First the relative acceleration $\delta\boldsymbol{a}$ of the deputy

relative to the chief in the *Hill*'s observer frame of the chief is recalled

$$\delta \boldsymbol{a} = \delta \ddot{\boldsymbol{r}}_g + \delta \boldsymbol{a}_{fc} + \delta \boldsymbol{d} + \boldsymbol{u} \tag{A.3.1}$$

Considering all the accelerations but the propulsion system of the deputy $\boldsymbol{u}$, it is desired to find suitable first order approximations for the norm of $\ddot{\boldsymbol{r}}_g$, $\delta \boldsymbol{a}_{fc}$ and $\delta \boldsymbol{d}$. Consistently with the rest of the presentation, the maximum norm of a vector or matrix, will be denoted by the notation $\|\|_+$. First the relative point mass gravity acceleration is isolated and rewritten in terms of the point mass potential U_{pm} as

$$\delta \ddot{\boldsymbol{r}}_g = -\frac{\mu}{r_{dep}^3}\boldsymbol{r}_{dep} + \frac{\mu}{r_{ch}^3}\boldsymbol{r}_{ch} = -\nabla U_{pm}(\boldsymbol{r}_{dep}) + \nabla U_{pm}(\boldsymbol{r}_{ch})$$

Considering that $\boldsymbol{r}_{dep} = \boldsymbol{r}_{ch} + \delta \boldsymbol{r}$ and $\|\delta \boldsymbol{r}\| \ll \boldsymbol{r}_{ch}$, a first order approximation for the relative acceleration due to point mass gravity is derived by means of a Taylor series expansion of $\nabla U_{pm}(\boldsymbol{r}_{dep})$ as follows

$$-\nabla U_{pm}(\boldsymbol{r}_{dep}) + \nabla U_{pm}(\boldsymbol{r}_{ch}) = -\nabla (U_{pm}(\boldsymbol{r}_{dep}) - U_{pm}(\boldsymbol{r}_{ch})) \approx -\nabla^2 U_{pm}(\boldsymbol{r}_{ch})\delta \boldsymbol{r}$$

Where the Taylor expansion $U_{pm}(\boldsymbol{r}_{dep}) = U_{pm}(\boldsymbol{r}_{ch}) + \nabla U_{pm}(\boldsymbol{r}_{ch})\delta \boldsymbol{r} + \mathcal{O}(\|dr\|^2)$ is applied to derive the RHS. The maximum relative acceleration due to point mass gravity is then upper bounded neglecting the higher order terms of the Taylor series

$$\boxed{\|\delta \ddot{\boldsymbol{r}}_g\|_+ \leq \|\nabla^2 U_{pm}(\boldsymbol{r}_{ch})\|_2 \|\delta \boldsymbol{r}\|_+}$$

It is recalled that the the 2-norm of the matrix $\nabla^2 U_{pm}(\boldsymbol{r}_{ch})$ is equal to the maximum singular value of the matrix.

Next the relative perturbation acceleration $\delta \boldsymbol{d}$ is upper bounded. The relative perturbation acceleration is unpacked as

$$\delta \boldsymbol{d} = \boldsymbol{d}_{zh,dep} + \boldsymbol{d}_{drag,dep} - \boldsymbol{d}_{zh,ch} - \boldsymbol{d}_{drag,ch} = \delta \boldsymbol{d}_{drag} + \delta \boldsymbol{d}_{zh}$$

The relative atmospheric drag acceleration $\delta \boldsymbol{d}_{drag}$ is approximated considering that the inertial atmospheric velocity of the chief and the deputy are

approximately the same so that $\dot{\boldsymbol{V}}_{atmo,ch} \approx \dot{\boldsymbol{V}}_{atmo,dep}$. In addition to that, the density variations over 1 km separation could be neglected when dealing with LEO orbits [[2],Section 2.3.3]. The differential drag acceleration is then approximated as

$$\delta \boldsymbol{d}_{drag} \approx (CD_{dep} - CD_{ch})\rho(\boldsymbol{r}_{ch})\|\boldsymbol{V}_{atmo,ch}\|^2 \hat{\boldsymbol{V}}_{atmo,ch}$$

A first order approximation for the maximum differential drag acceleration is then given by

$$\boxed{\|\delta \boldsymbol{d}_{drag}\|_+ \leq (CD_{dep} - CD_{ch})\|\rho(\boldsymbol{r_{ch}})\|_+ \|\boldsymbol{V}_{atmo,ch}\|_+^2}$$

On the other hand the relative acceleration due to high order zonal harmonics $\delta \boldsymbol{d}_{zh}$ is derived by applying the same approach developed for $\delta \ddot{\boldsymbol{r}}_g$ replacing U_{pm} with U_{zh}.

$$\delta \boldsymbol{d}_{zh} \approx \nabla^2 U_{zh}(\boldsymbol{r}_{ch})\delta \boldsymbol{r}$$

Due to the fact that the J_2 zonal harmonic is the highest zonal harmonic term and it is three order of magnitude higher than the successive zonal terms, an upper bound $\boldsymbol{d}_{zh}$ is given by considering only the J_2 potential as

$$\boxed{\|\delta \boldsymbol{d}_{zh}\|_+ \leq \|\nabla^2 U_{J_2}(\boldsymbol{r}_{ch})\|_2 \|\delta \boldsymbol{r}\|_+}$$

The last acceleration to be upper bounded is the fictitious acceleration $\delta \boldsymbol{a}_{fc}$ whose definition is recalled as

$$\delta \boldsymbol{a}_{fc} = -2\boldsymbol{\omega}_{\mathcal{H}/\mathcal{I}} \wedge \delta \boldsymbol{v} - \dot{\boldsymbol{\omega}}_{\mathcal{H}/\mathcal{I}} \wedge \delta \boldsymbol{r} - \boldsymbol{\omega}_{\mathcal{H}/\mathcal{I}} \wedge (\boldsymbol{\omega}_{\mathcal{H}/\mathcal{I}} \wedge \delta \boldsymbol{r})$$

The definition of $\boldsymbol{\omega}_{\mathcal{H}/\mathcal{I}}$ and $\dot{\boldsymbol{\omega}}_{\mathcal{H}/\mathcal{I}}$ is also recalled for convenience

$$
\begin{aligned}
\omega_r &= \frac{r_{ch}}{h} d_w \\
\omega_s &= 0 \\
\omega_w &= \frac{h}{r_{ch}^2} \\
\dot{\omega}_r &= \frac{\dot{r}_{ch}}{h} d_w - \dot{h} \frac{r_{ch}}{h^2} d_w + \frac{r_{ch}}{h} \dot{d}_w \\
\dot{\omega}_s &= 0 \\
\dot{\omega}_w &= \frac{\dot{h}}{r_{ch}^2} - 2\dot{r}_{ch} \frac{h}{r_{ch}^3}
\end{aligned}
\tag{A.3.2}
$$

In order to limit the complexity of the derivation it assumed that the chief orbit is nearly circular so that $\dot{\boldsymbol{\omega}}_{\mathcal{H}/\mathcal{I}}$ is approximately equal to zero. In addition it is noted that ω_r is at least three orders of magnitude lower than ω_w such that $\|\boldsymbol{\omega}_{\mathcal{H}/\mathcal{I}}\| \approx \frac{h}{r^2}$. Note that for circular orbits r_{ch} is constant and equal to the semimajor axis. Given the nearly circular chief orbit assumption, $\boldsymbol{a}_{fc}$ is upper bounded as

$$
\boxed{\|\boldsymbol{a}_{fc}\|_+ \leq 2\omega_w \|\delta \boldsymbol{v}\|_+ + \omega_w^2 \|\delta \boldsymbol{r}\|_+}
$$

The case of elliptical orbit could be derived assuming the less strong assumption that only $\dot{\omega}_r \approx 0$ but the derivation of the upper bound in this case is not developed further. Table A.1 summarises all the intermediate upper bounds which are valid in case of nearly circular orbits.

Term	Upper Bound
$\|\delta \ddot{\boldsymbol{r}}_g\|$	$\|\nabla^2 U_{pm}(\boldsymbol{r}_{ch})\|_+ \|\delta \boldsymbol{r}\|_+$
$\|\delta \boldsymbol{a}_{fc}\|$	$\boldsymbol{\omega}_w \|\delta \boldsymbol{v}\|_+ + \boldsymbol{\omega}_w^2 \|\delta \boldsymbol{r}\|_+$
$\|\delta \boldsymbol{d}_{zh}\|$	$\nabla^2 U_{J_2}(\boldsymbol{r}_{ch})\|_+ \|\delta \boldsymbol{r}\|_+$
$\|\delta \boldsymbol{d}_{drag}\|$	$\|(CD_{dep} - CD_{ch})\rho \|\boldsymbol{V}_{atmo,ch}\|^2$

Table A.1: Upper bounds on relative accelerations terms

A.4 Derivation of the maximum relative spacecraft dynamics acceleration time derivative

In this section, an upper bound on the time derivative of $\ddot{\boldsymbol{r}}_g$, $\delta \boldsymbol{a}_{fc}$ and $\delta \boldsymbol{d}$ is developed. The inertial relative acceleration $\delta \ddot{\boldsymbol{r}}$ of the deputy is related to the non-inertial relative acceleration $\delta \boldsymbol{a}$ as

$$\delta \ddot{\boldsymbol{r}} = \delta \boldsymbol{a} + 2\boldsymbol{\omega}_{\mathcal{H}/\mathcal{I}} \wedge \delta \boldsymbol{v} + \dot{\boldsymbol{\omega}}_{\mathcal{H}/\mathcal{I}} \wedge \delta \boldsymbol{r} + \boldsymbol{\omega}_{\mathcal{H}/\mathcal{I}} \wedge (\boldsymbol{\omega}_{\mathcal{H}/\mathcal{I}} \wedge \delta \boldsymbol{r}) \tag{A.4.1}$$

The inertial time derivative of the relative acceleration $\delta \dddot{\boldsymbol{r}}$ is related to the time derivative of the non-inertial relative acceleration $\delta \dot{\boldsymbol{a}}$ as

$$\begin{aligned}\delta \dddot{\boldsymbol{r}} =& \delta \dot{\boldsymbol{a}} + \boldsymbol{\omega}_{\mathcal{H}/\mathcal{I}} \wedge \delta \boldsymbol{a} + 2\dot{\boldsymbol{\omega}}_{\mathcal{H}/\mathcal{I}} \wedge \delta \boldsymbol{v} + 2\boldsymbol{\omega}_{\mathcal{H}/\mathcal{I}} \wedge (\delta \boldsymbol{a} + \boldsymbol{\omega}_{\mathcal{H}/\mathcal{I}} \wedge \delta \boldsymbol{v}) + \ddot{\boldsymbol{\omega}}_{\mathcal{H}/\mathcal{I}} \wedge \delta \boldsymbol{r} + \\ & \dot{\boldsymbol{\omega}}_{\mathcal{H}/\mathcal{I}} \wedge (\delta \boldsymbol{v} + \boldsymbol{\omega}_{\mathcal{H}/\mathcal{I}} \wedge \delta \boldsymbol{v}) + \dot{\boldsymbol{\omega}}_{\mathcal{H}/\mathcal{I}} \wedge (\boldsymbol{\omega}_{\mathcal{H}/\mathcal{I}} \wedge \delta \boldsymbol{r}) + \boldsymbol{\omega}_{\mathcal{H}/\mathcal{I}} \wedge (\dot{\boldsymbol{\omega}}_{\mathcal{H}/\mathcal{I}} \wedge \delta \boldsymbol{r}) + \\ & \boldsymbol{\omega}_{\mathcal{H}/\mathcal{I}} \wedge (\boldsymbol{\omega}_{\mathcal{H}/\mathcal{I}} \wedge (\delta \boldsymbol{v} + \boldsymbol{\omega}_{\mathcal{H}/\mathcal{I}} \wedge \delta \boldsymbol{r}))\end{aligned} \tag{A.4.2}$$

Where the transport theorem from equation (A.1.1) is used to derive equation (A.4.2) form equation (A.4.1). It order to reduce the complexity of the derivation, only the case of nearly circular orbits is developed analytically such that $\dot{\boldsymbol{\omega}}_{\mathcal{H}/\mathcal{I}} \approx 0$ and $\ddot{\boldsymbol{\omega}}_{\mathcal{H}/\mathcal{I}} \approx 0$. Given the nearly circular orbits assumption yields

$$\delta \dddot{\boldsymbol{r}} = \delta \dot{\boldsymbol{a}} + 3\boldsymbol{\omega}_{\mathcal{H}/\mathcal{I}} \wedge \delta \boldsymbol{a} + 3\boldsymbol{\omega}_{\mathcal{H}/\mathcal{I}} \wedge (\boldsymbol{\omega}_{\mathcal{H}/\mathcal{I}} \wedge \delta \boldsymbol{v}) + \boldsymbol{\omega}_{\mathcal{H}/\mathcal{I}} \wedge (\boldsymbol{\omega}_{\mathcal{H}/\mathcal{I}} \wedge (\boldsymbol{\omega}_{\mathcal{H}/\mathcal{I}} \wedge \delta \boldsymbol{r})) \tag{A.4.3}$$

Isolating $\delta \dot{\boldsymbol{a}}$ on the left side of equation (A.4.3), the resulting time derivative of the relative acceleration in the $\mathcal{H}$ is given by

$$\delta \dot{\boldsymbol{a}} = \delta \dddot{\boldsymbol{r}} \underbrace{-(3\boldsymbol{\omega}_{\mathcal{H}/\mathcal{I}} \wedge \delta \boldsymbol{a} + 3\boldsymbol{\omega}_{\mathcal{H}/\mathcal{I}} \wedge (\boldsymbol{\omega}_{\mathcal{H}/\mathcal{I}} \wedge \delta \boldsymbol{v}) + \boldsymbol{\omega}_{\mathcal{H}/\mathcal{I}} \wedge (\boldsymbol{\omega}_{\mathcal{H}/\mathcal{I}} \wedge (\boldsymbol{\omega}_{\mathcal{H}/\mathcal{I}} \wedge \delta \boldsymbol{r})))}_{\delta \dot{\boldsymbol{a}}_{fc}} \tag{A.4.4}$$

Where the inertial acceleration $\delta \dddot{\boldsymbol{r}}$ is the unpacked as

$$\delta \dddot{\boldsymbol{r}} = \frac{d}{dt}\ddot{\boldsymbol{r}} = \underbrace{\frac{d}{dt}(-\frac{\mu}{r_{dep}^3}\boldsymbol{r}_{dep} + \frac{\mu}{r_{ch}^3}\boldsymbol{r}_{ch})}_{\ddot{\boldsymbol{r}}_g} + \delta \dot{\boldsymbol{d}} + \dot{\boldsymbol{u}}$$

and

$$\delta \dot{\boldsymbol{a}} = \ddot{\boldsymbol{r}}_g + \delta \dot{\boldsymbol{a}}_{fc} + \delta \dot{\boldsymbol{d}} + \dot{\boldsymbol{u}}$$

The time derivative of the gravity acceleration $\ddot{\boldsymbol{r}}_g$ is rewritten in terms of the potential

$$\ddot{\boldsymbol{r}}_g = -\frac{d}{dt}\nabla(U(\boldsymbol{r}_{dep}) - U(\boldsymbol{r}_{ch})) \tag{A.4.5}$$

Applying the chain rule on equation (A.4.5) leads to

$$\ddot{\boldsymbol{r}}_g = -\nabla^2 U(\boldsymbol{r}_{dep})\dot{\boldsymbol{r}}_{dep} + \nabla^2 U(\boldsymbol{r}_{ch})\dot{\boldsymbol{r}}_{ch} \tag{A.4.6}$$

For small separations ($\|\delta\boldsymbol{r}\| \ll \|\boldsymbol{r}_{ch}\|$) the approximation $\dot{\boldsymbol{r}}_{ch} \approx \dot{\boldsymbol{r}}_{dep}$ is valid (note that $\dot{\boldsymbol{r}}$ indicates the inertial velocity). Additionally, $\boldsymbol{r}_{dep} = \boldsymbol{r}_{ch} + \delta\boldsymbol{r}$ so that a first order Taylor approximation on the deputy potential is given as $U_{pm}(\boldsymbol{r}_{dep}) = U_{pm}(\boldsymbol{r}_{ch}) + \nabla U_{pm}(\boldsymbol{r}_{ch})\delta\boldsymbol{r} + \mathcal{O}(\|\delta\boldsymbol{r}\|^2)$. Neglecting the higher order terms in the series, a first order approximation for $\ddot{\boldsymbol{r}}_g$ is obtained as

$$\delta\dot{\boldsymbol{a}}_g \approx -\nabla^3 U_{pm}(\boldsymbol{r}_{ch})\delta\boldsymbol{r}\ \dot{\boldsymbol{r}}_{ch} \tag{A.4.7}$$

Which is upper bound as

$$\boxed{\delta\dot{\boldsymbol{a}}_g \leq \sqrt{\lambda^2_{\partial x U_{pm}} + \lambda^2_{\partial y U_{pm}} + \lambda^2_{\partial z U_{pm}}}\|\delta\boldsymbol{r}\|_+\ \|\dot{\boldsymbol{r}}_{ch}\|_+} \tag{A.4.8}$$

Where $\lambda_{\partial x U_{pm}} := \|\frac{\partial}{\partial x}(\nabla^2 U)\|_2$,$\lambda_{\partial y U_{pm}} := \|\frac{\partial}{\partial y}(\nabla^2 U)\|_2$ and $\lambda_{\partial z U_{pm}} := \|\frac{\partial}{\partial z}(\nabla^2 U)\|_2$ It is note worth mentioning that $\nabla^3 U_{pm}(\boldsymbol{r}_{ch})$ is a three dimensional tensor of dimension $3x3x3$ in the form

$$(\nabla^3 U)_{ijk} = \frac{\partial}{\partial x_k}(\nabla^2 U)_{ij} \tag{A.4.9}$$

Next, the time derivative of the perturbing acceleration is unpacked as

$$\delta\dot{\boldsymbol{d}} = \delta\dot{\boldsymbol{d}}_{drag} + \delta\dot{\boldsymbol{d}}_{zh} \tag{A.4.10}$$

The differential drag acceleration is approximately given as $\dot{\boldsymbol{d}}_{drag}$

$$\delta\boldsymbol{d}_{drag} \approx (CD_{dep} - CD_{ch})\rho\|\hat{\boldsymbol{V}}_{atmo,ch}\|^2 \tag{A.4.11}$$

In order to limit the complexity of the derivation it is assumed that the chief orbit is nearly circular so that $\dot{\boldsymbol{V}}_{atmo,ch} \approx 0$. Hence $\delta\dot{\boldsymbol{d}}_{drag}$ becomes approximately

$$\boxed{\delta \dot{\boldsymbol{d}}_{drag} \approx 0} \tag{A.4.12}$$

On the other hand, the definition of $\delta \dot{\boldsymbol{d}}_{zh}$ is obtained exactly with the same procedure derived for $\delta \dot{\boldsymbol{a}}_g$ such that

$$\delta \dot{\boldsymbol{d}}_{zh} \leq \sqrt{\lambda^2_{\partial x U_{zh}} + \lambda^2_{\partial y U_{zh}} + \lambda^2_{\partial z U_{zh}}} \|\delta \boldsymbol{r}\|_+ \, \|\dot{\boldsymbol{r}}_{ch}\|_+ \tag{A.4.13}$$

It is recalled that the J_2 zonal term is the dominant zonal term by at least three orders of magnitude such that this is the only zonal term considered

$$\boxed{\delta \dot{\boldsymbol{d}}_{zh} \leq \sqrt{\lambda^2_{\partial x U_{zh}} + \lambda^2_{\partial y U_{zh}} + \lambda^2_{\partial z U_{zh}}} \|\delta \boldsymbol{r}\|_+ \, \|\dot{\boldsymbol{r}}_{ch}\|_+} \tag{A.4.14}$$

At last, the definition of $\dot{\boldsymbol{a}}_{fc}$ for nearly circular orbits is given by

$$\delta \dot{\boldsymbol{a}}_{fc} = -(3\boldsymbol{\omega}_{\mathcal{H}/\mathcal{I}} \wedge \delta \boldsymbol{a} + 3\boldsymbol{\omega}_{\mathcal{H}/\mathcal{I}} \wedge (\boldsymbol{\omega}_{\mathcal{H}/\mathcal{I}} \wedge \delta \boldsymbol{v}) + \boldsymbol{\omega}_{\mathcal{H}/\mathcal{I}} \wedge (\boldsymbol{\omega}_{\mathcal{H}/\mathcal{I}} \wedge (\boldsymbol{\omega}_{\mathcal{H}/\mathcal{I}} \wedge \delta \boldsymbol{r}))) \tag{A.4.15}$$

It is recalled that in case of nearly circular orbit, the term $\|\boldsymbol{\omega}_{\mathcal{H}/\mathcal{I}}\|$ is approximately constant and $\|\boldsymbol{\omega}_{\mathcal{H}/\mathcal{I}}\| \approx \frac{h}{a^2} = \omega_w$. Hence $\delta \dot{\boldsymbol{a}}_{fc}$ is upper bounded as

$$\|\delta \dot{\boldsymbol{a}}_{fc}\| \leq 3\omega_w \|\delta \boldsymbol{a}\|_+ + 3\omega_w^2 \|\delta \boldsymbol{v}\|_+ + \omega_w^3 \|\delta \boldsymbol{r}\|_+ \tag{A.4.16}$$

From the definition of $\|\delta \boldsymbol{a}\|$ in Section A.3 it is also possible to further rearrange equation (A.4.16) as

$$\boxed{\|\delta \dot{\boldsymbol{a}}_{fc}\| \leq 3\omega_w (\|\delta \ddot{\boldsymbol{r}}_g\|_+ + \|\delta \boldsymbol{a}_{fc}\|_+ + \|\delta \boldsymbol{d}\|_+ + \|\boldsymbol{u}\|_+) + 3\omega_w^2 \|\delta \boldsymbol{v}\|_+ + \omega_w^3 \|\delta \boldsymbol{r}\|_+} \tag{A.4.17}$$

Table A.2 summarises all the results obtained in this section

Term	Upper Bound
$\|\delta\dot{\boldsymbol{a}}_g\|$	$\sqrt{\lambda^2_{\partial xU_{pm}} + \lambda^2_{\partial yU_{pm}} + \lambda^2_{\partial zU_{pm}}}\|\delta\boldsymbol{r}\|_+ \ \|\dot{\boldsymbol{r}}_{ch}\|_+$
$\|\delta\dot{\boldsymbol{a}}_{fc}\|$	$3\omega_w\|\delta\boldsymbol{a}\|_+ + 3\omega_w^2\|\delta\boldsymbol{v}\|_+ + \omega_w^3\|\delta\boldsymbol{r}\|_+$
$\|\delta\dot{\boldsymbol{d}}_{zh}\|$	$\sqrt{\lambda^2_{\partial xU_{zh}} + \lambda^2_{\partial yU_{zh}} + \lambda^2_{\partial zU_{zh}}}\|\delta\boldsymbol{r}\|_+ \ \|\dot{\boldsymbol{r}}_{ch}\|_+$
$\|\delta\dot{\boldsymbol{d}}_{drag}\|$	0

Table A.2: Upper bounds on relative accelerations terms assuming circular chief orbit reference

Bibliography

[1] Ali Dorri, Salil S. Kanhere, and Raja Jurdak. "Multi-Agent Systems: A Survey." In: *IEEE Access* 6 (2018), pp. 28573–28593. ISSN: 2169-3536. DOI: 10.1109/ACCESS.2018.2831228.

[2] Simone D'Amico. "Autonomous formation flying in low earth orbit." PhD Thesis. TU Delft, 2010.

[3] Sabrina Corpino and Fabrizio Stesina. "Inspection of the cis-lunar station using multi-purpose autonomous Cubesats." In: *Acta Astronautica* 175 (2020), pp. 591–605.

[4] Yashwanth Nakka, Wolfgang Hoenig, and Soon-Jo Chung. "Information-Based Guidance and Control For On-orbit Inspection using Multiple Spacecraft." In: Jan. 2021.

[5] Aaron D. Ames et al. "Control barrier functions: Theory and applications." In: *2019 18th European control conference (ECC)*. IEEE, 2019, pp. 3420–3431.

[6] Jun Zeng, Bike Zhang, and Koushil Sreenath. *Safety-Critical Model Predictive Control with Discrete-Time Control Barrier Function*. July 2020.

[7] Pedro Roque et al. "Corridor MPC: Towards Optimal and Safe Trajectory Tracking." In: (2022).

[8] Xiao Tan and Dimos V. Dimarogonas. *Compatibility checking of multiple control barrier functions for input constrained systems*. arXiv:2209.02284 [cs, eess, math]. Sept. 2022. URL: http://arxiv.org/abs/2209.02284 (visited on 10/03/2022).

[9] Daniel Morgan et al. "Swarm-keeping strategies for spacecraft under J2 and atmospheric drag perturbations." In: *Journal of Guidance, Control, and Dynamics* 35.5 (2012), pp. 1492–1506.

[10] Guangyan Xu and Danwei Wang. "Nonlinear Dynamic Equations of Satellite Relative Motion Around an Oblate Earth." In: *Journal of Guidance, Control, and Dynamics* 31.5 (Sept. 2008), pp. 1521–1524. ISSN: 0731-5090. DOI: 10.2514/1.33616. URL: https://arc.aiaa.org/doi/10.2514/1.33616 (visited on 05/26/2022).

[11] Kyle T. Alfriend et al. *Spacecraft formation flying: Dynamics, control and navigation*. Vol. 2. Elsevier, 2009.

[12] Howard Curtis. *Orbital mechanics for engineering students*. Butterworth-Heinemann, 2013.

[13] Alessandro de Iaco Veris. *Practical Astrodynamics*. Springer Aerospace Technology. Cham: Springer International Publishing, 2018. ISBN: 9783319622194 9783319622200. DOI: 10.1007/978-3-319-62220-0. URL: http://link.springer.com/10.1007/978-3-319-62220-0 (visited on 12/18/2022).

[14] David A. Vallado. *Fundamentals of astrodynamics and applications*. Vol. 12. Springer Science & Business Media, 2001.

[15] Oliver Montenbruck, Eberhard Gill, and Fh Lutze. "Satellite orbits: models, methods, and applications." In: *Appl. Mech. Rev.* 55.2 (2002), B27–B28.

[16] Tom Keates. "Analytical Mechanics of Space Systems–Second Edition, H. Schaub and JL Junkins, American Institute of Aeronautics and Astronautics, 1801 Alexander Bell Drive, Suite 500, Reston, VA 20191-4344, USA. 2009. Distributed by Transatlantic Publishers Group, Unit 242, 235 Earls Court Road, London, SW5 9FE, UK,(Tel: 020-7373 2515; e-mail: richard@ tpgltd. co. uk). 793pp. Illustrated.\pounds 76.(10% discount available to RAeS members on request). ISBN 978-1-60086-721-7." In: *The Aeronautical Journal* 113.1149 (2009), pp. 747–747.

[17] Joshua Sullivan, Sebastian Grimberg, and Simone D'Amico. "Comprehensive survey and assessment of spacecraft relative motion dynamics models." In: *Journal of Guidance, Control, and Dynamics* 40.8 (2017), pp. 1837–1859.

[18] Adam W. Koenig, Tommaso Guffanti, and Simone D'Amico. "New state transition matrices for relative motion of spacecraft formations in perturbed orbits." In: *AIAA/AAS Astrodynamics Specialist Conference*. 2016, p. 5635.

[19] David Q. Mayne. “Model predictive control: Recent developments and future promise.” en. In: *Automatica* 50.12 (Dec. 2014), pp. 2967–2986. ISSN: 0005-1098. DOI: 10.1016/j.automatica.2014.10.128. URL: https://www.sciencedirect.com/science/article/pii/S0005109814005160 (visited on 05/04/2022).

[20] James B. Rawlings and Mayne David Q. *Model Predictive Control Theory and Design*. Inglese. Madison, Wis: Nob Hill Pub, Llc, 2009. ISBN: 9780975937709.

[21] H. Chen and F. ALLGöWER. “A Quasi-Infinite Horizon Nonlinear Model Predictive Control Scheme with Guaranteed Stability∗∗This paper was not presented at any IFAC meeting. This paper was accepted for publication in revised form by Associate Editor W. Bequette under the direction of Editor Prof. S. Skogestad.” en. In: *Automatica* 34.10 (Oct. 1998), pp. 1205–1217. ISSN: 0005-1098. DOI: 10.1016/S0005-1098(98)00073-9. URL: https://www.sciencedirect.com/science/article/pii/S0005109898000739 (visited on 08/07/2022).

[22] Lars Lindemann and Dimos V. Dimarogonas. “Control Barrier Functions for Signal Temporal Logic Tasks.” In: *IEEE Control Systems Letters* 3.1 (Jan. 2019), pp. 96–101. ISSN: 2475-1456. DOI: 10.1109/LCSYS.2018.2853182.

[23] Wei Xiao and Calin Belta. “Control barrier functions for systems with high relative degree.” In: *2019 IEEE 58th conference on decision and control (CDC)*. IEEE, 2019, pp. 474–479.

[24] Tengfei Liu. *Robust Event-Triggered Control of Nonlinear Systems*. eng. 1st ed. 2020.. Research on Intelligent Manufacturing. Singapore: Springer Singapore, 2020. ISBN: 9789811550133.

[25] Eduardo D. Sontag. *Mathematical Control Theory: Deterministic Finite Dimensional Systems*. en. Google-Books-ID: f9XiBwAAQBAJ. Springer Science & Business Media, Nov. 2013. ISBN: 9781461205777.

[26] Charles Henry Edwards. *Advanced calculus of several variables*. Courier Corporation, 2012.

[27] David G. Wright. “Tychonoff’s Theorem.” In: *Proceedings of the American Mathematical Society* 120.3 (1994), pp. 985–987. ISSN: 0002-9939. DOI: 10.2307/2160497. URL: https://www.jstor.org/stable/2160497 (visited on 08/09/2022).

[28] Stefan Scholtes. *Introduction to piecewise differentiable equations*. Springer Science & Business Media, 2012.

[29] Victor Nwankwo and Sandip Chakrabarti. "Theoretical Model of Drag Force Impact on a Model International Space Station Satellite due to Solar Activity." In: *TRANSACTIONS OF THE JAPAN SOCIETY FOR AERONAUTICAL AND SPACE SCIENCES SPACE TECHNOLOGY JAPAN* 12 (July 2014), pp. 47–53. DOI: 10.2322/tastj.12.47.

TRITA-EECS-EX- 2022:00

Bibliography

[1] Ali Dorri, Salil S. Kanhere, and Raja Jurdak. "Multi-Agent Systems: A Survey." In: *IEEE Access* 6 (2018), pp. 28573–28593. ISSN: 2169-3536. DOI: 10.1109/ACCESS.2018.2831228.

[2] Simone D'Amico. "Autonomous formation flying in low earth orbit." PhD Thesis. TU Delft, 2010.

[3] Sabrina Corpino and Fabrizio Stesina. "Inspection of the cis-lunar station using multi-purpose autonomous Cubesats." In: *Acta Astronautica* 175 (2020), pp. 591–605.

[4] Yashwanth Nakka, Wolfgang Hoenig, and Soon-Jo Chung. "Information-Based Guidance and Control For On-orbit Inspection using Multiple Spacecraft." In: Jan. 2021.

[5] Aaron D. Ames et al. "Control barrier functions: Theory and applications." In: *2019 18th European control conference (ECC)*. IEEE, 2019, pp. 3420–3431.

[6] Jun Zeng, Bike Zhang, and Koushil Sreenath. *Safety-Critical Model Predictive Control with Discrete-Time Control Barrier Function*. July 2020.

[7] Pedro Roque et al. "Corridor MPC: Towards Optimal and Safe Trajectory Tracking." In: (2022).

[8] Xiao Tan and Dimos V. Dimarogonas. *Compatibility checking of multiple control barrier functions for input constrained systems*. arXiv:2209.02284 [cs, eess, math]. Sept. 2022. URL: http://arxiv.org/abs/2209.02284 (visited on 10/03/2022).

[9] Daniel Morgan et al. "Swarm-keeping strategies for spacecraft under J2 and atmospheric drag perturbations." In: *Journal of Guidance, Control, and Dynamics* 35.5 (2012), pp. 1492–1506.

[10] Guangyan Xu and Danwei Wang. "Nonlinear Dynamic Equations of Satellite Relative Motion Around an Oblate Earth." In: *Journal of Guidance, Control, and Dynamics* 31.5 (Sept. 2008), pp. 1521–1524. ISSN: 0731-5090. DOI: 10.2514/1.33616. URL: https://arc.aiaa.org/doi/10.2514/1.33616 (visited on 05/26/2022).

[11] Kyle T. Alfriend et al. *Spacecraft formation flying: Dynamics, control and navigation*. Vol. 2. Elsevier, 2009.

[12] Howard Curtis. *Orbital mechanics for engineering students*. Butterworth-Heinemann, 2013.

[13] Alessandro de Iaco Veris. *Practical Astrodynamics*. Springer Aerospace Technology. Cham: Springer International Publishing, 2018. ISBN: 9783319622194 9783319622200. DOI: 10.1007/978-3-319-62220-0. URL: http://link.springer.com/10.1007/978-3-319-62220-0 (visited on 12/18/2022).

[14] David A. Vallado. *Fundamentals of astrodynamics and applications*. Vol. 12. Springer Science & Business Media, 2001.

[15] Oliver Montenbruck, Eberhard Gill, and Fh Lutze. "Satellite orbits: models, methods, and applications." In: *Appl. Mech. Rev.* 55.2 (2002), B27–B28.

[16] Tom Keates. "Analytical Mechanics of Space Systems–Second Edition, H. Schaub and JL Junkins, American Institute of Aeronautics and Astronautics, 1801 Alexander Bell Drive, Suite 500, Reston, VA 20191-4344, USA. 2009. Distributed by Transatlantic Publishers Group, Unit 242, 235 Earls Court Road, London, SW5 9FE, UK,(Tel: 020-7373 2515; e-mail: richard@ tpgltd. co. uk). 793pp. Illustrated.\pounds 76.(10% discount available to RAeS members on request). ISBN 978-1-60086-721-7." In: *The Aeronautical Journal* 113.1149 (2009), pp. 747–747.

[17] Joshua Sullivan, Sebastian Grimberg, and Simone D'Amico. "Comprehensive survey and assessment of spacecraft relative motion dynamics models." In: *Journal of Guidance, Control, and Dynamics* 40.8 (2017), pp. 1837–1859.

[18] Adam W. Koenig, Tommaso Guffanti, and Simone D'Amico. "New state transition matrices for relative motion of spacecraft formations in perturbed orbits." In: *AIAA/AAS Astrodynamics Specialist Conference*. 2016, p. 5635.

[19] David Q. Mayne. “Model predictive control: Recent developments and future promise.” en. In: *Automatica* 50.12 (Dec. 2014), pp. 2967–2986. ISSN: 0005-1098. DOI: 10.1016/j.automatica.2014.10.128. URL: https://www.sciencedirect.com/science/article/pii/S0005109814005160 (visited on 05/04/2022).

[20] James B. Rawlings and Mayne David Q. *Model Predictive Control Theory and Design*. Inglese. Madison, Wis: Nob Hill Pub, Llc, 2009. ISBN: 9780975937709.

[21] H. Chen and F. ALLGöWER. “A Quasi-Infinite Horizon Nonlinear Model Predictive Control Scheme with Guaranteed Stability∗∗This paper was not presented at any IFAC meeting. This paper was accepted for publication in revised form by Associate Editor W. Bequette under the direction of Editor Prof. S. Skogestad.” en. In: *Automatica* 34.10 (Oct. 1998), pp. 1205–1217. ISSN: 0005-1098. DOI: 10.1016/S0005-1098(98)00073-9. URL: https://www.sciencedirect.com/science/article/pii/S0005109898000739 (visited on 08/07/2022).

[22] Lars Lindemann and Dimos V. Dimarogonas. “Control Barrier Functions for Signal Temporal Logic Tasks.” In: *IEEE Control Systems Letters* 3.1 (Jan. 2019), pp. 96–101. ISSN: 2475-1456. DOI: 10.1109/LCSYS.2018.2853182.

[23] Wei Xiao and Calin Belta. “Control barrier functions for systems with high relative degree.” In: *2019 IEEE 58th conference on decision and control (CDC)*. IEEE, 2019, pp. 474–479.

[24] Tengfei Liu. *Robust Event-Triggered Control of Nonlinear Systems*. eng. 1st ed. 2020.. Research on Intelligent Manufacturing. Singapore: Springer Singapore, 2020. ISBN: 9789811550133.

[25] Eduardo D. Sontag. *Mathematical Control Theory: Deterministic Finite Dimensional Systems*. en. Google-Books-ID: f9XiBwAAQBAJ. Springer Science & Business Media, Nov. 2013. ISBN: 9781461205777.

[26] Charles Henry Edwards. *Advanced calculus of several variables*. Courier Corporation, 2012.

[27] David G. Wright. “Tychonoff’s Theorem.” In: *Proceedings of the American Mathematical Society* 120.3 (1994), pp. 985–987. ISSN: 0002-9939. DOI: 10.2307/2160497. URL: https://www.jstor.org/stable/2160497 (visited on 08/09/2022).

[28] Stefan Scholtes. *Introduction to piecewise differentiable equations*. Springer Science & Business Media, 2012.

[29] Victor Nwankwo and Sandip Chakrabarti. "Theoretical Model of Drag Force Impact on a Model International Space Station Satellite due to Solar Activity." In: *TRANSACTIONS OF THE JAPAN SOCIETY FOR AERONAUTICAL AND SPACE SCIENCES SPACE TECHNOLOGY JAPAN* 12 (July 2014), pp. 47–53. DOI: 10.2322/tastj.12.47.